ACCURATE ASTROPHYSICAL PARAMETERS FOR ALGOL-TYPE BINARY STARS

P. F. L. Maxted

A Thesis Submitted for the Degree of PhD
at the
University of St Andrews

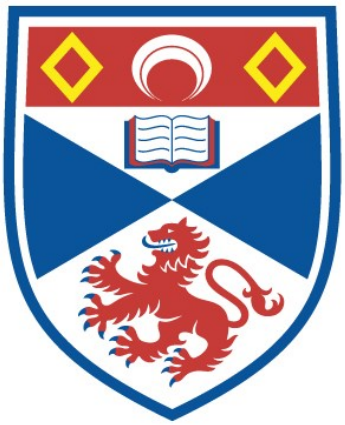

1995

Accurate astrophysical parameters for Algol-type binary stars

P.F.L. Maxted

10th August 1994

A thesis submitted to the University of St Andrews in application for the degree of Doctor of Philosophy

TK B 612

I, Pierre François Louis Maxted, hereby certify that this thesis, which is approximately 40,000 words in length, has been written by me, that it is, except where reference is made to others, a record of the work carried out by me, and that it has not been submitted in any previous application for a higher degree.

I was admitted as a research student under Ordinance No. 12 in October, 1991 and as a candidate for the degree of Doctor of Philosophy in October, 1992. The higher study for which this is a record was carried out in the University of St Andrews between 1991 and 1994.

In submitting this thesis to the University of St Andrews I understand that I am giving permission for it to be made available for the use in accordance with the regulations of the University Library for the time being in force, subject to any copyright vested in the work not being affected thereby . I also understand the the title and abstract will be published, and that a copy of the work may be made and supplied to any *bone fide* library or research worker.

P.F.L. Maxted, August 1994

I hereby certify that the candidate has fulfilled the conditions of the Resolution and Regulations appropriate for the degree of Doctor of Philosophy in the University of St Andrews and that the candidate is qualified to submit this thesis in application for that degree.

R.W. Hilditch, August 1994

FOR MY PARENTS

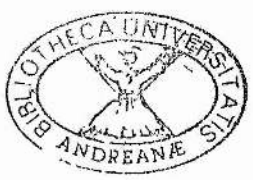

I would like to thank the following people who have all contributed to the speed and enjoyment with which this thesis has been completed:

Katrina, who made my final year more fun than I could have hoped for;

Graham Hill, for his generosity both in terms of data and advice;

The University of St Andrews Bridge Club, particularly my friends Erika, Aaron and Pete;

Contributors to the ZUVAD::GOSSIP conference; for much amusement;

Marek Sarna and Jean-Pierre De Greve, for providing me with their evolutionary models;

and to my supervisor Ron Hilditch, for his continual advice and encouragement.

The Isaac Newton Telescope is operated on the island of La Palma by the Royal Greenwich Observatory in the Spanish Observatorio del Roque de los Muchachos of the Instituto de Astrofisica de Canarias.

This research has made use of the Simbad database, operated at CDS, Strasbourg, France.

This research has been funded by PPARC (formerly SERC).

Abstract

We present new, accurate astrophysical parameters for both components of the six short-period Algol-type binary stars RZ Cas, AT Peg, TX UMa, AF Gem, RU UMi and HU Tau. The accuracy of the astrophysical parameters is ensured by the determination of a mass ratio for each of the systems from the spectroscopic orbits of both components via the cross correlation technique.

For RZ Cas and AT Peg we have developed a simple technique to correct the observed photometry for the presence of the secondary component. Spectral classification of the primary component of AT Peg was aided by the use of an improved Doppler tomography technique.

The systems RZ Cas, AT Peg, TX UMa, AF Gem and HU Tau are found to be apparently normal semi-detached Algol-type systems and accurate masses and radii have been determined with a typical precision of a few percent. For RU UMi we have been able to confirm the suspected semi-detached configuration.

We have compiled a list of nine Algol-type binary stars, five from this study, for which the observed astrophysical parameters have been determined accurately using a combination of both spectroscopic and photometric data in a self-consistent solution. The general model of non-conservative case B evolution adequately explains the properties of these systems as a group. Angular momentum loss via a magnetic stellar wind is shown to be an important factor in the evolution of these systems. However, there appear to be no published evolutionary models which can be used to estimate the properties of the progenitors of these systems. For the more massive systems the best available models predict periods that are too large by ~50–250% and luminosities for the faint components that are too high by factors of 10–20.

Contents

1 Introduction **1**

1.1 Introduction 1

1.2 A brief history of the study of Algol systems. 1

1.3 Observational characteristics of Algol systems. 2

1.4 Mass transfer 4

1.4.1 Mechanisms of accretion 4

1.4.2 Observational properties of accretion discs 5

1.5 Period changes and rotation rates. 6

1.6 The formation and evolution of Algol systems. 7

1.6.1 The evolution of single stars. 7

1.6.2 Evolution in an interacting binary system. 8

1.6.3 Models of case B evolution. 10

1.7 Overview of thesis 14

2 Observations and Reductions **19**

2.1 Introduction 19

2.2 The Dominion Astrophysical Observatory 1.2m coudé spectra 19

2.3 The Isaac Newton Telescope IDS spectra 20

2.4 The Leslie Rose RBS spectra 21

2.5 Radial velocity measurements 22

2.6 The light curves, their solutions and the radial velocity corrections 24

3 RZ Cassiopeiae **26**

3.1 Introduction 26

3.2 Spectroscopic observations and reductions 27

3.2.1 Observations 27

3.2.2 RV measures from Gaussian profiles 27

3.3 Spectroscopic results 28

3.3.1 Orbit 30

3.4 Spectral types and colour indices 30

3.4.1 Primary component 30

3.4.2 Secondary component 36

3.5 Solutions of the UBV light curves 39

3.5.1 Rotation of the primary 40

3.5.2 Results 41

3.6 Period jumps and associated phenomena 42

3.7 Additional observations 44

3.8 Conclusion 44

4 AT Pegasi **49**

4.1 Introduction 49

4.2 Spectroscopic observations and reductions 50

4.2.1 RV measures from Gaussian profiles 50

4.3 The spectroscopic orbit 50

4.4 Spectral types and colour indices 54

4.4.1 Reconstruction of the primary and secondary spectra 54

4.4.2 Strömgren photometry 54

4.5 Light curve solutions 56

4.5.1 Results 58

4.6 Conclusion 59

5 TX Ursae Majoris **61**

5.1 Introduction 61

5.2 Radial velocity measurements 62

5.3 The light curves and their solution 64

5.4 The absolute parameters of TX UMa 67

5.5 Conclusion 68

6 RU Ursae Minoris **71**

6.1 Introduction 71

6.2 Measurement of the radial velocities 71

6.2.1 Spectroscopic orbit 73

6.3 The solution of the light curves 74

6.4 Conclusion 77

7 AF Geminorum 80

7.1 Introduction 80

7.2 Radial velocity measurements 80

7.3 The light curves and their solution 83

7.3.1 The effective temperature of the primary component 83

7.3.2 Solution of the light curve 83

7.4 The absolute parameters of AF Gem 84

7.5 Conclusion 84

8 HU Tauri 89

8.1 Introduction 89

8.2 The spectroscopic orbit 90

8.2.1 Radial velocity measurements 90

8.2.2 The spectroscopic orbit 93

8.3 The light curve solutions 94

8.4 The absolute parameters 97

8.5 Conclusion 97

9 Comparison of accurate absolute parameters of Algol systems with evolutionary models 101

9.1 Introduction 101

9.2 A compilation of accurate absolute parameters for Algols. 102

9.2.1 Criteria for selection 102

9.2.2 The compilation 102

9.3 Comparison with evolutionary models 105

9.3.1 General properties 105

9.3.2 The evolutionary models of Iben & Tutukov, 1984 105

9.3.3 The evolutionary models of De Greve, 1993 110

9.4 Conclusion and future directions 112

A Automatic Rectification of spectra **118**

A.1 Introduction 118

A.2 The aim of rectification 118

A.3 The rectification algorithm 119

A.4 Using PRESS 121

A.5 XPRESS and DPRESS 124

B Tomography **125**

B.1 Introduction 125

B.2 The synthetic spectra 125

B.3 Summary of the method 127

B.4 Results 129

B.5 Conclusion 131

List of Figures

3.1 Symmetric CCF of RZ Cas v. Vega 29

3.2 Asymmetric CCF of RZ Cas v. Vega 29

3.3 Radial velocity measurements of RZ Cas and the adopted spectroscopic orbit . . 33

3.4 UV (IUE) spectra of standard A stars and RZ Cas 35

3.5 DDO observations of RZ Cas during primary minimum 37

3.6 The UBV light curves of RZ Cas and the adopted solutions 42

3.7 Residuals from the ephemeris of Herczeg & Frieboes-Conde 43

3.8 Y-cut through the red arm ISIS spectrum of RZ Cas 45

4.1 Radial velocity measurements of AT Peg and the adopted spectroscopic orbit . . 52

4.2 Spectra of AT Peg recovered using Doppler tomography 55

4.3 The light curve of AT Peg and the adopted solution 58

5.1 CCF of TX Uma 64

5.2 Radial velocity measurements for TX UMa and the adopted spectroscopic orbit . 65

5.3 The BV light curves of TX UMa and the adopted solutions 67

6.1 Radial velocity measurements of RU UMi and the adopted spectroscopic orbit . . 72

6.2 The R light curve of RU UMi and the adopted solution 75

6.3 RU UMi in the Hertzsprung–Russell diagram 78

6.4 RU UMi in the mass–radius plane 78

7.1 Radial velocity measurements of AF Gem and the adopted spectroscopic orbit . 83

7.2 The UBV light curves of AF Gem and the adopted solutions 86

8.1 Radial velocity measurements of HU Tau and the adopted spectroscopic orbit. . 93

8.2 The BV light curves of HU Tau and the solution for a detached configuration . . 96

8.3 The BV light curves of HU Tau and the adopted solutions 97

9.1 The Hertsprung-Russell diagram 106

9.2 The mass-radius plane 106

9.3 The M_{a0}–P_0 plane 109

9.4 Helium core mass estimates. 109

9.5 The mass gaining stars in the mass–radius plane 112

9.6 The mass donors in the mass–luminosity plane 115

9.7 The mass ratio–period plane 115

A.1 The rectification algorithm 120

B.1 The principle of Tomography as applied to binary star spectra 126

B.2 The RBS spectra of Vega and Hamal 128

B.3 A typical combined spectrum and the spectra recovered using tomography 130

B.4 Detail of spectra recovered using tomography and the original spectra for comparison. 131

B.5 The improvement in signal-to-noise for the primary 132

List of Tables

1.1 Critical initial separation in $R_\odot$ for interacting binary stars 9

1.2 Critical initial period in days for interacting binary stars 9

3.1 Measured radial velocities for RZ Cas 31

3.2 The spectroscopic orbit of RZ Cas 32

3.3 The combined spectroscopic orbit of RZ Cas 32

3.4 Strömgren photometry of RZ Cas 34

3.5 Mean UV colours of A type stars 35

3.6 Observed DDO colours of RZ Cas 38

3.7 DDO colour index estimates for RZ Cas. 39

3.8 DDO colours of some A type stars 39

3.9 Solutions to the UBV light curves of Chambliss 40

3.10 Absolute parameters of RZ Cas 41

3.11 Timings of minima of RZ Cas. 44

4.1 Measured radial velocities for AT Peg 51

4.2 The spectroscopic orbit of AT Peg 53

4.3 The combined spectroscopic orbit of AT Peg 53

4.4 Strömgren photometry of AT Peg 56

4.5 Light curve solution for AT Peg 57

4.6 Absolute parameters of AT Peg 57

5.1 Measured radial velocities for TX UMa 63

5.2 The spectroscopic orbit of TX UMa 66

5.3 Solutions to the BV light curves of TX UMa 68

5.4 Absolute parameters of TX UMa 68

6.1 Measured radial velocities for RU UMi 73

6.2 The spectroscopic orbit of RU UMi 74

6.3 Light curve solutions for RU UMi 76

6.4 Absolute parameters of RU Umi 76

7.1 Measured radial velocities for AF Gem 81

7.2 The spectroscopic orbit of AF Gem. 82

7.3 Solutions to the UBV light curves of AF Gem 85

7.4 Absolute parameters of AF Gem 85

8.1 Measured radial velocities for HU Tau 91

8.1 92

8.2 The spectroscopic orbit of HU Tau 94

8.3 Solutions to BV light curves of HU Tau 98

8.4 Absolute parameters of HU Tau 98

9.1 Observational data for the nine Algol systems 103

9.2 Accurate absolute parameters of nine Algol systems 107

Chapter 1

Introduction

1.1 Introduction

The study of Algol systems is one which is at once fascinating, challenging and rewarding but above all instructive. Algol itself was the first star to be recognised as an eclipsing binary over two hundred years ago and since then the study of similar systems has led to insights of major importance for study of all types of close binary systems. For example, the discovery by Joy (1941) of an accretion disc in RW Tau precedes the discovery of these structures in more active systems such as cataclysmic variables or X-ray binaries. Of fundamental importance in the study of these exotic systems, and other interacting systems such as W UMa-type contact binary systems, is the notion of mass transfer which was developed in the 1950's to resolve the "Algol paradox". Of no less importance was the evidence from the study of the Algol system AS Eri that this mass transfer may be non-conservative (Refsdal et al., 1974) i.e. that mass and angular momentum may be lost from the binary system.

The study of Algol systems is entering a new phase driven by advances in instrumentation and data analysis which will doubtless provide as many insights into the evolution of all binary stars as it has in the past.

1.2 A brief history of the study of Algol systems.

The study of Algol systems has a long history. It began in earnest when John Goodricke (1783) first noted the periodicity in the brightness variations of Algol (β Persei) and suggested that this was caused by the star being eclipsed by a dark body or by the presence of dark spots on

the rotating surface of the star. The eclipse hypothesis found strong support when Vogel (1889) discovered the radial velocity variations of Algol, and has since become an established fact.

Struve (1948) was among the first to notice that among eclipsing binaries there existed relatively many containing a bright main-sequence component in the spectral range mid-B to mid-A and a fainter component of lower mass and of similar radius and therefore the more highly evolved object. This is paradoxical since massive stars evolve much faster than less massive stars. He also drew attention to the fact that the secondary was close to the limit of dynamical stability, something that had been pointed out earlier by Walter (1931), and was emphasized later by Wood (1950). This prompted Crawford (1955) to formulate the important notion of mass transfer which was popularised by Hoyle (1957). Thus, by this time the essential elements existed to describe the nature and formation of Algol systems. Kuiper (1941) had already suggested that the Roche limit would affect the evolution of close binary stars, and Morton (1960) showed that mass transfer would occur extremely rapidly. The picture of interacting binary systems that was emerging at this time was reviewed by Paczyński (1971) and by Plavec (1970). The mechanisms described therein are essentially those that form the basis of our current understanding of Algol systems.

1.3 Observational characteristics of Algol systems.

The distinguishing feature of all Algol systems is their light curve. It consists of a deep primary eclipse with a much shallower secondary eclipse half a period later. Stars showing this kind of variability are known as EA type variables. However, it is important to note that a star showing EA type variability is not necessarily an Algol type system. It is quite possible that the system is simply a pair of unevolved main sequence stars as opposed to an evolved low mass star with a main-sequence early type companion. Budding (1984), in his catalogue of Algol systems, denotes these two different cases EA1 and EA2 for the unevolved and evolved systems respectively. To establish whether the system is evolved or not we need to know the astrophysical or absolute parameters (mass, radius and luminosity) of the two stars. The light curve gives us the radii of the stars relative to the separation of the stars, the relative luminosity of the two stars, and the inclination of the system to the line of sight. Combined with radial velocity curves for both stars and Kepler's laws, these give the absolute masses and radii directly. To establish the luminosities of the stars we need to find the effective temperature of one of the components, usually the brighter one. This can be estimated from its spectral type, photometric colours, or from a detailed analysis of its spectrum in the UV where contamination from the secondary is negligible. The effective temperature of the secondary component can then be derived using the luminosity ratio obtained from the light curve. Spectrophotometry is also a valuable tool for determination of the effective temperatures of both components (Etzel,

1988).

Given only one radial velocity curve the situation is more complicated since we have insufficient information to determine the absolute parameters of the system. In this case we must make some assumptions about the system such as the assumption that the primary is a main-sequence star. We may then use a relationship for, say, mass–luminosity or mass–radius applicable to these stars. However, it is difficult to determine the potentially large systematic error introduced by adopting this assumption in an individual case.

Another possibility arises since we know that for classical Algol systems the secondary star fills it Roche lobe. If we assume that this is the case for the system under investigation, we have a relationship between the mass ratio and the size of the secondary so the absolute parameters can be found. This method gives notoriously unreliable results when used with poor quality light curves and has led to much confusion. Even with the highest quality light curves the mass ratio derived by assuming a semi-detached configuration (the photometric mass ratio, q_{ptm}) can disagree significantly from the mass ratio derived directly from the spectroscopic orbit (the spectroscopic mass ratio, q_{sp}). A good example can be found in Chapter 5 for TX Uma.

Giménez & Garcia (1990) compared the mass ratios obtained using the two methods above to those obtained from double-lined spectra. Mass ratios obtained by assuming a main sequence primary star were reliable to within 10% with no systematic deviations. This shows that the primary star looks like a main sequence star despite the fact that it is accreting mass. The mass ratios derived by assuming the secondary fills its Roche lobe were much higher ($\sim$ 20%). Other methods for determining the mass ratio, such as combining the two previous methods, are discussed but are shown to be unreliable.

The radial velocity curves for Algol systems are not straightforward either. To derive accurate absolute parameters we require radial velocity curves for both components in order to fix the mass ratio. The faintness of the secondary relative to the primary has made this difficult but over the past ten years the use of solid-state detectors such as Reticon diode arrays and CCD's with their high quantum efficiencies and good red response in combination with the cross-correlation technique have made measurement of the secondary's radial velocity possible using telescopes of modest aperture (0.5m - 2.5m).

Mass transfer is a reliable indicator of the semi-detached nature of a binary system but if the mass transfer rate is too high then there will almost certainly be circumstellar matter which will confuse the radial velocities obtained for the primary component. The extent of this problem increases as the period of the system increases for reasons that will become apparent. An excellent example of this can be found in Popper (1989) in his study of twelve Algol system with a range of periods.

A typical Algol system consists of a primary of a few solar masses and of spectral type A or B with a G or K type secondary of a few tenths of a solar mass or more. These two properties make radial velocities of the secondaries of these systems extremely hard to determine. Many more Algols exist for which only one radial velocity curve has been established and the mass ratio has been determined indirectly by one of the methods described earlier. Budding (1989) studied the statistical properties of observed Algols based on his catalogue (1984). The periods of these systems ranges from a day or less up to several tens of days, the average is 7.5 days but most have a period of about 2.5 days. No definite Algols have been found with a primary mass less than $1.2\,M_{\odot}$, which is in keeping with evolutionary models, although very low mass systems such as R CMa, Z Dra and RT Per, may have had odd evolutionary histories (Yungelson et al., 1989). However at higher masses the situation is not so clear. The most most massive classical Algol is RZ Sct with a primary mass of about $13.5\,M_{\odot}$ and maybe as much as $18\,M_{\odot}$.

1.4 Mass transfer

Another common property of Algol systems is the mass transfer from the secondary star to the primary star. This takes place in the form of a stream of matter leaving the secondary star at the inner Lagrangian point. The hydrodynamical properties of this stream were studied by Lubow & Shu (1975) using a multiple length scale approach. They assumed a synchronously rotating system with an isothermal stream in which the thermal velocity was some small fraction ϵ of the orbital velocity. They found that the stream leaves the inner Lagrangian point as a highly anisotropic stellar wind forming a stream of width $\sim \epsilon$d, d being the separation of the components. For a full range of mass ratios, the angle the stream makes with the line of stellar centres varies only from 19.5 to 28.4 degrees. The width of this stream remains nearly constant as it falls towards the companion star, narrowing somewhat as it reaches its closest first approach to the companion at a distance $\tilde{\omega}_{min}$.

1.4.1 Mechanisms of accretion

The fate of the matter in the stream is determined primarily by the geometry of the system. In widely separated systems ($r < \tilde{\omega}_{min}$, r being the primary's radius) the stream does not hit the mass gaining star and it does not have sufficient energy to escape from the system. The stream therefore orbits the star. However as the stream approaches periastron on its first orbit (second approach) it will intersect itself forming a shock. The processes "downstream" of this shock will be complicated. However Lubow & Shu showed that there exists a steady state scenario in which the incoming and returning segments of the stream intersect forming a permanent disc around the mass gaining star (provided of course that the mass transfer continues). Viscous

forces cause the disc to spread so that angular momentum is lost from the outer edge allowing matter to settle onto the star at the inner edge. This type of disc is called a steady Keplerian disc, and some of its properties are described by Smak (1989) and by Hubeny(1989). A general description of accretion discs is described in Frank et al. (1992).

In less widely separated systems where $r > \tilde{\omega}_{min}$, the stream will hit the mass gaining star. In this case two possibilities exist depending again on the geometry of the system. If we consider the quantity r_h which is the radius of a circular Keplerian orbit having the same angular momentum as the stream, then the two cases are distinguished by $r > r_h$ and $r < r_h$. For the case $r > r_h$ the matter in the stream has insufficient angular momentum to escape from the surface of the star and so will simply accrete directly onto the star, possibly in the form of a hot spot and/or an equatorial bulge. If the mass transfer rate increases temporarily then the matter may form a transient accretion disc which is likely to be highly turbulent and asymmetric. The velocities of the particles in such a disc are referred to (incorrectly) as "sub-Keplerian", meaning that their tangential velocity is less than that of a particle at the same radius in a circular Keplerian orbit i.e. the particles are near apastron in their their elliptical orbits.

Smak (1989) also considers the case $r < r_h$, in which the matter in the stream has too much angular momentum to remain on the surface of the star and so will "splash". By computing particle trajectories and modeling the splash as a simple reflection he found that under the condition of steady mass transfer rate the disc formed by a splash and the Keplerian discs described earlier are qualitatively similar. However the way this discs forms and its appearance when mass transfer rates are variable will clearly be different.

1.4.2 Observational properties of accretion discs

Accretion discs in Algols are not as spectacular as those in other systems such as cataclysmic variable stars or X-ray binaries simply because the matter is falling into a relatively "shallow" potential well and so does not lose much gravitational potential energy. Discs in Algols tend therefore to be fairly cool, a few thousand Kelvin depending on the mass transfer rate. Nevertheless, these discs may contribute significantly to the total luminosity of the system (Smak, 1989) and they will certainly affect the shape of the light curve. For example, the obscuration of the disc by the fainter star produces broad shallow wings around primary eclipse. Accretion discs are most noticeable spectroscopically in the form of double peaked emission lines. These lines are particularly useful since their profiles vary during primary eclipse as different parts of the disc are eclipsed. Thus, time-resolved spectroscopy is a valuable tool for unravelling the structure of these discs (Kaitchuck, 1989; Peters, 1989).

1.5 Period changes and rotation rates.

One of the most easily observed properties of an Algol system is that which was first observed by John Goodricke, the system's period. The advent of photoelectric photometry has enabled timings of minima to be made which are accurate to a few seconds. Clearly, such timings are very sensitive to changes in the period of the system and are therefore a good tool to investigate the behaviour of systems over the long term. Since mass is being transferred from the less massive to the more massive star, the period of the system should increase monotonically, provided the mass transfer is conservative. However O-C diagrams (observed minus computed times of minima against time) for many Algol systems show both increases and decreases in period alternating randomly on a time scale of years and of order $\Delta P/P \sim 10^{-5}$. One possible explanation is that the mass transfer in non-conservative. However mass loss rates from these systems via stellar winds are far too low to account for these period changes (as is the case for RS CVn binaries).

Biermann & Hall (1973) proposed a mechanism that has been used successfully to describe these period changes in which the mass transfer rate is variable. If the mass transfer rate suddenly increases then a "lump" of matter will fall onto the mass gaining star. If the angular momentum of this matter is stored in the outer layers of the star, the orbital angular momentum is decreased at the expense of the rotational angular momentum of the star. This leads to an increase in the period. Since the mass gaining star is now rotating asynchronously, tidal forces will tend to reduce its rotation until it reaches synchronism. This effectively restores the the orbital angular momentum to the value it would have taken had the angular momentum not been temporarily stored in the outer layers of the star. This effect can be simplified by considering two phases of mass transfer; an active phase where all the angular momentum carried by the mass is stored in the outer layers of the mass gaining star and a quiet phase where the mass transfer rate is low and tidal forces transfer the rotational angular momentum back into orbital angular momentum. This simplified approach predicts an O-C diagram comprising upwardly curving parabolic segments. An example of the application of the hypothesis to obtain mass transfer rates is given for the case of U Cep and strong evidence for the processes involved at work is found in our study of RZ Cas.

The Biermann-Hall hypothesis clearly requires that the mass gaining star rotates asynchronously for at least part of the time. Rotation rates are therefore important for understanding the mass transfer process. The usual way of obtaining rotation rates is to observe the line broadening in spectra to obtain a value of the projected rotational velocity $V_{rot} \sin i$, i being the inclination obtained from the light curve. A variation of this method is described by Hill (1990),in which the cross correlation function is used to measure $V_{rot} \sin i$. This is possible because the cross correlation function is strongly determined by the mean shape of the lines in the spectrum and so its width is dependent on $V_{rot} \sin i$. The method is particularly effective in

the case of double stars with faint components since the cross correlation technique can detect companion stars two or three magnitudes fainter than the primary.

Van Hamme & Wilson (1990) describe an alternative method using analysis of light curves to obtain the ratio of the polar and equatorial radii. This can be used to estimate the rotation rate fairly accurately for fast rotating stars where the polar flattening due to rotation is fairly large. There is however strong disagreement between values obtained by the two methods for some systems. This can be accounted for if the rotation is latitude dependent. In the case of a fast rotating equatorial belt for example, the photometric method will produce a large rotation rate since the ratio of radii will be large. The spectroscopic method will produce a low value for the rotation rate because the gravity darkening effect will make the fast rotating regions appear darker so only the slow rotating regions are seen. These considerations aside, the authors find some evidence emerging for a group of systems which are rotating at or near their centrifugal limits, so-called "double-contact" systems.

Period changes may also be indicative of a magnetic cycle, similar to the solar activity cycle, operating in the subgiant components of Algol systems. This is a consequence of the convective atmospheres and rapid rotation of these stars which combine to make them active dynamo stars. A 32y magnetic cycle was proposed by Soderhjelm (1980) in his comprehensive study of Algol. Similarly Berrington & Hall (1994) in their study of SW Cyg find a 96y magnetic cycle to be the best explanation of the observed period variations.

1.6 The formation and evolution of Algol systems.

1.6.1 The evolution of single stars.

In order to understand the evolution of binary stars, it is first necessary to know how stars evolve "normally" i.e. when they are well separated from any companion stars. The description here is based on the work of Iben (1965a,b; 1966 a,b,c). Though much work has been done in the field of stellar evolution since, Iben's analysis is sufficiently accurate for our purposes and has the merit of dealing with the mass range we are concerned with in a uniform manner.

We start with a chemically homogeneous star in the mass range 0.5–15 $M_{\odot}$, with a hydrogen burning core, which has contracted until it reaches equilibrium i.e. a star on the Zero–age main sequence (ZAMS). The star fuses hydrogen in its core principally by the proton-proton reaction in less massive stars, giving way to the more efficient CNO cycle at higher masses, producing helium. As the helium concentration builds up, hydrogen burning becomes less efficient so the core contracts slowly, raising the temperature and thus the rate of hydrogen

fusion, the star thus becomes more luminous. The contraction of the core also causes the outer layers of the star to expand.

For a star of around one solar mass this process continues for about ten billion years, after which the star's luminosity and radius will have doubled and the concentration of hydrogen in the centre will have been depleted to the extent that hydrogen burning stops in the core, though it continues in a shell around the helium rich core. The temperature in the core is insufficient to burn helium and so the core contracts. The gravitational potential energy released during this contraction heats up the hydrogen burning shell surrounding the core increasing the rate of hydrogen burning. This increased luminosity causes the outer layers of the star to expand. This phase of the evolution corresponds to the subgiant and red giant branch of the HR diagram. When the star reaches the tip of the red giant branch the helium core has become degenerate and so cannot contract any further. When the temperature and pressure in the core are sufficient to start helium burning this will happen explosively because the core is degenerate. This "helium flash" causes the star to evolve away from the red giant tip. The evolution of the star after this stage need not concern us here.

The scenario is much the same for stars between half a solar mass up to about three solar masses. Above three solar masses the evolution is significantly different because the star has a convective core which keeps the central regions of the star chemically homogeneous. When the hydrogen in the core of the star is exhausted we are left with an isothermal helium core surrounded by a thick hydrogen burning shell (provided the core mass is not great enough to start helium burning straight away). As hydrogen is fused to form helium the mass of the core relative to the total mass of the star, q_0 gradually increases. This continues until q_0 reaches a value of about 0.1. This limit is called the Schönberg-Chandrasekhar limit, q_{SC}, and it arises because the maximum pressure at the surface of the core decreases strongly with core mass. At this point the evolution proceeds extremely rapidly as the core collapses and the outer layers of the star expand, just half million years for a seven solar mass star to increase its radius from 2.4 solar radii to 72.4 solar radii. The luminosity barely changes during this phase, which corresponds to the Hertzsprung gap on the HR diagram, because the gravitational energy released by the core collapsing is used up in "lifting" the outer layers of the star. The behaviour of the star once it reaches the red giant branch is complex, involving successive expansions and contractions of the outer layers and is extremely sensitive to the mass of the star. Again, these later stages of evolution need not concern us here.

1.6.2 Evolution in an interacting binary system.

Interacting binary systems are defined to be those in which mass transfer will occur (excluding stellar wind effects). More precisely we can say that this will occur if the limit of dynamical

Table 1.1: Critical initial separation in $R_\odot$ for interacting binary stars

Primary mass	q=1	q=0.5	q=0.2
$3\,M_\odot$	85	74	62
$5\,M_\odot$	191	165	137
$9\,M_\odot$	621	533	451
$15\,M_\odot$	1489	1279	1081

Table 1.2: Critical initial period in days for interacting binary stars

Primary mass	q=1	q=0.5	q=0.2
$3\,M_\odot$	37	34	29
$5\,M_\odot$	97	89	78
$9\,M_\odot$	428	394	341
$15\,M_\odot$	1202	1107	959

stability of a star, its Roche lobe, is at some time smaller than the size the star would have been if it had evolved normally. If we assume that the orbits are circular and synchronised, which is generally true for such close systems, then we can calculate for a given mass ratio the size of the Roche lobe of the primary star (defined from here on as the initially more massive star, even though it is observed in a classical Algol system as the less massive fainter star) relative to the separation of the stars. If we then have an evolutionary model for a star of a given mass we can simply calculate the minimum separation for which the size of the primary's Roche lobe is always larger than the size of the star (ignoring the effect of distortion to the shape of the star on its evolution). This is done for the models of Iben in Table 1.1 and again in terms of the period in Table 1.2 for three mass ratios (taken from Plavec, 1967).

Should the separation be smaller than this value initially, or fall below this value, say by angular momentum loss (AML) via a magnetic stellar wind (Yungelson et al., 1989), then the evolution of the primary star will be affected because at some time the primary will expand to fill its Roche lobe and so lose mass. This can occur during any of the periods during which the star is expanding. The nomenclature that has become standard in the field was devised by Kippenhahn & Weigert (1967) and Lauterborn (1970) as follows:

Case A: The primary fills its Roche lobe during its main sequence expansion phase while it is still burning hydrogen in its core.

Case B: The primary fills its Roche lobe once it has stopped burning hydrogen in its core and before helium ignition.

Case C: The primary fills its Roche at after helium ignition in the core.

This is clearly a simplistic scheme and more detailed evolutionary models require a more complex scheme, usually based on the same notation, to deal with intermediate cases and evolution of the secondary star leading to double-degenerate systems, cataclysmic variables etc. Of these three cases, B is the most common since it is associated with the lifetime of the star during which expansion is greatest. It is also the mechanism which is assumed to produce a classical Algol system and is described in more detail below. Case A is more complex in that it generally leads to a contact binary system for which evolutionary models do not exist beyond the contact stage. Case C evolution is the most difficult case to model since it involves a common envelope phase in which the primary expands to engulf the secondary. A thorough discussion of case C evolution is to be found in Pastetter & Ritter (1989). It is believed that the system loses large amounts of angular momentum and mass as the secondary spirals in through the outer layers of the primary, possibly producing a planetary nebula, and resulting in a cataclysmic variable consisting of the core of the primary and the main sequence secondary.

1.6.3 Models of case B evolution.

In the simplest case we can model the evolution through case B mass transfer of a binary system under the following assumptions:

1. The internal structure of the stars is spherical.
2. Mass transfer starts when the volume of the star equals the volume of its Roche lobe.
3. The orbit is circular.
4. The mass transfer rate is calculated by keeping the volume of the Roche lobe and the star equal.
5. The primary (mass losing star) is in hydrostatic equilibrium.
6. The effect on the primary of the evolution of the secondary is negligible.
7. The total mass is conserved.
8. Angular momentum is conserved.

Early calculations such as Paczynski (1967) and Kippenhahn & Weigert (1967) made use of all these assumptions. Evolution of the secondary star will clearly become important if the secondary star's radius exceeds the size of its Roche lobe since the system will become a contact system. The effects of contact occurring in case A and early case B mass transfer is reviewed by De Greve (1989). The effects of accretion onto a main sequence star have been studied by Ulrich & Berger (1976), Kippenhahn & Meyer-Hofmeister (1977), Neo et al. (1977) Flannery &

Ulrich (1977), Packet & De Greve (1979), Sarna & Fedorova (1989) and Hellings (1983). These allow us to distinguish between systems where the expansion of the secondary is large enough for the system to form a contact system and those in which it is not. Calculations treating the simultaneous evolution of both components have been done by Benson (1970), De Greve (1985) and Packet & De Greve (1990). Grids of evolutionary models for both components have been published by de Loore & De Greve (1991) and De Greve (1993) for the mass ranges 9 to 40 $M_\odot$ and 3 to 8 $M_\odot$ respectively. These sophisticated models include the effects of non-conservative mass transfer, stellar wind mass loss and magnetic stellar winds.

A more sophisticated model for rapid mass transfer was studied by Kolb and Ritter (1990) for a system of initial masses $2\,M_\odot$ and $1\,M_\odot$ with initial separation $8\,R_\odot$. These parameters were chosen to be similar to a system studied by Kippenhahn et al. (1967). The two models had no significant differences. In general it was found that evolutionary models calculated by constraining the primary to its Roche lobe are good if: the mass transfer rate is not sensitive to the degree of filling of the Roche lobe; the pressure scale height in the primary is much less than its radius and the phases when mass transfer stops and restarts are not important for calculating the evolution of the system. Another method uses a mass transfer rate given by Jedrzedec (1969):

$$\dot{M} \sim \left(\frac{\Delta R_1}{R_1}\right)^{n+1.5} \tag{1.1}$$

where:

n=polytropic index

R_1 = radius of star

$\Delta R_1 = R_1 - R_{cr}$

R_{cr} is the radius beyond which the star will lose mass. This is usually assumed to be the radius of the sphere of equal volume to the Roche lobe of the star (r_1). This assumption is only strictly valid in the case of a synchronously rotating star. Plavec (1958) and Kruszewski (1963) studied the more difficult case of non-synchronous rotation and found little difference between the two cases. In the mass range $0.8 < \frac{M_1}{M_2} < 20$ the equivalent radius is given to better than 2% by:

$$\frac{r_1}{A} = 0.38 + 0.2 \log \frac{M_1}{M_2} \tag{1.2}$$

$$A = \frac{(M_1 + M_2)\, J^2}{G\,(M_1 M_2)^2} \tag{1.3}$$

where A is the separation of the components and J the orbital angular momentum (Paczynski, 1971). This is simply a generalisation of the usual method for calculating mass transfer rates, which is equivalent to taking $\Delta R_1 = 0$.

Yungelson (1973) studied the effect of non-conservative mass transfer on the evolution of the initially more massive stars in systems evolving through case B with initial masses of $1.3\,M_\odot$ and $1.5\,M_\odot$. He calculated both conservative and non-conservative evolution assuming 25% mass loss from the system lost as a stellar wind. He found his non-conservative models gave better results compared to observed systems on the the period–mass ratio and luminosity–mass ratio planes.

Given a close binary star which will undergo case B mass transfer its evolution can, in its essentials, be studied using the method of Kippenhahn and Weigert (1967), provided that the expansion of the secondary is not too great. This is usually the case for primary masses less than about $16\,M_\odot$. In this case evolution of the binary is as follows.

The binary system will evolve as two separate main sequence stars until the primary has depleted the hydrogen in its core sufficiently for core hydrogen fusion to cease. Hydrogen burning will continue in a shell around the core and the star's outer layers will expand. When the outer layers reach the critical radius, mass transfer will begin. Assuming all the mass is transferred to the secondary ("conservative evolution") and that the orbital angular momentum is unchanged, the Roche lobe around the primary will shrink, and so more mass is transferred and so on until the mass ratio is reversed i.e. the primary is now the less massive star. At this point further mass transfer will result in an increase in the size of Roche lobe around the primary and so this phase of mass transfer stops. The time scale for this rapid mass transfer (RMT) is extremely short and is found to be of the order of the Kelvin - Helmholtz or thermal time scale:

$$t_{K-H} = \frac{GM_1^2}{R_1 L_1} = 3.1 \times 10^7 \text{years} \frac{M^2}{RL} \tag{1.4}$$

M, R, L all in Solar units.

Since this time scale is short this phase of binary star evolution should be rarely seen. However, examples do exist, notably β Lyrae. The further evolution of the system will depend upon the nature of the remnant of the primary. If the initial mass of the primary was greater than about $3\,M_\odot$ then the remnant will have started helium burning in its core before RMT. Once RMT is complete we are left with a main-sequence secondary and a helium burning

primary. This situation looks similar to a Wolf-Rayet star. For initial primary masses below $3\,M_\odot$ the remnant will have a degenerate helium core and a hydrogen burning shell. This means that the outer layers of the star are still expanding and so mass transfer is still going on, but at a much lower rate than during RMT. This is a classical Algol system. This phase of slow mass transfer will continue until either helium ignition occurs, which causes the star to shrink, or the hydrogen burning shell can no longer support slow mass transfer. This will occur once the star reaches a radius given by:

$$\log \frac{R_{max}}{R_\odot} = C + 5.3 \log \frac{M}{M_\odot} \tag{1.5}$$

where $3.6 < C < 4.1$ depending on composition and the mixing length parameter.

This is the standard scenario for the evolution of classical Algol systems i.e. that they are the remnants of case B RMT undergoing a phase of slow mass transfer. However this explanation is insufficient to account for specific systems since it neglects the effects of mass loss which, as Popper showed for AS Eri, must be taken into account in order for case B evolution to produce Algol systems from reasonable initial periods and masses.

Also it is clear that case B may not be the only way of producing Algol type systems. Packet & De Greve (1990) modelled eight systems with primary masses $3\,M_\odot$ and $5\,M_\odot$ and mass ratios 0.7 and 0.9 with periods in the range 0.74 days to 1.62 days. The periods were chosen to give case A evolution which started mass transfer at 50% and 75% of the core hydrogen burning phase. The system of initial masses $5\,M_\odot$ and $4.5\,M_\odot$ and with initial period 0.95 days is discussed in particular. This system undergoes a mass ratio reversal following a phase of relatively slow mass transfer during which the secondary (gainer) hardly changes its radius. This is followed by a long-lived phase of slow mass transfer before the accelerated nuclear burning in the core of the secondary causes a further case A mass ratio reversal in the opposite direction. This is followed by another phase of slow mass transfer before the system eventually evolves into contact. The situation is similar for the other systems studied. In general they conclude that an Algol system is a candidate for case A evolution if:

1. its period is in the range 1.2 to 2 days,
2. its mass ratio is in the range 1.2 to 3,
3. both components lie near the main-sequence in the mass-luminosity diagram, the HR diagram and the mass-radius diagram.

Tout & Eggleton (1988) showed that the effects of stellar wind mass loss are also important when studying late case B evolution i.e. RMT starts when the primary is at the base of the Red Giant Branch on the HR diagram. If the effects of stellar wind mass loss are neglected,

we find that RMT starts when the primary has developed a deep convective envelope. In this case the process of mass transfer occurs on a hydrodynamical time-scale ($\sim$ 10-1000 years). This rate of mass transfer will lead to common envelope evolution probably resulting in either planetary nebula ejection and a short period system (P$\sim$ 0.5 days) or coalescence and a fast rotating single red giant star. However, there are observed Algol systems with orbital periods and masses which suggest they must have undergone late case B evolution. The authors resolve this paradox by considering the mass loss due to an enhanced stellar wind, similar to those seen in RS CVn systems, where the stellar wind is enhanced by the the tidal or other interactions due to the star's companion by a factor of about 100. In this scenario the mass loss may be sufficient to reduce the the mass ratio to below its critical value of about 0.7 in which case when Roche lobe over-flow (RLOF) does occur, it will be on a slow time scale and so the system looks like an Algol system. The mass loss may even be sufficient to prevent the primary ever filling its Roche lobe in which case it will evolve into a white dwarf of unusually low mass (0.3 $M_{\odot}$compared to >0.6 $M_{\odot}$ for single white dwarfs). The mass loss may of course not be enough to prevent mass loss on a hydrodynamical time scale. Evolutionary models are presented for each case using a crude estimate of the mass loss due to the stellar wind (assumed to be lost from the system) for components with initial masses of $2\,M_{\odot}$ and $1.818\,M_{\odot}$. The system with an initial orbital period of 10 days evolves into an Algol system as described above with an orbital period at the start of slow mass transfer of 19 days and a mass ratio q=0.52. The evolution is followed though the phase of slow mass transfer until the primary becomes a white dwarf, by which time the secondary has a mass of 2.41 $M_{\odot}$ and the period has increased to 148 days.

1.7 Overview of thesis

The evolutionary scenario above for the evolution of classical Algol systems is only correct insofar as it adequately describes the basic features of EA2 type systems i.e. a main-sequence star with a less massive subgiant companion. However as De Greve(1989) points out we can only be sure that the model is correct if we study individual systems to see whether or not evolutionary models exist which satisfactorily explain the current state of the system. In particular the following problems need to be addressed:

1. The assumption of conservative mass transfer is clearly unrealistic and the manner in which it affects the evolution of the system needs to be investigated.
2. It is not clear that the scenario above is the only way of forming a classical Algol system
3. The extent to which actual systems conform to our standard picture of them needs to be investigated; for example,whether the assumptions of circular orbits and synchronous

rotation are justified.

4. The slow mass transfer phase has associated with it such phenomena as equatorial bulges, gas streams and accretion discs which are worthy of study in their own right.

The increase in sophistication of evolutionary models needs a complementary increase in the sophistication of the observational techniques used to study actual systems. This is being achieved both by increasing the number of systems observed and by using better quality data from larger telescopes and more sensitive detectors. These higher quality data require the use of more elaborate analyses such as cross-correlation for spectroscopic data along with accurate light-curve synthesis codes. Used together these methods can provide absolute parameters with accuracies of a few percent.

As a continuation of the work already done at St. Andrews and elsewhere to provide accurate absolute parameters for close binary systems we have used the cross correlation method to derive spectroscopic orbits based on Reticon and CCD spectra for both components of six known or suspected Algol systems in the period range 0.5–3 days. We also present light curve solutions for all six systems and thus obtain absolute parameters for the six systems consistent with both the photometric and spectroscopic data including the non-Keplerian distortions to the radial velocity measurements. This work has been aided by the use of the Doppler tomography technique (Bagnuolo & Gies, 1991) which has been developed and extended to cope with the particular problems associated with extracting the individual spectra from composite spectra of Algol systems. We have also derived a simple method for correcting the observed colours of the primary star for the presence of the secondary.

For five of the systems considered the data are of sufficient quality for accurate absolute parameters to have been derived. The precision of the absolute parameters varies but the masses and radii presented have uncertainties of a few percent. For the best cases the precision is comparable to the precision obtained for less complicated detached systems (1–2%).

The observations and data reduction are described in Chapter 2. These six systems are discussed individually in Chapters 3-8. In particular we have concentrated on deriving reliable absolute parameters for these systems using published photometry and the light-curve synthesis program LIGHT2. The evolutionary status of most of these systems and other well studied Algols systems is discussed in Chapter 9.

Bagnuolo W.G., Gies D.R., 1991. ApJ, **376**, 266.

Benson, R.S., 1970. PhD Thesis, Univ. California, Berkeley.

Berrington R.C., Hall D.S., 1994. AJ, **107**, 1868.

Biermann P., Hall D.S., 1973. A&A, **27**, 249.

Budding E., 1984. C.D.S. Bull., **27**, 91.

Budding E., 1989. Algols, Batten A.H..Kluwer Academic Publishers, Dordrecht205

Crawford J.A., 1955. AJ, **121**, 71.

Etzel P.B., 1988. In: New directions in spectrophotometry, p.79, Philip A.G.D., Hayes D.S., Adelman S.J. (ed.), L. Davies Press, Schenectady NY.

Flannery B.P., Ulrich R.K., 1977. ApJ, **212**, 533.

Frank J. King A.R., Raine D.J., 1992. Accretion Power in Astrophysics, C.U.P..

Giménez A., Garcia J.M., 1990. In: Active Close Binaries, p.121, İbanoğlu (ed.), Kluwer Academic Publishers, Dordrecht.

Goodricke, J., 1783. Phil. Trans. Roy. Soc., **73**, 474.

De Greve J.P., 1985. A&A, **142**, 367.

De Greve, J.P., 1989. In: Algols, p.127, Batten A.H. (ed.), Kluwer Academic Publishers, Dordrecht.

De Greve J.P., 1993. A&AS, **1993**, 97.524

Hill G., 1993. Proc. Coll. Seoul ,Nov 1990, in press.

Hellings, 1983. Astrophys. Spa. Sci., **96**, 37.

Hoyle F., 1955. Frontiers of Astronomy, Wm Heineman,London.195-202

Hubeny I., 1989. In: Algols, p.117, Batten A.H. (ed.), Kluwer Academic Publishers, Dordrecht.

Iben I. Jnr., 1965a. ApJ, **142**, 1447.

Iben I. Jnr., 1965b. ApJ, **143**, 483.

Iben I. Jnr., 1966a. ApJ, **141**, 993.

Iben I. Jnr., 1966b. ApJ, **143**, 505.

Iben I. Jnr., 1966c. ApJ, **143**, 516.

Jedrzedec, E., 1969. Msc Thesis. Warsaw Univ.

Joy. A.H., 1941. PASP, **54**, 35.

Kaitchuck, R.H., 1989. In: Algols, p.23, Batten A.H. (ed.), Kluwer Academic Publishers, Dordrecht.

Kippenhahn R., Kohl K., Weigert A., 1967. Z. Astrophys., **66**, 58.

Kippenhahn R., Meyer-Hofmeister, 1977. A&A, **54**, 539.

Kippenhahn R., Weigert A., 1967. Z.Astrophys, **65**, 251.

Kuiper G.P., 1941. ApJ, **93**, 133.

Kołb U., Ritter H., 1990. A&A, **236**, 385.

Kruszewski, 1963. Acta Astron., **13**, 106.

de Loore C., De Greve J.P., 1991. A&AS, **594**, 453.

Lauterborn, D., 1970. A&A, **7**, 150.

Levine R.H., 1981. In: Solar Phenomena in Stars and Stellar Systems, p.235, Bonnet R.M., Dupree A.K. (ed.), Reidel.

Lubow, S.H. and Shu, F.H., ApJ. 1975, **198**, 383.

Morton D.C., 1960. ApJ, **132**, 146.

Neo, S., Miyaji, S., Nomoto, K.and Sugimoto, D. , 1977. Publ. Astron . Soc. Japan, **29**, 249.

Packet W., De Greve, J.P., 1980. A&A, **230**, 97.

Paczynski, B., 1971. ARA&A, **9**, 183.

Paczynski, 1967. Acta Astron., **17**, 355.

Pastetter L. and Ritter, H., 1989. A&A, **214**, 186(PR).

Peters, G.J., 1989. In: Algols, p.23, Batten A.H. (ed.), Kluwer Academic Publishers, Dordrecht.

Plavec, M., 1958. 8th Liege Coll.', **20**, 411.

Plavec, M., 1970. PASP, **82**, 957.

Plavec, M., 1967. In: On the evolution of double stars, p.84, J.Dommanget (ed.), Belgium.

Popper D.M., 1989. ApJSS, **71**, 595.

Refsdal, S., Roth, M.L., Weigert A., 1974. A&A, **36**, 113.

Sarna M.J., Fedorova A.V., 1989. A&A, **208**, 111.

Smak, J., 1989. In: Algols, p.107, Batten A.H. (ed.), Kluwer Academic Publishers, Dordrecht.

Söderhjelm S., 1980. A&A, **89**, 100.

Struve, O., 1948. Ann. Astrophys., **11**, 117.

Tout C.A., Eggleton P.P., 1988. ApJ, **334**, 357.

Ulrich, R.K., Berger, H.L., 1976. ApJ, **206**, 509.

van Hamme, W., Wilson, R.E., 1990. AJ, **100**, 1981.

Vogel, H.C., 1889. Sitzungsber. Prüss. Akad.. p. 1045

Walter, K., 1931. Veröff. Königsberg Sterw., **2**.

Wood, F.B., 1950. ApJ, **112**, 196.

Yungelson L.R., 1973. Sov. Astron. AJ, **16**, 864.

Yungelson L.R., Tutukov A.V., Fedorova A.V., 1989. In: Algols, p.141, Batten A.H. (ed.), Kluwer Academic Publishers, Dordrecht.

Chapter 2

Observations and Reductions

2.1 Introduction

In this chapter we describe the instruments used to obtain the spectrographic material used in this study and discuss the methods used to reduce the spectra and derive the spectroscopic orbits. The spectroscopy presented in this study comes from three sources. The spectroscopic orbits for RZ Cas, AT Peg and TX UMa are based on spectra obtained with the Dominion Astrophysical Observatory's (DAO) coudé spectrograph on the 1.2m telescope. Spectroscopy obtained using the intermediate dispersion spectrograph (IDS) attached to the 2.5m Isaac Newton telescope (INT) on the island of La Palma was used to derive orbits for AF Gem and RU UMi. For HU Tau observations obtained at the DAO were used in conjunction with spectra obtained at the St Andrews University Observatory using the Richardson-Brealey spectrograph (RBS) attached to the 0.5m Leslie Rose telescope (LRT).

2.2 The Dominion Astrophysical Observatory 1.2m coudé spectra

The spectroscopic observations obtained at the DAO described here were generously provided by Dr Graham Hill. They were obtained as part of a much larger programme to study spectroscopic binaries with poorly determined orbits – specifically those that appear in the *Seventh Catalogue of the Orbital Elements of Spectroscopic Binary Systems* (Batten et al., 1978) with orbits rated 'c–e'. The data were provided in the form of spectra linearized in wavelength, $0.3 Å pxl^{-1}$ over the spectral range $\lambda\lambda$4000-4510Å with a typical S/N ratio for the spectra of $\sim$ 50–100 and a resolution measured from the FWHM of an arc line of 0.9Å. The spectra required rectification

prior to analysis with VCROSS(Hill, 1982; Hill & Fisher, 1986) in the cross-correlation process. For AT Peg and RZ Cas the spectra were rectified using REDUCE(Hill, 1982; Hill & Fisher, 1986) by dividing the spectrum by a smooth function fitted through manually selected regions of continuum. For the other systems the spectra were rectified using PRESS, an automatic routine described in Appendix A. A discussion of the relative merits of the two methods can also be found therein.

2.3 The Isaac Newton Telescope IDS spectra

Following an application for telescope time we were awarded seven nights (4–10 February 1993) at the Observatorio Roque de los Muchachos to use the intermediate dispersion spectrograph (IDS) on the 2.5m Isaac Newton telescope (INT). The 500mm camera and Jobin-Yvon R1200B grating were used to give a dispersion of $16.7 \text{Å}\,\text{mm}^{-1}$. The detector used was an EEV CCD detector which gave a wavelength coverage ≈ 500 Å. All spectra were centered on 4275Å and a window 100 pixels wide ($\cong 30''$) in the spatial direction was used. Integration times were 1000s and a thorium-argon arc was observed before and after every observation of a star. Three nights were lost due to poor weather and a further half night due to instrument failure. The slit width was chosen such that one slit width projected onto two pixels at the detector to give adequate sampling of the spectra, although a few spectra of AF Gem were obtained with a slightly wider slit. The seeing was generally very good (less than $1''$). While this is good for the efficiency of the spectrograph it did cause problems with the measured radial velocities of brighter stars. This is simply a consequence of image motion within the slit during the shorter exposures used for these stars causing an error in the measured radial velocity. We do not expect the spectra of the program stars to be affect in this manner because the longer exposure times and the use of an auto-guider should have provided uniform illumination of the slit. We estimated the resolution of the spectra by measuring the average full-width half-maximum (FWHM) of the lines in a typical arc and found a value of 0.88Å (1.05Å for the AF GEM spectra obtained with a wider slit).

Preliminary reductions of the CCD images were made via the STARLINK package FIGARO (Shortridge, 1987). Bias subtraction was achieved by forming a normalised median bias map for each night from between 5 to 10 exposures of 0 seconds. This image was then subtracted from every other image taken that night using the median value in the overscan region to set the bias level for that image. Flat-field images were obtained each night using a tungsten lamp. A master flat-field was formed for each night by forming the median image of all the flat fields obtained during the same night. The spectral response of the instrument to the tungsten lamp was removed by extracting the spectrum of the response across the entire image, smoothing this spectrum, and dividing the master flat-field row-by-row by this smooth function. All other

images taken on the same night were then divided by this master flat-field to correct for small scale variations in sensitivity. The removal of cosmic ray events was done automatically using the routine BCLEAN which searches for these events by comparing each pixel to the mean value in neighbouring pixels. We chose parameters such that any pixel that exceeded the mean value in its neighbours by 10σ and at least 500 counts was considered to be a cosmic ray event and was "patched" by setting its value to the mean value of the neighbouring pixels. There were typically about 10 such events in an exposure of 1000s.

The underlying night sky spectrum was subtracted from the images using the routine POLYSKY and we then used optimal extraction routines of Horne (1986) to convert the two dimensional images into one dimensional spectra. This provides a higher signal-to-noise ratio for the resulting spectrum than simple addition in the spatial direction, particularly for faint images. This is achieved by first using the routine PROFILE to form normalised profiles of the image in the spatial direction. The intensity of the star in each spectral element is then determined using the routine OPTEXTRACT, which forms the sum of the pixels in the spatial direction weighted by the value of the profile at that point. This enables all of the light collected to be used without increasing the noise in the final spectrum due to faint pixels at the edge of the image. The spectra were then linearized in wavelength, $0.373\text{Å}\,\text{pxl}^{-1}$ over the spectral range $\lambda\lambda$4035–4495Å. The use of a thorium-argon arc caused some problems since there are a large number of lines due to thorium which were not resolved at the dispersion used. This made measurements of the wavelength of most lines unreliable. From the hundreds of lines in the spectrum only 12 lines were found to give reliable wavelengths. Deviations from a standard plate were fitted using a fifth order polynomial (although a linear fit would have been adequate), the error associated with the fit was generally 0.6-0.8μm.

2.4 The Leslie Rose RBS spectra

HU Tau was observed extensively during the winter of 1992-93 and few spectra also obtained during the following season using the Richardson-Brealy spectrograph (RBS) attached to the 0.5m Leslie Rose Telescope (LRT) with a Reticon diode array detector (Edwin, 1989). A 1800 lines/mm grating is used to give a dispersion of approximately $25\text{Å}\,\text{mm}^{-1}$. The pixel size on the detector is 15μm which is well matched to a fixed slit width of 3" on the sky i.e. the projected slit width corresponds to two pixels at the detector. The slit width is also well matched to the typical seeing at St Andrews. By measuring the mean FWHM of lines in an arc we find that the resulting spectra have a resolution of 0.9Å at 4500Å.

An LED within the spectrograph directly illuminates the detector. This enables flat field images to be obtained to allow for small scale variations in sensitivity across the detector. In

general one or two flat field images were obtained on each clear night. These showed little sign of variation from night-to-night and so normalised median flat field images were formed for each month's observations using all the flat field images obtained during that month. Pixel-to-pixel variations from month-to-month were found to be constant to within a few tenths of a percent. All spectra were divided by the appropriate flat field image before further use.

Observations of all stars is accompanied by the observation of a copper argon arc for wavelength calibration. The FIGARO routine ARC was used to first identify a few prominent lines and to then automatically find other identifiable lines in a typical spectrum. Approximately 50 lines were found in a 700Å interval around 4300Å. The resulting line list was then used in the wavelength calibration of subsequent spectra within REDUCE. Deviations from a standard plate were fitted using a fifth order polynomial and the mean error associated with the fit was $0.86 \pm 0.1\mu$m.

2.5 Radial velocity measurements

To measure the radial velocities of both components of the Algol systems studied we used the cross-correlation technique (CCT) in the form of the program VCROSS. The use of the CCT is now well established in various forms all of which use a template spectrum to measure the radial velocity of a program star by comparing the two spectra at a range of relative velocity shifts. It is clear that if the template spectrum is similar to the program star's spectrum then the two spectra will correspond when the induced relative velocity shift is equal in size but opposite in sign to the actual relative velocity shift. The implementation of this technique can be done in hardware as in Griffin's (1967) highly successful photoelectric radial velocity spectrometer and subsequent similar instruments in which a spectrum is imaged onto a negative template spectrum in the form of a mask. The amount of light produced by this combination is measured by a photomultiplier for a range of shifts in the mask's position. A dip in the amount of light detected is observed when the two spectra correspond and the radial velocity is then simply found from the mask's position. This form of cross-correlation works best for slowly rotating late-type stars where the large number of narrow lines produce extremely reliable radial velocities.

The mathematical basis for the software implementation of the CCT is the cross-correlation function (CCF):

$$\mathrm{CCF} = \int_{-\infty}^{\infty} f(t)g(t+T)dt$$

This is simply a measure of the similarity of two functions f and g as a function of a relative shift T. If for the two functions f and g we adopt two spectra with logarithmic

wavelength scales we find that the effect of the Doppler shift is uniform in wavelength i.e. :

$$T = \log \lambda_1 - \log \lambda_0 = \log(1 + v/c)$$

For digital spectra and fast Fourier transforms (FFTs) this results in the following expression for the Lth point of the CCF:

$$C_I(z_L) = a(M \cdot I)^{-1} \sum_{J=1}^{M} G(f_J) T(-f_J) e^{2\pi i f_J z_L}$$

where :

$C_I(z_L)$ is the Lth point of the CCF for a radial velocity shift z_L,

$G(x_i)$ is the digital program spectrum of size N described below,

$T(x_i)$ is the digital template spectrum of size K described below,

$$J = \begin{cases} N & \text{if } (K-L) \geq N \\ (K-L) & \text{if } (K-L) < N \end{cases}$$

$$I = \begin{cases} N & \text{if } (K-L) \geq N \\ (K-L) & \text{if } (K-L) \leq N \end{cases}$$

In order to produce a good peak in the CCF the spectra must be linearized and rectified. Rectification removes effects due to low order components of the FFT. To avoid problems associated with the finite length of the data set the spectrum is extended by 20% at each end by adding a cosine function that runs from the last data point to the mean level of the spectrum. These are then the functions G and T used in the expression above.

In practice the user of VCROSS can ignore much of the above and simply supply the program with two spectra and a file which describe the regions of the spectra and the range of radial velocity shifts for which the cross-correlation is to be performed. The program will then calculate the CCF and a range of options are then possible. Usually the resulting CCF is plotted and the user can use a variety of methods to measure the function. There is a choice of three analytical functions; parabolic, Lorentzian and Gaussian. These can be fitted individually to a single peak. It is also possible to form a standard profile by storing a measured CCF or by producing theoretical profiles and using these in subsequent measurements. Alternatively, two or more of these functions can be fitted simultaneously to selected regions of the CCF. This feature is particularly useful for binary systems where the peaks due to each component are blended. The use of VCROSS to measure radial velocities for different types of binary stars and the techniques employed are discussed in more detail by Hill (1993). The template stars and regions of spectrum used in this study are described individually for each system in subsequent chapters. The measured radial velocities were used to determine the spectroscopic orbits using

the program RVORBIT (Hill, 1987). In general, two solutions are presented for each system, "uncorrected" and "corrected". The first solution is simply the solution of the spectroscopic orbit for the measured radial velocities. The need for correcting this orbit and the method employed is discussed below.

2.6 The light curves, their solutions and the radial velocity corrections

The absolute parameters for the six systems studied were derived using the spectroscopic orbit in combination with the solution of published light curves. To derive these solutions we used the program LIGHT2 (Hill, 1979; Hill & Rucinski, 1993). It is particularly important in Algol systems to determine the mass ratio of the system spectroscopically since the size and the shape of the secondary component is constrained by the Roche lobe which is determined by the mass ratio. However the calculation of the mass ratio is also dependent upon the solution of the light curve. This is because we must include the effects of the ellipticity of the components, the rotation of the components during eclipse (Rossiter effect), and the mutual heating of the components (reflection effect). These effects result in the center of light not being coincident with the center of mass for a star in a close binary system. These effects produce radial velocities that cannot be described by a simple Keplerian orbit and so the corrections for these effects that must be applied are often called "non-Keplerian corrections". The radial velocities of the secondary components of Algol systems are particularly susceptible to these effects. They are noticeably non-spherical and the hemisphere facing the hotter component is heated by several hundred degrees. The combination of these effects is sufficient to produce differences between the observed and actual radial velocities of as much as 10%.

The calculation of these corrections is done within LIGHT2 by assuming that the spectral lines produced at each integration point are Gaussians with the width matched to the resolution of the spectrograph used. The intensity weighted mean over the visible surface of the star of these profiles shifted by the projected rotational velocity at each point is then formed to produce a theoretical profile. It is possible to fit these profiles directly to the CCF within VCROSS but for the systems studied here the peaks in the CCF due to the secondary component were generally too weak and the corrections for the primary too small to warrant producing separate profiles for each CCF. The corrections for both components were simply applied by taking the intensity weighted mean of the projected rotational velocity at each integration point. The typical size of these corrections are less than $1\,\mathrm{km\,s^{-1}}$ for the primary and 10-$20\,\mathrm{km\,s^{-1}}$ for the secondary.

The solutions to the light curves are discussed individually for each system in subsequent chapters.

Batten A.H., Fletcher J.M., MacCarthy D.G., 1989. Publ. Dom. Astrophys. Obs., **17**, 1.

Edwin R.P., 1989. The Observatory, **109**, 173.

Griffin R.F., 1967. ApJ, **148**, 465.

Hill G., 1979. Publ. Dom. Astrophys. Obs., **15**, 297.

Hill G., 1982. Publ. Dom. Astrophys. Obs., **16**, 59.

Hill G., 1987. RVORBIT user's manual, internal publication of the Dom. Astrophys. Obs.

Hill G., 1993. In: New frontiers in binary star research, p.38, Leung J.C. and Nha, I.-S. (ed.), Korea.

Hill G., Fisher W.A., 1986. Publ. Dom. Astrophys. Obs., **16**, 193.

Hill G., Rucinski S.M., 1993. In: Light curve modeling of eclipsing binary stars, p.135, Milone E.F. (ed.), Springer-Verlag, Berlin.

Hill G., Fisher W.A., Poeckert R., 1982. Publ. Dom. Astrophys. Obs., **16**, 43.

Horne K., 1986. PASP, **98**, 609.

Shortridge K., 1987. Starlink FIGARO users guide, Rutherford Appleton Laboratory.

Chapter 3

RZ Cassiopeiae

3.1 Introduction

RZ Cassiopeia is a bright, short-period, Algol system with deep, fast eclipses ($V_{max}=6^m.2$, P=1.195 days, $V_{min}=7^m.9$, D=5hrs). These properties make it ideal for photometric study and many times of primary minimum have been published. The period variations of RZ Cas have been studied in some detail by several authors but most recently by Hegedüs et al. (1991) who found some evidence for periodicity in the period changes and raised the question of apsidal motion again. Other notable studies are those of Herczeg & Frieboes-Conde (1974) and Hall et al. (1976), who used its exceptionally well defined O-C curve as a test of the Biermann-Hall hypothesis (Biermann & Hall, 1973; Hall, 1975) namely, that the observed variations in times of minima about a linear ephemeris are due to mass transfer episodes between the two components of a binary. Some evidence for this hypothesis is presented in this chapter.

The light curve near primary minimum of RZ Cas is notable for its instability. Although RZ Cas is a partially eclipsing system, several workers have found a flat bottom to primary minimum with varying durations of up to 22 minutes. A recent example can be found in Nakamura et al. (1991), who present photometry in seven colours of one primary minimum with a flat bottom lasting 14 minutes. Olson (1982) describes these and other disturbances to the light curve and presents multi-colour photometry which is shown to be consistent with the hypothesis of hot and cool spots on the surface of the primary component.

For such a bright system, spectroscopic studies are surprisingly rare. Batten et al. (1989) cite only three, that of Duerbeck and Hänel (1979) being the most recent. They present a radial velocity curve for the primary component and find from the metallic lines a circular orbit and a spurious eccentricity from the hydrogen lines, indicative of circumstellar material.

Chambliss (1976) presents complete light curves in three colours (approximately UBV) together with solutions by three methods (Russell-Merrill, Kopal-Jurkevich and Wood). Hegedüs et al. also present light curves (BV) and solve for the absolute parameters using Kopal's frequency domain method. RZ Cas is also a radio source (Drake et al., 1986; Umana et al., 1991) and an X-ray source (Schmitt et al. 1990).

In this study we use new spectroscopic data to derive directly and for the first time a reliable mass ratio for RZ Cas. Ultraviolet spectra and *uvby* photometry are used to establish the effective temperature of the primary. DDO photometry is presented which appears to show composition anomalies in the secondary component. The light curves of Chambliss are solved with the new mass ratio.

3.2 Spectroscopic observations and reductions

3.2.1 Observations

The spectroscopic observations by GH included here were made between 1985 and 1992 with the Dominion Astrophysical Observatory's coudé spectrograph on the 1.2m telescope. Details of the observation and reduction can be found in Chapter 2. To derive the primary radial velocities the cross correlation functions (CCFs) of the spectra were measured by fitting Gaussian profiles by least squares. The template spectrum was that of 72 Oph (HD 165777,A4IVs). The radial velocity of 72 Oph was measured from the CCF using Vega as a template (rv=$-14\pm1.5\,\mathrm{km\,s^{-1}}$, Khalesseh and Hill, 1991) and was taken to be -34.4$\mathrm{km\,s^{-1}}$. For the secondary component the template spectrum was that of HD 154417, a standard radial velocity star (rv=$-17.4\pm0.3\,\mathrm{km\,s^{-1}}$, G0V). A 40Å window around the hydrogen lines was excluded from the cross correlation process since their great width broadens the CCF intolerably.

3.2.2 RV measures from Gaussian profiles

The CCFs produced with 72 Oph as a template showed a large peak corresponding to the primary which, for most spectra, was well represented by a Gaussian profile. The exceptions were those spectra in which the primary and secondary peaks were blended and spectra which showed asymmetric peaks. Whenever the secondary peak was visible it was also measured using a Gaussian profile and the overall fit was then very good. The asymmetric peaks pose more of a problem. It should firstly be noted that the asymmetry is not due to blending between the primary and secondary peaks since the asymmetry took the form of a broad wing on the opposite side of the primary peak to the expected position of the secondary peak. This is

demonstrated in Fig. 3.1 and Fig. 3.2. Indeed, the secondary peak was occasionally well seen in spectra showing an asymmetry in the primary peak. For the purposes of deriving the radial velocity the peak was measured using the sum of two Gaussian profiles, one for the primary peak and one to account for the presence of the wing. This produced a much better fit to the CCF and gave radial velocities which looked more realistic as judged by eye from the maximum of the CCF. The cause of these asymmetries will be discussed later. It should be noted that all the various methods used to measure the primary radial velocities and solve for the primary semi-amplitude gave similar results.

The CCF produced with HD 154417 as a template again showed a large peak corresponding to the primary as well as a smaller peak corresponding to the secondary. The weakness of this latter feature as well as its position in the wings of the primary peak make measurements difficult. It is particularly important to find a profile which accurately matches that of the primary peak in the wings. This was achieved by producing a synthetic profile taken from the CCF of Vega against a spectrum of Vega which was then convolved with a rotational broadening function to match the rotation of the primary component of RZ Cas. The CCF was then measured using the synthetic profile to represent the primary peak and a Gaussian profile for the secondary peak.

The non-Keplerian effects and rotational distortions are expected to be quite large for the secondary. In previous work these corrections have been neatly accounted for by using synthetic profile fitting (Hill & Rucinski, 1993). However the peaks in the CCFs for the secondary were too small to use this method and so these corrections have simply been applied in terms of a velocity shift at each phase calculated from the intensity weighted mean of the projected rotational velocity over the visible surface of the star. No attempt has been made to fit synthetic profiles to the primary CCF since the Gaussian profiles are quite adequate and non-Keplerian effects for the primary are found to be small ($< 0.3\,\mathrm{km s^{-1}}$) for all phases used in this study.

3.3 Spectroscopic results

Although the photometric and spectroscopic results are presented separately, it is to be emphasized that the two are by no means independent. A process of iteration has been employed whereby preliminary results from one are used to find approximate results in the other until a solution is found that is consistent with all the data.

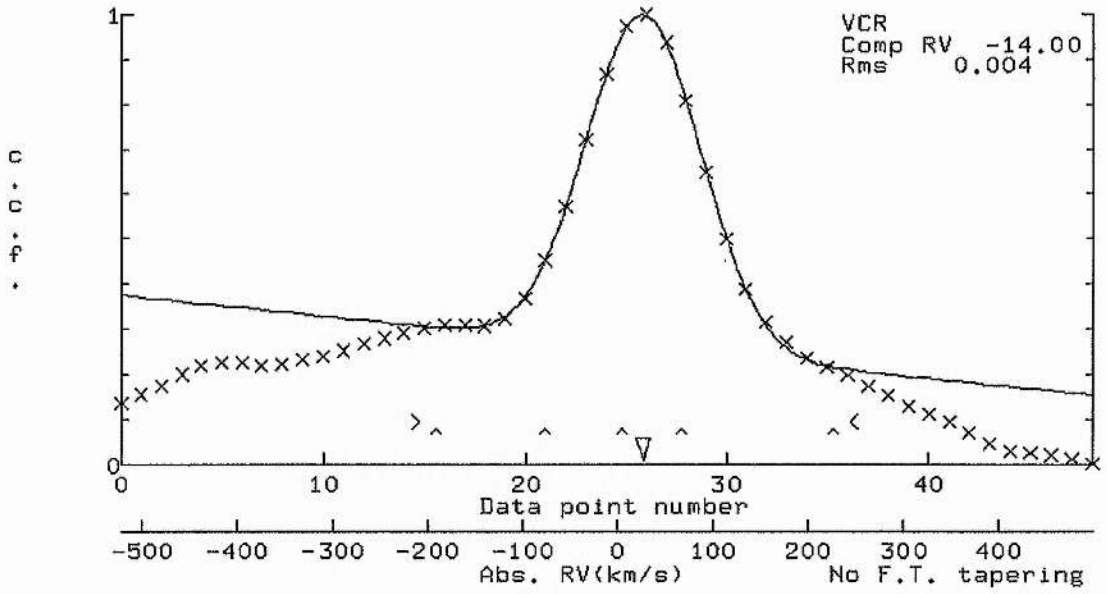

Figure 3.1: Symmetric CCF of RZ Cas v. Vega

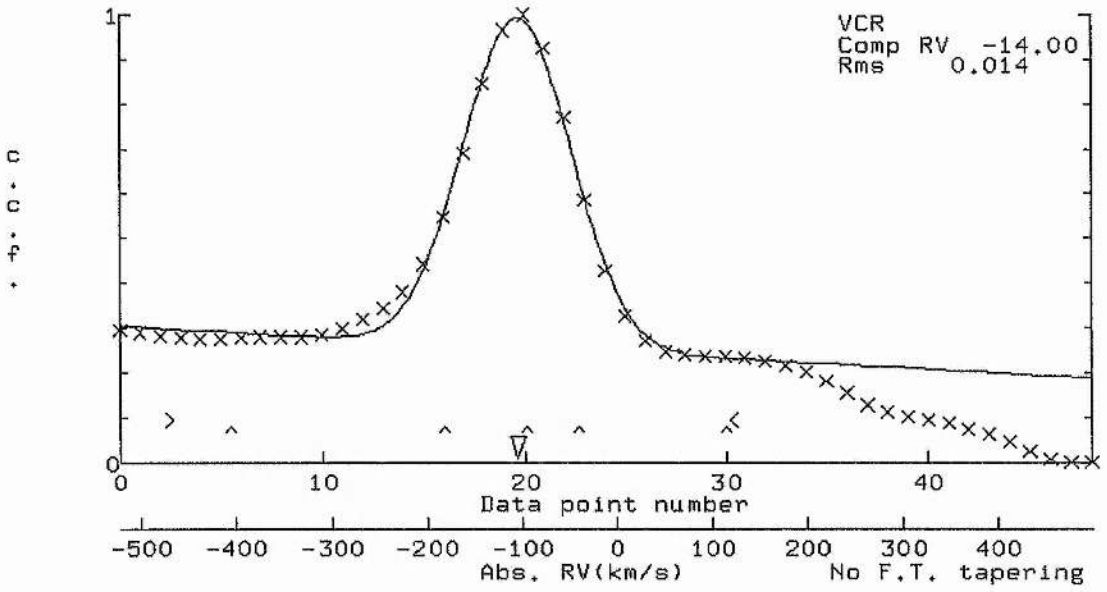

Figure 3.2: Asymmetric CCF of RZ Cas v. Vega

3.3.1 Orbit

The radial velocity measurements for the primary and secondary components are shown in Table 3.1. A period jump of RZ Cas caused some problems in our attempts to solve for the orbit since the radial velocity data span this jump which is, unfortunately, not well covered by observations. We therefore decided to leave the period and time of maximum positive velocity (T_+) as well as the semi-amplitude and the systemic velocity as free parameters in the least-squares solution of the orbit. Solutions for the primary's orbit were attempted with the eccentricity as a free parameter but these showed the eccentricity to differ negligibly from zero. The adopted, uncorrected primary spectroscopic orbit is shown in Table 3.2 together with previously published orbits. The spectroscopic orbit of the secondary was solved independently in a similar fashion, the systemic velocities of the two solutions providing a check on the methods used. The solution is also shown in Table 3.2. The resultant combined spectroscopic orbit is presented in Table 3.3 under the heading "Uncorrected". Also shown in Tables 2 and 3 are spectroscopic orbits corrected for the ellipticity of the components, which introduces systematic errors (non-Keplerian effects). These are calculated from the solutions to the light curves described below as an intensity weighted mean of the projected rotational velocities. For RZ Cas the corrections to the radial velocities of the secondary component are between 5 and 10 $\mathrm{km\,s^{-1}}$ which are enough to alter the mass ratio by $\sim$ 5%. The corrections to the primary radial velocity are small ($< 0.3\,\mathrm{km\,s^{-1}}$) but are included for the sake of consistency. The corrected radial velocities and adopted solution are shown in Fig. 3.2.

3.4 Spectral types and colour indices

3.4.1 Primary component

The spectral type of the primary has been classified as A2V (Chambliss ,1976) and A3V (Duerbeck and Hänel, 1979). From our own analysis we find a spectral type for the primary of A3V.

Hilditch and Hill (1975) present Strömgren *uvby* data for RZ Cas at eight phases including six at or near primary eclipse. They list the colour indices (u-b), (v-b), (b-y) and the V magnitude. Given any two observations of a colour index at phases where the luminosity ratio of the two components differs, e.g. one observation at quadrature and one during primary eclipse, and given an estimate of the luminosity ratio in one of the filter bandpasses, we can solve for the colour indices of the individual components as follows.

Given observed colour indices at phases 1 and 2, $(x-y)_1$ and $(x-y)_2$, and the luminosity

Table 3.1: Measured radial velocities for RZ Cas in kms^{-1}. The phase is calculated from the ephemeris of Herczeg & Frieboes-Conde (HJD min I=2429875.6902 + 1.1952473)

HJD-2400000	Phase	Uncorrected		Corrected		
		RV_{pri}	RV_{sec}	RV_{pri}	RV_{sec}	Wt
45905.9524	0.6699	11.88	-245.4	12.11	-251.89	1
45906.9584	0.5115	-46.08	-48.5	-46.08	-30.45	0
45908.9713	0.1956	-120.47	126.6	-120.35	130.24	1
46327.0038	0.9412	-14.10		-24.63		1
46331.9704	0.0965	-82.12		-81.80		1
46367.8702	0.1320	-97.24		-96.94		1
46473.8016	0.7592	28.46	-240.8	28.57	-247.67	1
46473.8231	0.7772	26.91	-228.7	26.96	-234.35	1
46473.8450	0.7955	23.10	-227.1	23.08	-231.65	1
46473.8693	0.8158	19.53		19.43	-237.70	1
46473.8946	0.8370	20.41	-235.3	20.31	-216.63	1
46473.9189	0.8573	12.39	-214.8	11.72		1
46474.8182	0.6097	-2.44		-2.26		1
46474.8755	0.6576	12.23	-211.7	12.45	-217.42	1
46474.9137	0.6896	22.33	-214.4	22.55	-221.51	1
46475.6775	0.3286	-108.61		-108.83		1
46487.6584	0.3524	-103.49	152.4	-103.71	159.16	1
46488.5996	0.1399	-106.16		-105.87		1
46488.7826	0.2930	-112.18		-112.37		1
46668.0050	0.2388	-116.39	145.4	-116.44	151.44	1
46668.0099	0.2429	-117.77		-117.83		1
46685.8954	0.2068	-109.39	154.6	-109.32	158.79	1
46685.9235	0.2303	-111.51	170.3	-111.54	175.86	1
47065.9452	0.1743	-102.89	155.2	-102.70	157.68	1
47065.9758	0.1999	-107.64	156.4	-107.56	160.15	1
47101.9582	0.3045	-111.04	160.4	-111.26	168.12	1
47101.9700	0.3143	-110.22	154.9	-110.44	162.45	1
48929.9027	0.6486	8.2	-230.6	6.69	-235.53	1
48929.9190	0.6623	10.8	-230.0	11.15	-235.72	1

Table 3.2: The spectroscopic orbit of RZ Cas.Values in bold type are assumed, numbers in parentheses are errors in the final digits

	This Paper		Horak (1952)	Duerbeck & Hänel (1979)	
	Uncorrected	Corrected			
Primary					
$\gamma(\mathrm{km\,s^{-1}})$	-45.0 ± 0.7	-45.5 ± 0.7	40 ± 2	-45.5 ± 1.1	-46.6 ± 1.1
$K_p(\mathrm{km\,s^{-1}})$	71.2 ± 0.8	70.9 ± 0.8	68 ± 2	70.5 ± 1.4	70.1 ± 1.5
e	**0.000**	**0.000**	0.01 ± 0.03	0.024 ± 0.023	**0.000**
$\omega(^\circ)$	—	—	240 ± 160	87 ± 2	—
Period (days)	1.195249(13)	1.195254 (14)	N/A	**1.1952528**	**1.1952528**
$T_+ - 2440000$	7118.038(8)	7118.038(10)	N/A	**1396.3792**	**1396.3792**
Secondary					
$\gamma(\mathrm{km\,s^{-1}})$	-41 ± 3	-41 ± 4	—	—	—
$K_s(\mathrm{km\,s^{-1}})$	208 ± 4	213 ± 4	—	—	—
e	**0.000**	**0.000**	—	—	—
Period (days)	1.195227(11)	1.195228 (10)	—	—	—
$T_+ - 2440000$	7118.628(8)	7118.628(8)	—	—	—

Table 3.3: The combined spectroscopic orbit of RZ Cas

Parameter	Uncorrected	Corrected
$m_p \sin^3 i / \mathrm{M}_\odot$	2.07 ± 0.04	2.16 ± 0.07
$m_s \sin^3 i / \mathrm{M}_\odot$	0.71 ± 0.03	0.715 ± 0.02
$(a_p + a_s) \sin i / 10^6$ km	4.24 ± 0.06	4.68 ± 0.07
m_p / m_s	2.92 ± 0.065	3.02 ± 0.07

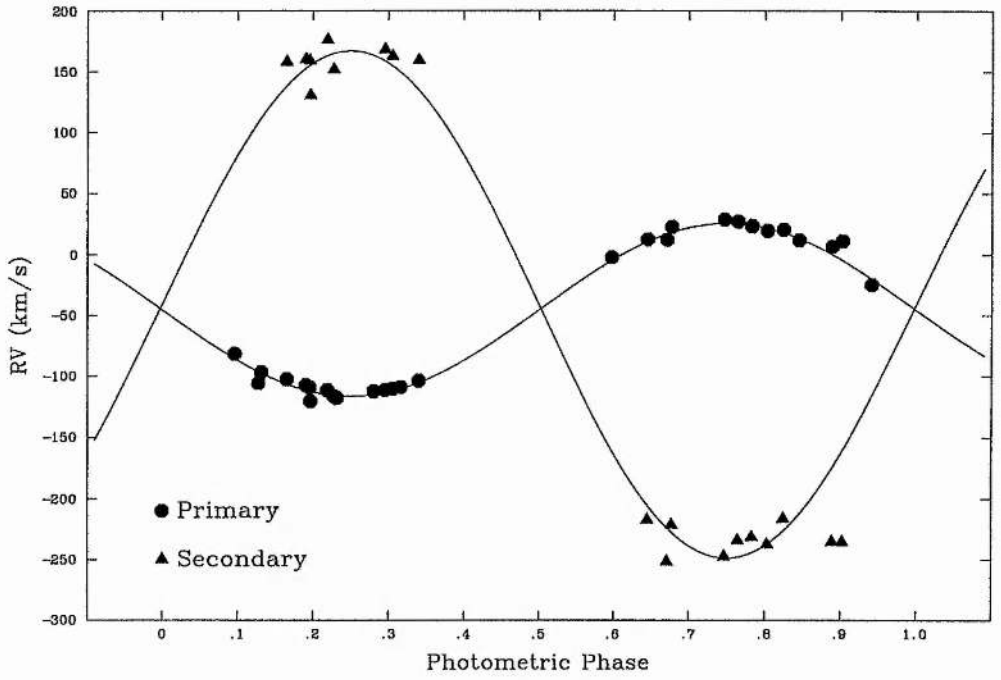

Figure 3.3: Radial velocity measurements of RZ Cas and the adopted spectroscopic orbit. The radial velocity measurements have been corrected for non-Keplerian effects

ratio of the two components in the y filter bandpass at the two phases, L_1 and L_2, the colour indices of the individual components, $(x-y)_{\rm pri}$ and $(x-y)_{\rm sec}$, are given by:

$$(x-y)_{\rm pri} = -2.5 \times \log\{[(1+L_2)10^{-0.4(x-y)_2} - (1+L_1)10^{-0.4(x-y)_1}]/(L_2-L_1)\} \qquad (3.1)$$

and

$$(x-y)_{\rm sec} = -2.5 \times \log\{[L_2(1+L_1)10^{-0.4(x-y)_1} - L_1(1+L_2)10^{-0.4(x-y)_2}]/(L_2-L_1)\}. \quad (3.2)$$

Clearly for small values of $L_2 - L_1$, small errors in the observed colour indices will translate into large errors in the solution; we therefore set a lower limit to $(L_2 - L_1/L_2 + L_1)$ of 1, i.e. the luminosity ratio must change by a factor of at least 2.

This can be repeated for all suitable pairs of observations and the mean value together with its standard deviation found. Note that the main source of error comes from the estimate of the luminosity ratio. The size of this error can be estimated by performing the calculation using estimates of the luminosity ratio in the both filter bandpasses. For our calculations we used the luminosity ratios generated by LIGHT2 with the adopted solution shown in Table 3.9 and black-body fluxes modified to produce realistic *uvby* fluxes. The results are shown in Table 3.4 with standard errors and the number of pairs used to solve for the colour index. The colours for the primary star are stable to within $0\overset{\rm m}{.}01$, those of the secondary to much more than this. We therefore consider only the primary in the subsequent discussion. Lester et al. (1986) provide

Table 3.4: Strömgren photometry of RZ Cas

Notes	$(u\text{-}b)$	n	$(v\text{-}b)$	n	$(b\text{-}y)$	n
l_p/l_s in x of (x-y):						
Primary	1.449 ± 0.009	11	0.223 ± 0.005	13	0.032 ± 0.003	13
Secondary	2.46 ± 0.09		1.09 ± 0.03		0.86 ± 0.02	
l_p/l_s in y of (x-y):						
Primary	1.445 ± 0.008	11	0.225 ± 0.004	13	0.034 ± 0.003	13
Secondary	3.08 ± 0.59		1.69 ± 0.16		1.03 ± 0.05	
Adopted primary values:	1.447 ± 0.008		0.224 ± 0.005		0.033 ± 0.003	

normalized $uvby\beta$ indices for various temperatures and compositions. Although the agreement with observations is occasionally poor, notably for A stars in the m_1 index, we are fortunate in that the indices are normalised so as to agree with five standard star observations, one of which is a normal A3V star. From the adopted colour indices shown in Table 3.4 we form the following indices: $(b\text{-}y)$=0.033 ± 0.003, $c_1 = 1.00 \pm 0.015$, $m_1 = 0.191 \pm 0.006$. Comparison with the theoretical indices computed for stars with various compositions shows the primary component of RZ Cas to be an unreddened A3V star with $T_{\rm eff} \simeq 8600K \pm 100K$,a surface gravity $\log g \approx 4.25$ and a composition similar to the Sun. (This is consistent with the results of Perry et al. (1982) who find that reddening is insignificant in all directions away from the Sun out to a minimum distance of 75pc, RZ Cas being at a distance of 73 ± 2pc)

A low resolution ultraviolet spectrum of RZ Cas taken with the IUE satellite near mid-secondary eclipse is available in the IUE data bank. This has the virtue of being negligibly affected by the secondary component. Comparison with standard star spectra, particularly the position of the steep continuum slope between 1200Å and 1600Å confirms the spectral type of A3V and shows no sign of reddening (Fig. 3.3). This region of the spectrum is also sensitive to characteristics of the λ Bootis class of stars (A-type stars with metallic lines too weak for the spectral type as determined from the ratio of the K line to Balmer line strengths), but none of these characteristics are seen in RZ Cas.

Following the method of Hill and Ebbighausen (1984) we have used the UV fluxes of Thompson et al. (1978) to estimate the spectral type of the primary since these fluxes are negligibly affected by the presence of the secondary. We form the colour indices $\lambda\lambda$2740-V, $\lambda\lambda$2365-V and $\lambda\lambda$1565-V where the V magnitude is corrected for the presence of the secondary with a luminosity ratio generated by LIGHT2 using the adopted parameters shown in Table 3.9. The reddening as given by Thompson et al. ($E(B-V) = 0.43(1565-2740) - 0.46(1565-2365) + 0.06$) is found to be $E(B-V)$=-$0\overset{\rm m}{.}02 \pm 0\overset{\rm m}{.}05$, again indicating that the system is probably unreddened.

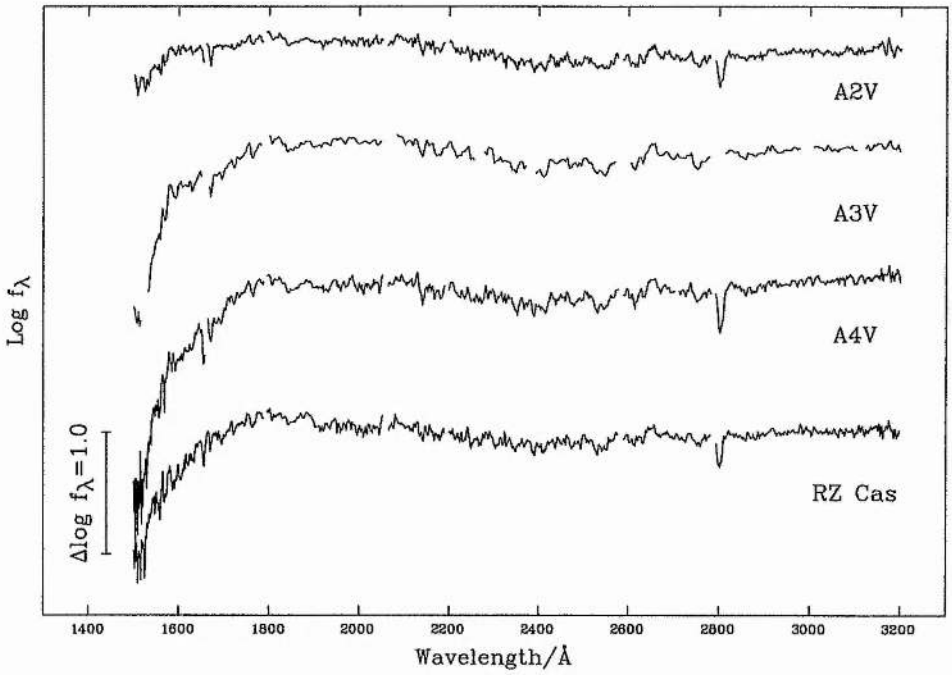

Figure 3.4: UV (IUE) spectra of standard A stars and RZ Cas.From top to bottom: HD80081,A2V; HD216956,A3V; HD97603,A4V; RZ Cas

Thus we find the following colour indices for RZ Cas: $\lambda\lambda$2740-V=$0^m.47\pm0^m.02$; $\lambda\lambda$2365-V=$0^m.35\pm0^m.05$; $\lambda\lambda$1565-V=$1^m.48\pm0^m.07$.

Table 3.5 shows mean UV colour indices for main-sequence and near-main-sequence A2–A5 stars compiled from the catalogue of Thompson et al. (all corrected for reddening where appropriate). All three colour indices indicate a spectral type of about A4–A5 but unfortunately no information is available as to the timing of these observations and so this estimate must be regarded with caution.

Table 3.5: Mean UV colours of A type stars

Spectral	2740-V		2365-V		1565-V		
type	value	σ	value	σ	value	σ	n
A2	0.23	0.08	0.09	0.09	0.20	0.25	8
A3	0.28	0.08	0.17	0.09	0.56	0.32	19
A4	0.35	0.08	0.30	0.07	1.55	0.21	5
A5	0.45	0.11	0.40	0.12	1.81	0.37	9
RZ Cas	0.47	0.02	0.35	0.05	1.48	0.07	

For the purposes of this analysis we therefore assume the primary component of RZ Cas to be an unreddened main-sequence A3V star with Solar composition.

3.4.2 Secondary component

Chambliss suggests a spectral type for the secondary of approximately G5 IV. The temperature of the secondary component derived from the light curve solutions presented below would indicate a spectral type for the secondary of approximately K0. The surface gravity and mean radius derived from the light curve solutions suggest luminosity classes of III and IV respectively.

A set of narrow- and intermediate-band interference filters conforming to the specification of the DDO photometric system (McClure, 1976) was employed in the Peoples' photometer attached to the 0.5m Leslie Rose Telescope at the University Observatory, St Andrews. One night of photometric observations (1975 January 23/24) is presented here consisting of 39 observations of RZ Cas during a primary eclipse obtained by RWH. Observations (not reported here) were also obtained of a nearby comparison star to confirm the constancy of the zero-point of the photometer. Only the 41, 42, 45 and 48 filters of the DDO system were used. Since the colour indices C(41-42), C(42-45), C(45-48) are specified entirely by those filters and do not depend on the particular telescope/photometer system used, we have been able to use the transformation coefficients (or scale factors) for this filter set established by RWH from extensive observations at Kitt Peak National Observatory (reported in Hilditch, 1981). Accordingly, 18 observations of 14 DDO standard stars obtained in 1975 January 23/24 were used to determine extinction coefficients and zero points for the transformation of the observations to the standard system. The colour indices and m(48) magnitude for RZ Cas given in Table 3.6 are those transformed directly to the standard system by means of the standard star observations. The rms errors of the standard star observations about the mean transformation are $\pm 0\overset{m}{.}019$, $\pm 0\overset{m}{.}020$, $\pm 0\overset{m}{.}008$ and $\pm 0\overset{m}{.}02$ in C(41-42), C(42-45), C(45-48) and m(48) respectively. The values for RZ Cas are expected to be of similar accuracy. No evidence was found for zero-point or extinction drifts during the night.

The difficulties involved in interpreting these data stem from the accuracy with which we can estimate the luminosity ratio of the two components in any one filter bandpass. Our best estimates of luminosity ratios are those generated with LIGHT2 using modified blackbody fluxes, which produce realistic broad-band fluxes, but only for the Johnson UBVRI and Strömgren *uvby* systems. However, both the Strömgren *b* filter and the DDO 48 filter are centered in a region of stellar spectrum devoid of strong spectral features and are separated by only $\sim$ 100Å, so the luminosity ratio in both will be approximately equal. We can refine our estimate by interpolating from the *uvby* fluxes the luminosity ratio at the bandpass of the 48 filter at any given phase. By generating luminosity ratios at phases near primary eclipse we

can synthesize light curves for the $C(45-48)$ colour index for various values of $C(45-48)_{\rm sec}$, the colour index of the secondary component. A value of the colour index of the primary, $C(45-48)_{\rm pri}$, is adopted so as to produce the correct value of $C(45-48)$ outside of eclipse. The various values of $C(45-48)_{\rm sec}$ then give different eclipse depths and the best fit can be readily seen. This is shown in the upper panel of Fig. 3.4, for the values of $C(45-48)_{\rm sec}$ shown in Table 3.7.

The upper curve corresponds to $C(45-48)_{\rm sec}=1.2$, the lower curve to $C(45-48)_{\rm sec}=1.5$, the best fit occurring at a value of $C(45-48)_{\rm sec}\simeq 1.4$. Also shown in Table 3.7 are the adopted values of $C(45-48)_{\rm pri}$ which can be compared to values for similar stars shown in Table 3.8 (from McClure and Van den Bergh,1968).

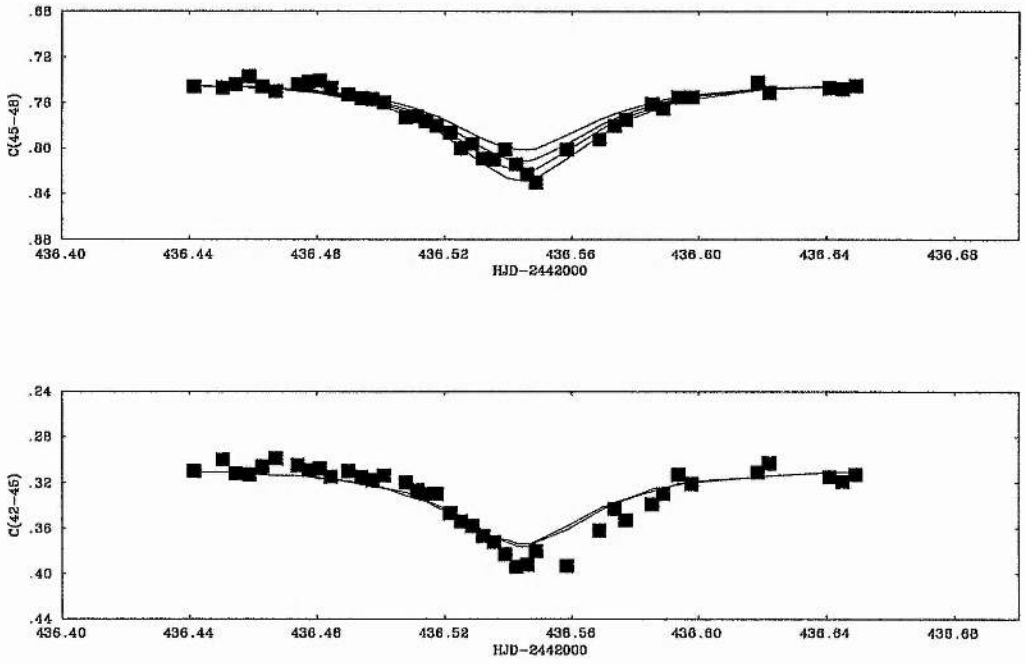

Figure 3.5: DDO observations of RZ Cas during primary minimum. See text for explanation

Adopting a value of $C(45-48)_{\rm sec}=1.4$ and the corresponding value of $C(45-48)_{\rm pri}$ we can calculate the luminosity ratio in the bandpass of the 45 filter. We can then synthesize light curves for the $C(42-45)$ colour index in a similar fashion. Unfortunately, the large value of $C(45-48)_{\rm sec}$ implies a large luminosity ratio in the bandpass of the 45 filter (≈ 40 outside of eclipse). In this case only an unreasonably large value of $C(45-48)_{\rm sec}$ ($\gtrsim 2$) will provide a good fit to the $C(42-45)$ light curve. Since this colour index is a measure of the break in the continuum due to the G band (CH) ,taken at face value this implies an extremely large carbon abundance for the secondary component. A compromise can be made by adopting solutions with values of $C(45-48)_{\rm sec}=1.2$ or 1.3 and $C(42-45)_{\rm sec}=1.2$ or 1.3 respectively, which are

Table 3.6: Observed DDO colours of RZ Cas

HJD-2442000	C(41-42)	C(42-45)	C(45-48)	m(48)
436.4504	0.0655	0.300	0.747	6.401
436.4545	0.0631	0.312	0.744	6.433
436.4587	0.0676	0.313	0.737	6.436
436.4628	0.0671	0.306	0.746	6.487
436.4670	0.0577	0.299	0.750	6.494
436.4739	0.0709	0.305	0.744	6.551
436.4774	0.0685	0.309	0.742	6.603
436.4808	0.0691	0.308	0.741	6.652
436.4843	0.0601	0.315	0.747	6.686
436.4898	0.0623	0.310	0.753	6.764
436.4940	0.0656	0.315	0.756	6.819
436.4974	0.0721	0.318	0.757	6.879
436.5009	0.0669	0.314	0.760	6.952
436.5078	0.0596	0.320	0.773	7.087
436.5113	0.0708	0.327	0.772	7.176
436.5141	0.0767	0.330	0.776	7.279
436.5175	0.0697	0.330	0.780	7.369
436.5217	0.0747	0.347	0.786	7.452
436.5251	0.0677	0.354	0.800	7.571
436.5286	0.0641	0.358	0.796	7.671
436.5321	0.0661	0.367	0.809	7.735
436.5355	0.0653	0.372	0.810	7.808
436.5390	0.0674	0.383	0.801	7.861
436.5425	0.0462	0.394	0.814	7.920
436.5459	0.0720	0.392	0.823	7.953
436.5487	0.0573	0.380	0.830	7.943
436.5688	0.0559	0.362	0.792	7.576
436.5736	0.0682	0.343	0.780	7.445
436.5771	0.0657	0.353	0.775	7.320
436.5854	0.0549	0.339	0.761	7.150
436.5889	0.0640	0.330	0.765	7.049
436.5937	0.0698	0.313	0.755	6.944
436.5979	0.0769	0.321	0.755	6.875
436.5584	0.0539	0.393	0.801	7.795
436.6186	0.0736	0.311	0.742	6.613
436.6221	0.0821	0.303	0.751	6.580
436.6408	0.0715	0.315	0.747	6.425
436.6450	0.0631	0.319	0.748	6.402
436.6491	0.0870	0.313	0.745	6.418

Table 3.7: DDO colour index estimates for RZ Cas.

$C(45-48)_{\rm sec}$	$C(42-45)_{\rm sec}$	$C(45-48)_{\rm pri}$	$C(42-45)_{\rm pri}$
1.2	1.2	0.728	0.289
1.3	1.3	0.725	0.290
1.4	$\gtrsim 2$	0.722	$\lesssim 0.29$
1.5	—	0.720	—

Table 3.8: DDO colours of some A type stars

HD	Sp.Ty	E(B-V)	C(41-42)	C(42-45)	C(45-48)
97603	A4V	0.03±0.01	0.055	0.32	0.74
154494	A3IV	0.05±0.03	0.05	0.32	0.73
173880	A3V	0.03±0.01	0.07	0.33	0.71

the colours of normal K4-5 stars of luminosity class III-IV, but these values give poor fits to both light curves. The $C(42-45)$ light curve and the two nearly identical synthetic light curves are shown in the lower panel of Fig. 3.4.

The $C(41-42)$ colour index shows no change during primary eclipse which implies a value of $C(41-42) \simeq 0.065$ for both components. This colour index measures the strength of CN absorption band shortward of $\lambda 4216$, but in the light of the results above it is not clear how this value should be interpreted.

The question of the spectral type and surface composition of the secondary component can only be answered conclusively by obtaining a good spectrum of the secondary. Given that the system is partially eclipsing, this can only be obtained by using image reconstruction techniques such as tomography (Bagnuolo & Gies,1991), preferably with spectra obtained in the near-infrared where the luminosity ratio is less extreme.

3.5 Solutions of the UBV light curves

To derive absolute parameters we have used the UBV light curves of Chambliss (1976) and the program LIGHT2 (Hill, 1979; Hill & Rucinski, 1993). The light curves of Hegedüs et al. are of inferior quality to those of Chambliss and are not considered here. The assumptions are those given in earlier papers, those of importance being that the secondary rotates synchronously and the values of β, the gravity brightening exponent, for the hot and cool components are 0.25 and 0.08 respectively. The mean primary temperature was fixed at 8600K. Solutions attempted with the secondary's radius as a free parameter either failed to converge to a solution or showed

Table 3.9: Solutions to the UBV light curves of Chambliss. Values in bold type are fixed, formal errors are quoted below other quantities.

	Uncorrected			Corrected			Adopted
	U	B	V	U	B	V	
r_p	0.2452	0.2429	0.2407	0.2419	0.2436	0.2436	0.243
	± 0.0021	± 0.0018	± 0.0012	± 0.0030	± 0.0014	± 0.0018	± 0.002
r_s		**0.2708**			0.2683[a]		0.2683
							0.0017[b]
$< T_p >$		**8600**			**8600**		8600
$< T_s >$	5019	4858	4613	4850	4774	4609	4700
	± 99	± 75	± 40	± 165	± 94	± 54	± 200
m_p/m_s		**2.92**			**3.02**		3.02
							± 0.07
$i/^\circ$	83.27	82.80	82.79	83.09	82.92	83.06	83.0
	± 0.13	± 0.11	± 0.05	± 0.17	± 0.08	± 0.10	± 0.1
$\beta_{\rm sec}$	0.83	0.57	0.40	1.23	0.73	0.47	0.7
	± 0.18	± 0.12	± 0.07	± 0.23	± 0.15	± 0.09	± 0.3
σ(mags)	0.010	0.007	0.006	0.012	0.008	0.007	—

a:Fixed at Roche limit. b:From error in mass ratio

the secondary to be in contact with its Roche lobe. We therefore constrained the secondary to its Roche lobe (as defined from the mass ratio) in all the solutions. Free parameters in the solutions were: the polar radius of the primary component relative to the semi-major axis of the relative orbit (r_p); the effective temperature of the cool component at its pole (although mean temperature $< T_s >$ is quoted here) ; the inclination of the orbital plane (i) and the albedo of the secondary component($\beta_{\rm sec}$).

3.5.1 Rotation of the primary

It is important to establish the rotation rate of the primary component before attempting a solution to the light curve since the rotation introduces distortions to the shape of the star and, via gravity brightening, to the intensity distribution on the surface of the star. For this study we used the determinations for RZ Cas of Fukuda(1982) who quotes $V_{\rm rot} \sin i = 85$ km s^{-1} which agrees well with the earlier determination of Olson (1968) who quotes $V_{\rm rot} \sin i = 82$ km s^{-1}. For our light curve solutions we fixed the ratio $V_{\rm rot}$(actual)/$V_{\rm rot}$(synchronous) = 1.2 resulting in a value for $V_{\rm rot} \sin i = 83$ km s^{-1}.

Table 3.10: Absolute parameters of RZ Cas

	Primary	Secondary
Mass	$2.205 \pm 0.075\,M_\odot$	$0.73 \pm 0.02\,M_\odot$
Mean Radius	$1.67 \pm 0.03\,R_\odot$	$1.94 \pm 0.03\,R_\odot$
Mean Temperature	$8600K \pm 100K$	$4700K \pm 200K$
Log ($L/L_\odot$)	1.12 ± 0.02	0.16 ± 0.08
Mean log g	4.34 ± 0.02	3.73 ± 0.02
Absolute bolometric magnitude	1.89 ± 0.06	4.2 ± 0.2
Bolometric correction	-0.06	-0.45
Absolute visual magnitude	1.96 ± 0.06	4.7 ± 0.2

3.5.2 Results

The best fit solutions to the light curves are shown in Table 3.9 for both the uncorrected and corrected mass ratios. The albedo found for the corrected U solution (1.23 ± 0.23) is curious, but probably reflects the problems associated with this filter (telluric features, Balmer decrement) rather than any physical phenomenon. Also shown are the values adopted for subsequent calculations. In particular the values shown were used to calculate the absolute parameters shown in Table 3.10. The symbols r_p and r_s refer to the polar radii of the two components relative to the semi-major axis of the relative orbit, $< T_p >$ and $< T_s >$ are their mean effective temperatures. The light curves of Chambliss and their solutions using the corrected mass ratio are shown in Fig. 3.5. In common with Chambliss we find the residuals to be small ($\sim \pm 0.01$mags) but not random, being either systematically positive or negative in given portions of the light curve. In particular, the calculated light curve is too low at quadrature. It is also noticeable that in all three light curves second quadrature is lower than first quadrature by $\sim \pm 0.005$mags. A likely explanation for this difference may be starspots on the cool component. If we assume that the secondary rotates synchronously we find $V_{rot} \sin i = 83\,km\,s^{-1}$. Rotation rates as large as this in late-type stars are linked with chromospheric activity. Further evidence for such activity comes from the detection of RZ Cas at radio wavelengths. For example, from two observations using the VLA at 6cm, Umana et al. (1991) derived brightness temperatures for RZ Cas of 4.26×10^8K and 11.1×10^8K. Assuming the source of the radio flux to be gyrosynchrotron radiation from mildly relativistic electrons they derived a mean magnetic field strength for the seven Algol systems detected of $15 < B < 150$ Gauss. Also, the observations of Schmitt et al. (1990) using the EINSTEIN satellite at X-ray wavelengths show emission that is well represented by a model corona at a temperature of log T=7.57, which is a value appreciably higher than that found in other late-type stars but is typical of RS CVn systems. Indeed, with respect to the activity of the cool component, Algol systems share many characteristics with RS CVn systems. These systems show distortions to their light curves which are attributed to

starspot activity on the cool component. Similar activity is seen in the infrared light curves of the prototype Algol system, β Per (Richards,1990). Infrared light curves of RZ Cas would certainly shed further light on this matter.

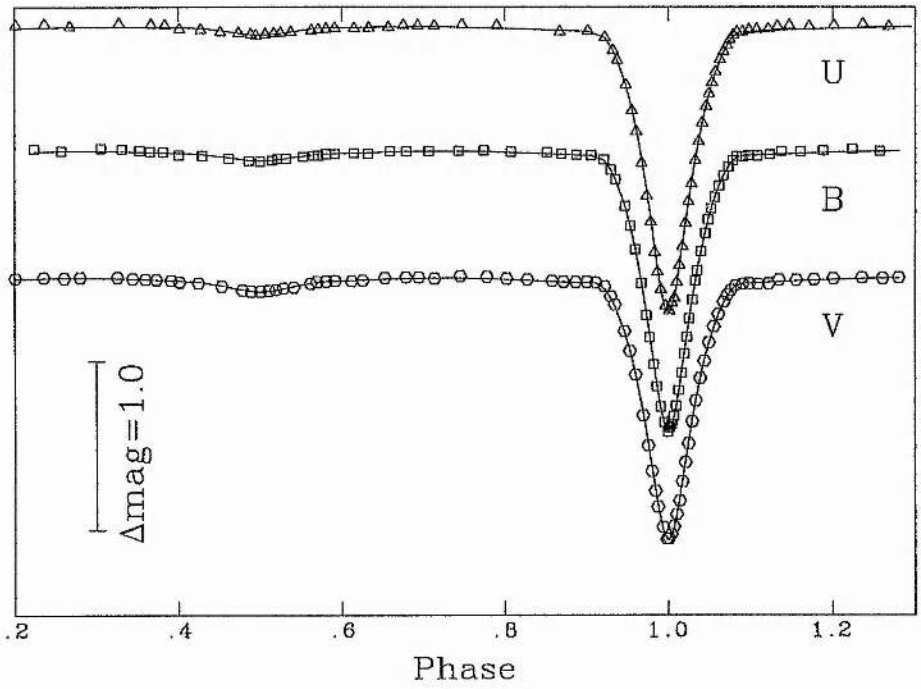

Figure 3.6: The UBV light curves of RZ Cas and the adopted solutions

3.6 Period jumps and associated phenomena

The O-C diagram for RZ Cas using the linear ephemeris of Herczeg & Frieboes-Conde (HJD min. I = 2429875.6902 + 1.1952473) is shown in Fig. 3.6. The dates of the spectroscopic observations presented here are indicated. The period jump around HJD 2446500 is clearly seen, the size is found to be $\Delta P/P \approx 10^{-5}$. Spectra taken at about this time (group 1, $2446000 < HJD < 2447000$) differed from the others (group 2) in two respects. Firstly, only group 1 spectra showed an asymmetry in the form of a wing on one side of the CCF which could not be attributed to the presence of the secondary component. This wing always appeared on the right hand side of the CCF (more positive in velocity space). Secondly, it was also noted that all the group 1 spectra, even those without noticeable wings, produced CCFs that were wider than the CCFs produced using group 2 spectra. The measured full width at half maximum (FWHM) of the CCFs of the two groups differed by ~20%. Applying the Mann-Whitney test to the two groups showed them to be different with respect to their FWHM at the 99% confidence level. From these two facts (the period jump and the abnormal spectra) we conclude that

a mass transfer episode was observed resulting in regions of the primary component rotating asynchronously. Not only does this account for the increased width in the FWHM of the CCFs, it also explains the period jump observed at this time because angular momentum is transferred from the orbital motion and stored in the outer layers of the primary component. This angular momentum is then gradually restored to the orbital motion via tidal interaction between the components as described by Biermann and Hall (1973). The wing observed on the CCF may well be due to one of the phenomena associated with mass transfer such as an accretion stream, a hot spot on the surface of the primary component or a highly unstable, highly asymmetric accretion disk (accretion bulge may be a more suitable term in this case). Herczeg & Frieboes-Conde find that period jumps occur in RZ Cas every 2.5–3 years on average which is in fair agreement with the timescale of 6.8 years for a period increase and subsequent decrease found by Hall et al.; therefore spectroscopic and photometric monitoring over a timescale of a few years would almost certainly shed more light on the mass transfer mechanisms at work in RZ Cas.

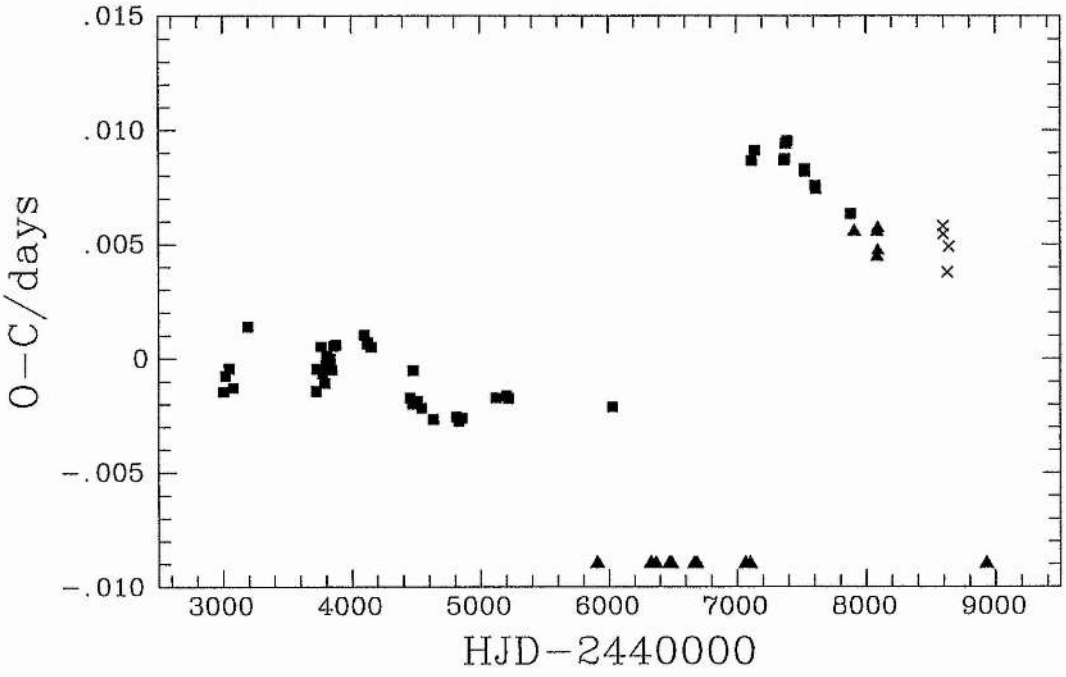

Figure 3.7: Residuals from the ephemeris of Herczeg & Frieboes-Conde. Crosses indicate timings from this paper, small triangles are timings from Hegedüs et al., small squares indicate timings gleaned from IBVS, large triangles show dates of mid-exposure of spectra presented in this paper

Table 3.11: Timings of minima of RZ Cas.

HJD of Min I	n
2448600.4403	201
2448601.6352	675
2448631.5146	1163
2448643.4680	581

3.7 Additional observations

RZ Cas was observed during the winter of 1991-92 with the Twin Photometric telescope and new automatic photometers (Edwin & Gears, 1992) at the University Observatory, St Andrews. We used HD 16393 as our comparison star only to learn later that Hegedüs et al. (1991) had found it to be variable by a hundredth of a magnitude or so. However these variations are small and should not have a large effect on timings of primary minimum. Our four new times of primary minimum are presented in Table 3.11 together with the number of points used to derive them via the method of parabolic curve fitting. They are also shown in Fig. 3.6. We would warn other workers not to use HD 16393 as a comparison star for RZ Cas unless its constancy (or otherwise) can be verified.

RZ Cas was also observed with the red and blue arms of the ISIS spectrograph on the William Herschel Telescope at La Palma, Canary Islands in 1992 (January 15/16, 23:40 UT). A cross section of the spectrum taken in the red arm at right angles to the direction of dispersion (Y-cut) has revealed a companion star to RZ Cas at a separation of $\sim$5" and a position angle of 123°. This companion is approximately 6.6 magnitudes fainter at 7800Å than RZ Cas at the time that spectrum was taken (very near primary minimum).There is no sign of the star in the spectrum taken in the blue arm. A magnified view of the Y-cut through the red spectrum is shown in Fig. 3.7 with the full Y-cut inset for comparison. The existence of a companion star was subsequently verified by the observations of Narusawa & Okyudo (1993) whose CCD observations showed a star with a V magnitude of 13–14 approximately 6" east of RZ Cas.

3.8 Conclusion

The ability of the cross-correlation technique to measure reliably the radial velocities of the faint secondary component coupled with analysis of good quality multi-colour light curves has enabled accurate absolute parameters for both components of RZ Cas to be found. It is hoped that these will be used to study the evolutionary status of RZ Cas as has been done for U Sge (Sarna & De Greve, 1993), β Per (Sarna,1993), TV Cas (De Greve et al., 1985) and a few other

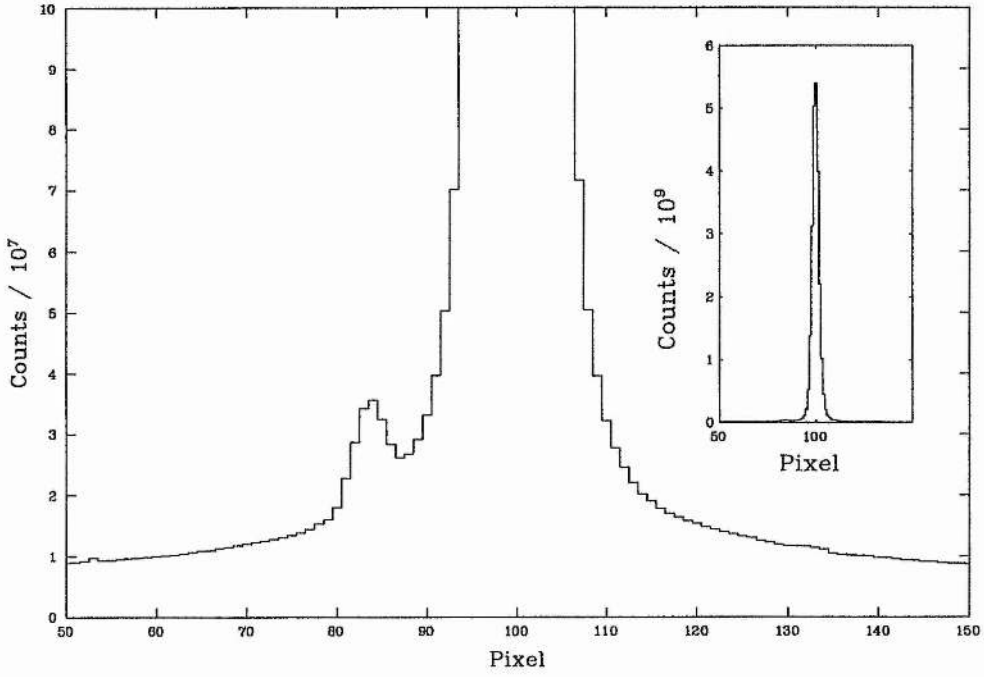

Figure 3.8: Y-cut through the red arm ISIS spectrum of RZ Cas

systems. In this regard it is worth noting that Sarna finds that the carbon abundance must be accurately known in order to constrain the models, certainly better than the 50% error in the estimate available to him for β Per. The Strömgren photometry presented above gives a good estimate of the metallicity of the primary, but ideally a high resolution UV spectrum, preferably taken near mid-secondary eclipse should be used to determine the composition of the primary component spectroscopically. The best hope for a reliable secondary spectrum from which to derive abundances lies with image-reconstruction techniques for which near-infrared spectra would provide the best chance of reliable results. Tomography has already been shown to be successful in this regard and the data set obtained would have the added bonus of improving the radial velocity determinations of the secondary and thus improve the accuracy of the primary mass estimate.

The curious phenomenon of the transient flat bottom to primary eclipse is certainly not due to a total eclipse in RZ Cas since the eclipse is found to be partial both from the analysis of the light curves of Chambliss ($\alpha \simeq 0.81$ from our analysis or indeed that of Chambliss) and from the analysis of Hegedüs et al. of their own B and V light curves taken at a different epoch from which they conclude "that the possibly flat bottom of the primary minimum could not be caused by a total eclipse". It therefore seems that Olson's hypothesis of hot and cool spots on the surface of the hot component is the most likely explanation for the peculiarities seen in primary eclipse. Since the cool component of RZ Cas is also likely to show starspots, infrared

light curves of RZ Cas with good phase coverage would certainly be of interest.

The observations of distortions to the CCFs in conjunction with the period jump observed at that time must be regarded as good evidence in support of the Biermann-Hall hypothesis. This conclusion has a bearing on the interpretation of the period variations of RZ Cas and similar systems in that ascribing any periodicities of these variations to the light-time effect due to orbital motion about one or more companions must be regarded as uncertain without further evidence. RZ Cas in certainly worthy of further photometric study with, in particular, new timings of minima become increasingly more valuable with time. The precision of the spectroscopy now available warrants a modern light curve of high precision in a standard system such as the *uvby* system or Utrecht Photometric system (UPS) (Heintz & Van Gent,1989).

The evolutionary status of RZ Cas is discussed in Chapter 9.

Bagnuolo W.G., Gies D.R.,, 1991. ApJ, **376**, 266.

Batten A.H., Fletcher J.M., MacCarthy D.G., 1989. Publ. Dom. Astrophys. Obs., **17**, 1.

Biermann P., Hall D.S., 1973. A&A, **27**, 249.

Chambliss C.R., 1976. PASP, **88**, 22.

Drake S.A., Simon T., Linsky J.L., 1986. AJ, **91**, 1229.

Duerbeck H.W., Hänel A., 1979. A&AS, **38**, 155.

De Greve J.P., de Landtsheer A.C., Packet W., 1985. A&A, **142**, 367.

Edwin R.P., Gears R.T., 1992. PASP, **104**, 1234.

Fukuda I., 1982. PASP, **94**, 271.

Hall D.S., 1975. Acta Astron., **25**, 1.

Hall D.S., Keel W.C., Neuhaus G.H., 1976. Acta Astron., **26**, 239.

Hegedüs T., Szatmáry K., Vinkoó J., 1991. Ap&SS, **187**, 57.

Heintz J.R.W., Van Gent R.H., 1989. Space Sci. Rev., **50**, 257.

Herczeg T.,Frieboes-Conde H., 1974. A&A, **30**, 259.

Hilditch R.W., 1981. MN, **196**, 305.

Hilditch R.W., Hill G., 1975. Mem. RAS, **79**, 101.

Hill G., 1979. Publ. Dom. Astrophys. Obs., **15**, 297.

Hill G., Ebbighausen E.G., 1984. AJ, **89**, 1256.

Hill G., Rucinski S.M., 1993. In: Light curve modeling of eclipsing binary stars., p.135, Milone E.F. (ed.), Springer-Verlag,Berlin.

Horak H.G., 1952. ApJ, **115**, 61.

Khalesseh B., Hill G., 1991. A&A, **244**, 75.

Lester J.B., Gray R.O., Kurucz L.K., 1986. ApJS, **61**, 509.

McClure R.D., 1976. AJ, **81**, 182.

McClure R.D., Van Den Bergh S., 1968. AJ, **73**, 313.

Nakamura Y., Narusawa S., Kamada M., 1991. IBVS, **3641**.

Narusawa S., Okyudo M., 1993. Annu. Rep. Nishi-Harima Astron. Obs., **3**, 11.

Olson E.C., 1968. PASP, **80**, 185.

Olson E.C., 1982. ApJ, **259**, 702.

Perry C.L., Johnston L., Crawford D.L., 1982. AJ, **87**, 1751.

Richards M.T., 1990. ApJ, **350**, 372.

Sarna M.J., 1993. MN, **262**, 534.

Sarna M.J.,De Greve J.P., 1993. In: Proc. 3rd DAEC meeting,Meudon,France,1992. The feedback of chemical evolution on the stellar content of galaxies.(in press).

Schmitt J.H.M.M., Collura A.,Sciortino S.,Vaiana G.S., Harnden F.R.JR., Rosner R., 1990. *ApJ*, **365**, 704.

Thompson G.I.,Nandy K.,Jamar C. et al., 1978. Catalogue of stellar UV Fluxes.

Umana G., Catalano S., Rodono M., 1991. A&A, **249**, 217.

Chapter 4

AT Pegasi

4.1 Introduction

AT Peg (HD 210892, P=1.146 days, α(2000.0)=22h13.4m, δ = +8°25.5′, A4V+G) is one of many eclipsing binary systems of $\sim 10^{th}$ magnitude (V=9.5–10.3) which is suspected of being an Algol type system. The only previous spectroscopic study for this system is that of Hill & Barnes (1972) who present radial velocity data for the primary component and estimate a spectral type for the primary of A7V. They also derive absolute parameters under the assumption that the secondary component fills its Roche lobe. They find no trace of the secondary component in any of their spectra. The only available light curve for AT Peg is that of Cristaldi & Walter (1963) at a wavelength of 4540Å, although the spectral response of the system used is not available. The most recent analysis of the period variations of AT Peg is that of Güdür et al. (1987) who derive two different quadratic ephemerides, one from all available data, the other from photoelectric data only.

In this chapter we describe the derivation of the spectroscopic orbit from DAO spectra. The mass ratio derived is used to solve the light curve of Cristaldi & Walter which in turn is used to derive corrections for non-Keplerian effects in the spectroscopic orbit. The spectral type of the primary is established from a spectrum reconstructed from the available combined spectra using tomography. This is found to be in agreement with the available *uvby* photometry.

4.2 Spectroscopic observations and reductions

To derive the primary radial velocities the cross correlation functions (CCFs) of the spectra were measured by fitting Gaussian profiles by least squares. The template spectrum was that of 72 Oph (HD 165777,A4IVs). The radial velocity of 72 Oph was measured from the CCF using Vega as a template (rv=$-14 \pm 1.5 kms^{-1}$, Khalesseh and Hill, 1991) and was taken to be $-34.4 kms^{-1}$. For the secondary component the template spectrum was that of HD 154417, a standard radial velocity star (rv=$-17.4 \pm 0.3 kms^{-1}$, G0V). A 40Å window around the hydrogen lines was excluded from the cross correlation process since their great width broadens the CCF intolerably. The region around the G band was also excluded from the cross correlation process when the template spectrum was that of HD 154417.

4.2.1 RV measures from Gaussian profiles

The CCFs produced with 72 Oph as a template showed a large peak corresponding to the primary and in most cases a much weaker peak corresponding to the secondary. The primary and, when present, secondary peaks were both measured simultaneously by fitting Gaussian profiles by least squares. The quality of the fits was extremely good.

The CCF produced with HD 154417 as a template again showed a large peak corresponding to the primary as well as a smaller peak corresponding to the secondary. The peaks were again measured simultaneously using Gaussian profiles, the quality of the fits being more variable due to spurious features affecting the shapes of some peaks.

Non-Keplerian effects are expected to be quite large for the secondary. In previous work these corrections have been neatly accounted for by using synthetic profile fitting (Hill & Rucinski, 1993). However the peaks in the CCFs for the secondary were too small to use this method and so these corrections have simply been applied in terms of a velocity shift at each phase calculated from the intensity weighted mean of the projected rotational velocity over the visible surface of the star. No attempt has been made to fit synthetic profiles to the primary CCF since the Gaussian profiles are quite adequate and non-Keplerian effects for the primary are found to be small ($< 0.3 kms^{-1}$) for all phases used in this study.

4.3 The spectroscopic orbit

The radial velocity measurements for the primary and secondary components are shown in Table 4.1. The ephemerides adopted for the solution of the primary and secondary orbits were

Table 4.1: Measured radial velocities for AT Peg in $km\,s^{-1}$. Residuals are for corrected velocities and adopted orbit

HJD-2400000	Phase	Uncorrected		Corrected		O-C	
		RV_{pri}	RV_{sec}	RV_{pri}	RV_{sec}	Primary	Secondary
47037.8392	0.7176	-90.79	207.18	-91.12	215.18	-1.6	13.0
47037.8743	0.7482	-86.83	202.15	-87.28	210.33	-1.2	15.6
47068.6902	0.6364	-79.83	193.17	-79.55	196.45	2.6	10.0
47068.7082	0.6725	-85.69	201.87	-85.55	207.32	-0.1	—
47068.7315	0.6521	-85.24	—	-85.26	—	3.1	7.6
47068.8256	0.7546	-85.55	178.69	-86.02	186.83	-1.1	-5.5
47068.8672	0.7909	-78.69	—	-79.09	—	-3.4	—
47404.6923	0.8124	-66.38	168.42	-66.73	174.43	1.5	17.4
47408.6784	0.2904	85.09	-148.26	84.83	-151.70	0.8	13.2
47408.7017	0.3108	80.95	—	80.69	—	3.6	—
47452.6588	0.6652	-96.34	175.83	-96.31	180.80	-8.8	-17.0
47510.5840	0.2074	101.48	-178.31	101.68	-185.42	3.5	9.4
47786.8046	0.2215	96.10	-189.27	96.20	-195.42	-1.3	-2.0
47786.8295	0.2432	94.35	-171.67	94.28	-176.36	-0.8	11.9
47786.8566	0.2668	92.58	-170.09	92.32	-173.53	1.8	5.0
47786.8875	0.2938	83.19	-151.87	82.93	-155.31	0.0	7.3
47787.7389	0.0367	52.96	—	53.27	—	1.4	—
47787.8490	0.1328	85.63	-191.04	86.11	-198.52	-3.3	-22.1
47787.8896	0.1682	96.33	-151.46	96.74	-159.58	0.7	30.9
48461.7920	0.1764	99.01	-169.53	99.39	-177.64	2.4	14.7
48516.8695	0.2338	88.29	-173.79	88.29	-179.10	-8.0	11.8

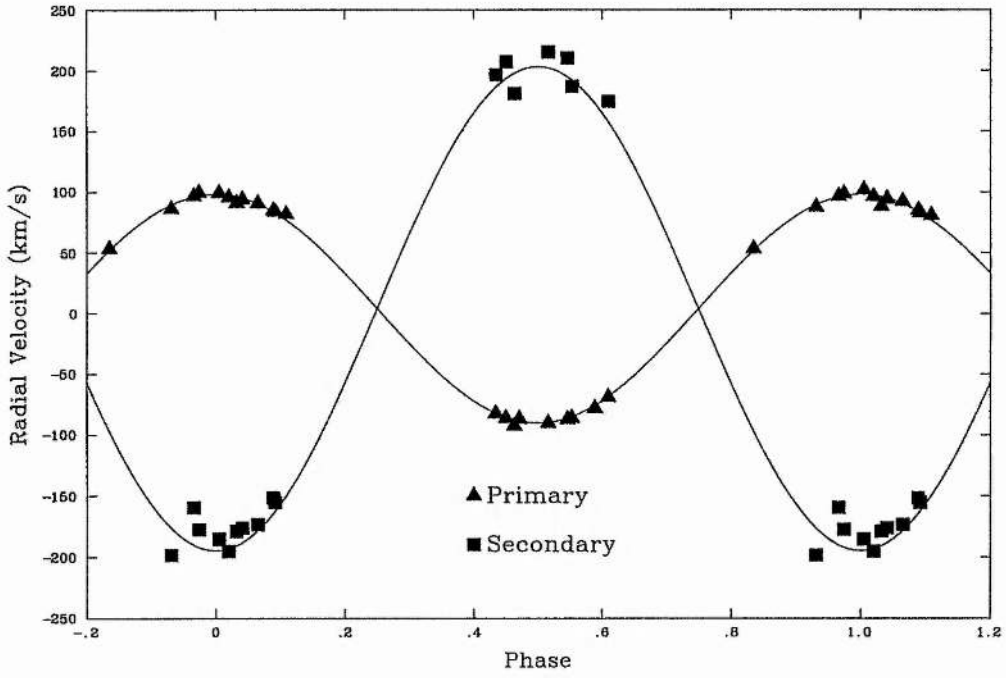

Figure 4.1: Radial velocity measurements of AT Peg and the adopted spectroscopic orbit. The radial velocity measurements have been corrected for non-Keplerian effects

derived from a least squares fit to the 14 most recent timings of primary minimum cited in Güdür et al. and are shown in Table 2. T_+ is the epoch of maximum positive radial velocity and other symbols have their usual meanings. Solutions for the primary's orbit were attempted with the eccentricity as a free parameter but these showed the eccentricity to differ negligibly from zero. The adopted, uncorrected primary spectroscopic orbit is shown in Table 4.2 together with the previously published orbit of Hill & Barnes. The spectroscopic orbit of the secondary was solved independently in a similar fashion. The systemic velocity was initially left as a free parameter but was subsequently fixed at the value derived from the the solution of the primary orbit since the two values were not significantly different. The choice of systemic velocity had little effect on the value of the secondary semi-amplitude. The adopted solution is also shown in Table 4.2. The resultant combined spectroscopic orbit is presented in Table 4.3 under the heading "Uncorrected". Also shown in Tables 2 and 3 are spectroscopic orbits corrected for the ellipticity of the components, which introduces systematic errors (non-Keplerian effects). These are calculated from the solution to the light curve described below by forming the intensity weighted mean of the projected rotational velocities. For AT Peg the corrections to the radial velocities of the secondary component are between 5 and $10 kms^{-1}$ which are enough to alter the mass ratio by $\sim 5\%$. The corrections to the primary radial velocity are small ($< 0.3 kms^{-1}$) but are included for the sake of consistency. The corrected radial velocities and adopted solution are shown in Fig. 4.1.

Table 4.2: The spectroscopic orbit of AT Peg

	This Paper		Hill & Barnes
	Uncorrected	Corrected	
Primary			
$\gamma(kms^{-1})$	4.2 ± 0.6	4.1 ± 0.6	3.9 ± 1.0
$K_p(kms^{-1})$	93.9 ± 0.7	94.1 ± 0.7	87.6 ± 1.5
e	**0.000**	**0.000**	0.0024
			± 0.016
$\omega(^\circ)$	—	—	305 ± 37
Period (days)	**1.1460765**	**1.1460765**	**1.146080**
$T_+ - 2440000$	**2661.5281**	**2661.5281**	0819.735
			± 0.003
Secondary			
$\gamma(kms^{-1})$	**4.2**	**4.1**	—
$K_s(kms^{-1})$	193 ± 3	199 ± 3.5	—
e	**0.000**	**0.000**	—
Period (days)	**1.1460765**	**1.1460765**	—
$T_+ - 2440000$	**2662.1011**	**2662.1011**	—

Table 4.3: The combined spectroscopic orbit of AT Peg

Parameter	Uncorrected	Corrected
$m_p \sin^3 i / \mathrm{M}_\odot$	1.89 ± 0.05	2.04 ± 0.06
$m_s \sin^3 i / \mathrm{M}_\odot$	0.92 ± 0.02	0.96 ± 0.025
$(a_p + a_s) \sin i / \mathrm{R}_\odot$	6.50 ± 0.07	6.64 ± 0.08
m_p / m_s	2.05 ± 0.04	2.115 ± 0.04

4.4 Spectral types and colour indices

4.4.1 Reconstruction of the primary and secondary spectra

Hill & Barnes estimate the spectral type of the primary component to be A7V from photographic spectra. Given a set of binary spectra with radial velocities measured or estimated for both components, and a luminosity ratio, it is possible to reconstruct the individual spectra using an iterative procedure known as tomography (Bagnuolo & Gies, 1991). Some of the properties of this technique as when applied to Algol systems are discussed in Appendix B. Briefly, the recovery of the primary spectrum is found to be reliable but in its present implementation, recovery of the secondary spectrum is possible only under limited conditions. In particular, the recovered secondary spectrum is disrupted by corresponding strong features in the primary spectrum, such as the hydrogen lines and strong metallic lines. This is a consequence of the large and rapid change in the luminosity ratio near these features. Since there are a large number of strong metallic lines in the primary spectrum of AT Peg, the secondary spectrum presented here will not be reliable. However, it is reassuring to note that there is at least some resemblance to a late-type spectrum. In any case, the secondary has only a small effect on the appearance of the primary spectrum. Two regions of recovered spectra are shown in Fig. 4.2 together with a typical combined spectrum and stars of known spectral type for comparison. Note the increase in the quality of the primary spectrum that results from combining several spectra. From this spectrum we estimate the spectral type of the primary component to be A4V. Details of the reconstruction are as follows: 22 spectra where used in the reconstruction using the iterative least squares technique after being smoothed over a 0.6Å interval, 50 iterations were used, and little change in the spectra was noted after 30 iterations. From the light curve solution we obtain luminosity ratios in the sense primary/secondary of 16.5 and 14.6 at the wavelengths 4250Å and 4450Å. The uncorrected radial velocities shown in Table 4.1 were used where available, otherwise radial velocities derived from the adopted spectroscopic orbit were used. The initial input spectra were featureless and the damping constant was fixed at a value of 0.3.

4.4.2 Strömgren photometry

Hilditch and Hill (1975) present Strömgren *uvby* data for AT Peg at four phases including two at or near primary eclipse. They list the colour indices (u-b), (v-b), (b-y) and the V magnitude. Given any two observations of a colour index at phases where the luminosity ratio of the two components differs, e.g. one observation at quadrature and one during primary eclipse, and given an estimate of the luminosity ratio in one of the filter bandpasses, we can solve for the colour indices of the individual components as described in Chapter 3. The adopted colour

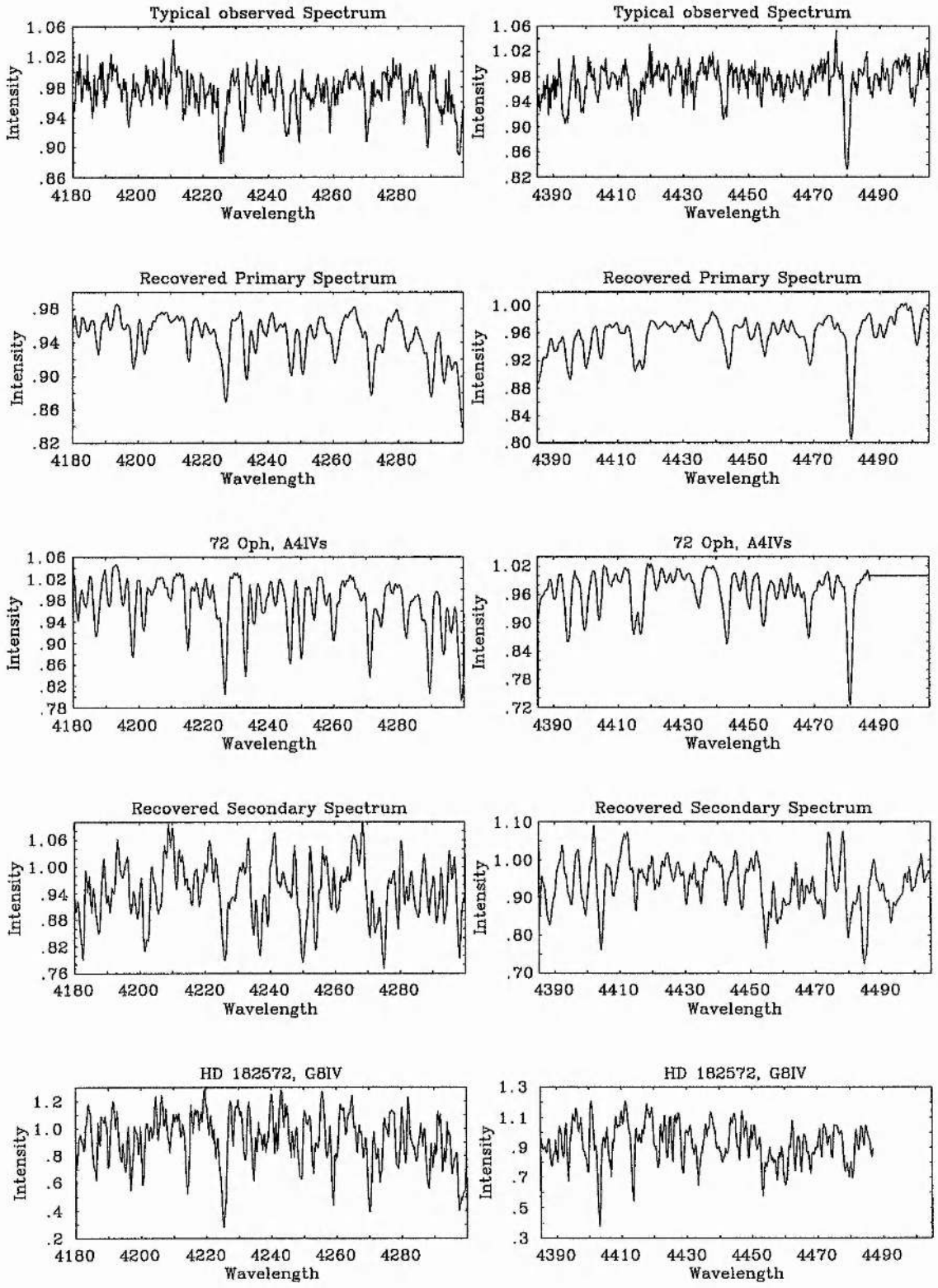

Figure 4.2: Spectra of AT Peg recovered using Doppler tomography

Table 4.4: Strömgren photometry of AT Peg

Notes	$(u\text{-}b)$	n	$(v\text{-}b)$	n	$(b\text{-}y)$	n
Primary						
L(p/s) in :						
x of (x-y)	1.42 ± 0.03	3	0.24 ± 0.02	3	0.08 ± 0.02	3
y of (x-y)	1.47 ± 0.02	3	0.27	1	0.08 ± 0.02	3
Adopted	1.45 ± 0.02		0.24 ± 0.02		0.08 ± 0.02	
Secondary						
L(p/s) in :						
y of (x-y)	2.63 ± 0.20	3	1.40 ± 0.45	3	0.50 ± 0.12	3
y of (x-y)	1.55 ± 0.01	3	1.70	1	0.50 ± 0.10	3
Adopted	—		—		0.50 ± 0.10	

indices are shown in Table 4.4 where n refers to the number of pairs of observations used to derive the mean colour index. The adopted spectral type of the primary implies a value of $T_{eff} \approx 8400$K (Schmidt-Kaler, 1982). Lester et al. (1986) tabulate Strömgren colour indices for stars of selected compositions for a range of temperatures. Interpolating between models shows good agreement between a model star of Solar composition and $T_{eff} \approx 8400$K and the adopted values for AT Peg with a reddening of E(b-y)=0.02 ± 0.02. The value of $(b\text{-}y)$ obtained for the secondary appears to be reliable and implies a spectral type of mid to late G (Manfroid et al., 1987), which is consistent with the temperature derived from the light curve solution.

4.5 Light curve solutions

The only light curve available for AT Peg is that of Cristaldi & Walter. The light curve is of good quality in terms of the scatter of points about the mean curve ($\sim 0^m.01$) but is not well defined in terms of the spectral response of the system used, although the authors quote a wavelength for the light curve of 4540Å. Güdür et al. report observations of AT Peg in the Johnson B and V bands but their individual observations are not available. For this analysis we used the light curve of Cristaldi & Walter, assuming a bandpass similar to the Johnson B filter with a central wavelength of 4540Å , and the program LIGHT2 (Hill, 1979; Hill & Rucinski, 1993). The assumptions used are the same as those for the similar system RZ Cas except that synchronous rotation was assumed for both components and the albedo of the secondary component was fixed at a value of 0.5. Solutions were attempted with a detached configuration but these failed to converge to a solution and so a semi-detached configuration was assumed in all subsequent calculations, i.e. the secondary is constrained to the Roche lobe as defined

Table 4.5: Light curve solution for AT Peg

Parameter	Uncorrected	Corrected
r_p	0.266	0.268
Formal error	$\pm$0.020	$\pm$0.020
r_s	**0.2977**[a]	**0.2953**[a]
Formal error	$\pm$0.0015[b]	$\pm$0.0015[b]
$< T_p >$	**8400**	
$< T_s >$	4910	4900
Formal error	$\pm$70	$\pm$70
Mass ratio(p/s)	**2.05**	**2.115**
Inclination	76.02	76.24
Formal error	$\pm$0.08	$\pm$0.08
σ(mags)	0.011	0.011

a:Fixed at Roche limit. b:From error in mass ratio

Table 4.6: Absolute parameters of AT Peg

	Primary	Secondary
Mass	$2.22 \pm 0.065\,M_\odot$	$1.05 \pm 0.025\,M_\odot$
Mean Radius	$1.86 \pm 0.025\,R_\odot$	$2.15 \pm 0.03\,R_\odot$
Mean Temperature	$8400K \pm 100K$	$4900K \pm 200K$
Log ($L/L_\odot$)	1.19 ± 0.025	0.38 ± 0.07
Mean log g	4.25 ± 0.02	3.80 ± 0.015
M_{bol}	1.72 ± 0.06	3.75 ± 0.2
Bolometric correction	-0.04	-0.35
M_V	1.76 ± 0.06	4.1 ± 0.2

by the mass ratio. The temperature of the primary star was initially fixed at 7850K to match the spectral type of A7V reported by Hill & Barnes but was later fixed at a value 8400K to correspond to the spectral type derived above. All calculations dependent upon results from the light curve solution were repeated using parameters derived from the solution shown in Table 4.5 under the heading "Corrected" and these are the results reported here. In general the change in primary temperature and use of a corrected mass ratio does not alter significantly the results. Free parameters in the solutions were: the polar radius of the primary component relative to the semi-major axis of the orbit, the effective temperature of the cool component at its pole, and the inclination of the orbital plane.

4.5.1 Results

The results of the light curve solution using both corrected and uncorrected mass ratios are shown in Table 4.5. The symbols r_p and r_s refer to the polar radii of the two components relative to the semi-major axis, $< T_p >$ and $< T_s >$ are their mean effective temperatures. The fit to the observed light curve is very good. In particular there are no systematic trends in the residuals which appear to be scattered randomly about the fit with a mean scatter of about $0^m.01$. Errors quoted in Table 4.5 are formal errors derived from the solution and may not reflect the true uncertainty in these values. This is true in particular for the temperature of the secondary component which is dependent upon the colour of the light curve, which is not well defined. However, the results of the Strömgren photometry presented above confirm that the temperature quoted in Table 5 is at least approximately correct. The light curve and adopted solution using the corrected mass ratio are shown in Fig. 4.3.

From the parameters shown in Table 3 derived from the corrected spectroscopic orbit and the corresponding light curve solution shown Table 5 we obtain the absolute parameters for AT Peg shown in Table 6.

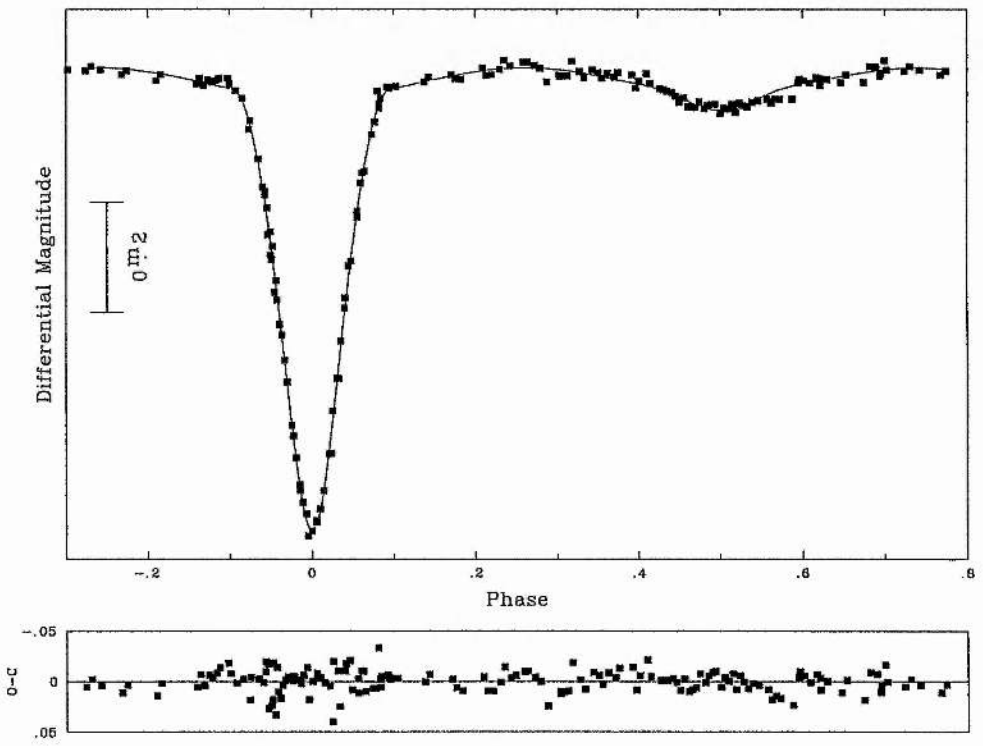

Figure 4.3: The light curve of AT Peg and the adopted solution

4.6 Conclusion

The ability of the cross-correlation technique to obtain reliable radial velocities for faint companion stars in binary systems has enabled the suspected semi-detached configuration of AT Peg to be confirmed and the absolute parameters of the system to be found. The quality of the spectroscopic orbit warrants photometric data of similar quality. We look forward to the publication of the light curves of Güdür et al. and subsequent analysis with the use of the spectroscopic mass ratio derived here. AT Peg certainly merits further study, in particular timings of primary minimum become increasingly valuable with time. Meaningful comparisons with evolutionary models would benefit from knowledge of the surface abundance of elements such as carbon. For the primary component of AT Peg, analysis of high resolution UV spectra, as has been done for other Algol systems by Cugier (1989), would provide valuable information as to the nature of the primary component. Since AT Peg is a partially eclipsing system, analysis of the secondary would require high quality spectroscopy in conjunction with image processing techniques similar to those presented here in order to obtain a spectrum of the secondary uncontaminated by the primary component. The near-infrared region would provide the best chance of extracting a reliable secondary spectrum since the luminosity ratio is more favourable at these wavelengths. The evolutionary status of AT Peg is discussed in Chapter 9.

Bagnuolo W.G., Gies D.R., 1991. ApJ, **376**, 266.

Cugier H., 1989. A&A, **214**, 168.

Cristaldi S., Walter K., 1963. Astron. Nachr., **287**, 103.

Güdür N., Sezer C., Gülmen O., 1987. IBVS, **2978**.

Hilditch R.W., Hill G., 1975. Mem. RAS, **79**, 101.

Hill G., 1979. Publ. Dom. Astrophys. Obs., **15**, 297.

Hill G., 1982. Publ. Dom. Astrophys. Obs., **16**, 59.

Hill G., Barnes J.V., 1972. PASP, **84**, 430.

Hill G., Rucinski S.M., 1993. In: Light curve modeling of eclipsing binary stars., p.135, Milone E.F. (ed.), Springer-Verlag,Berlin.

Khalesseh B., Hill G., 1991. A&A, **244**, 75.

Lester J.B., Gray R.O., Kurucz L.K., 1986. ApJS, **61**, 509.

Manfroid J., Oblak E., Pernier B., 1987. A&ASS, **69**, 505.

Schmidt-Kaler T.H., Physical parameters of the stars. In: Landolt-Bornstein New Series. Volume 2b, astronomy and astrophysics–stars and star clusters, eds. K. Schaifers, H.H. Voigt, New York, Springer-Verlag.

Chapter 5

TX Ursae Majoris

5.1 Introduction

TX UMa (HD 93033, P=3.0632 days, α(2000.0)=10h45m20.45s, δ=+45°33′58″, B8V+G0III-IV, V=7.06–8.76) is a system that has attracted much attention from observers since the discovery of its radial velocity variations by Pearce (1932) in 1925 and the subsequent independent discovery of its eclipsing nature by Rugumer (1931) and Schneller (1931). Several light curves have been published, mostly in the Johnson UBV system. The optical light curve is characterised by a deep primary eclipse ($\Delta m_V = 1.7$) and a much shallower secondary eclipse. All attempts to find solutions to the light curve have run into difficulty. Koch (1961) describes a range of problems he encountered in attempting to find a consistent solution of his UBV light curves, Hill and Hutchings (1973) discuss their solutions to the same light curves from a more technical point of view. The most comprehensive photometric study of TX UMa is that of Papoušek et al. (1985) comprising 6980 observations of the B magnitude over the course of 17 years. Kreiner and Tremko (1980) analysed the majority of these data and found variations in the depth of primary eclipse of as much as $0^m.11$. The most recent of many analyses of the period variations of TX UMa is that of Hric and Komžík (1992). From their data it is evident that the period is essentially constant for long periods of time ($\sim$ 20 years) but that variations occur in the form of period jumps of size $\Delta P/P \approx 2 \times 10^{-5}$. If it is assumed that the period variations are due to conservative mass transfer, they find the amount of transferred matter to be $\Delta M \approx 2.5 \times 10^{-5} M_\odot$.

There have been several spectroscopic orbits published for TX UMa, that of Swensen and McNamara (1968) being the most frequently quoted although the orbits of Grewing and Herczeg(1966), Hiltner (1945) and Hric et al. (1990) are all similar in that they all find a small eccentricity and a value for $K_1 \approx 53 \mathrm{kms}^{-1}$ (although Grewing and Herczeg find $K_1 =$

66.7kms^{-1}). There appears to be a fair degree of intrinsic scatter in the radial velocities and so the small eccentricity found may be suspect. Swensen and McNamara also note variations in the appearance of the spectra apparently, independent of phase, with regard to the cores of the hydrogen lines which at times appear sharp and are at other times poorly defined.

Allbright and Richards (1993) used variations in the profile of Hα in 105 CCD spectra with good phase coverage to discuss the circumstellar material present in TX UMa. Their technique involves subtracting theoretical Hα profiles for the two component stars from the observed profiles. The remaining "difference profiles" can then be analysed to determine the distribution of circumstellar material in the system. They find evidence for material located high out of the orbital plane. This material causes excess absorption during primary eclipse. It takes the form of an asymmetric rotating disk with most of the material located in the region of the supposed impact site on the primary star of the stream of material from the cool component. They also find that the amount of circumstellar material is variable, but only on a time scale longer than four orbital cycles.

5.2 Radial velocity measurements

The radial velocity measurements presented here are based on 19 DAO spectra (see Chapter 2). The spectra were rectified using PRESS as described in Appendix 1. To derive the primary radial velocities we used a spectrum of Vega (A0Va, rv=-14±1.5km/s) as a template to form the cross-correlation functions. The CCFs showed a large peak corresponding to the primary blended with a weaker peak due to the cool component. The two peaks were measured simultaneously by fitting two Gaussian profiles by least squares. The quality of the fits was very good.

To derive the radial velocities of the cool component we used two template spectra to form the CCFs, one of HD 154417 (G0V, rv=-17.4 ± 0.3kms^{-1}), the other of 54 Aql (F8V, rv=0.1 ± 0.3kms^{-1}). Despite the large luminosity ratio at the wavelength of the spectra, the CCFs showed a large narrow peak corresponding to the secondary component and a slightly weaker and broader peak due to the primary. An example is shown in Fig. 5.1. The strength of the peak in the CCF due to the secondary is due to the large number of metallic lines in the spectrum of the secondary compared to the relatively featureless primary. However, the presence of spurious features in the CCF's makes the measurement of the secondary's radial velocities less certain than those for the primary. In general we used Gaussian profiles fitted by least squares to as much of the secondary's peak as appeared free from noise and blending with the primary. The radial velocity measurements obtained for both templates for the secondary component are shown in Table 5.1 under the heading "Uncorrected". Also shown in Table 5.1 under the heading "Corrected" are the radial velocities for the secondary component corrected for non-

Table 5.1: Measured radial velocities for TX UMa in $km\,s^{-1}$. The phase is calculated from the ephemeris of Hric and Komžík (HJD min I = 2448594.47957 + 3.0633292E)

HJD-2400000	Phase	Primary	Secondary			
			HD 154417		54 Aql	
			Uncorrected	Corrected	Uncorrected	Corrected
47510.980	0.300	-52.42	185.85	197.30	180.30	191.75
47511.000	0.306	-50.72	186.53	198.10	190.34	201.91
47511.018	0.312	-49.98	177.19	188.74	177.44	188.99
47511.033	0.317	-53.68	180.21	191.65	175.97	187.41
47512.061	0.653	31.55	-174.82	-185.36	-176.21	-186.75
47512.075	0.657	40.85	-185.80	-196.50	-186.46	-197.16
47512.089	0.662	40.21	-187.34	-198.17	-193.95	-204.78
48398.777	0.114	-47.95	108.26	109.38	—	—
48398.822	0.129	-44.11	—	—	—	—
46474.945	0.094	-40.49	91.43	92.33	—	—
46487.870	0.314	-47.73	193.28	204.81	192.84	204.37
48703.801	0.687	42.57	-189.43	-200.92	-179.66	-191.15
48703.855	0.705	48.30	-211.18	-222.56	-205.26	-216.64
48703.888	0.716	46.83	-204.69	-215.83	-202.13	-213.27
48703.904	0.721	45.44	-200.50	-211.51	-199.70	-210.71
48703.939	0.732	50.25	-205.13	-215.77	-194.42	-205.06
48703.957	0.738	44.74	-192.67	-203.08	-188.91	-199.32
48704.005	0.754	51.55	-177.53	-186.81	-176.83	-186.11
48704.025	0.760	43.00	—	—	—	—

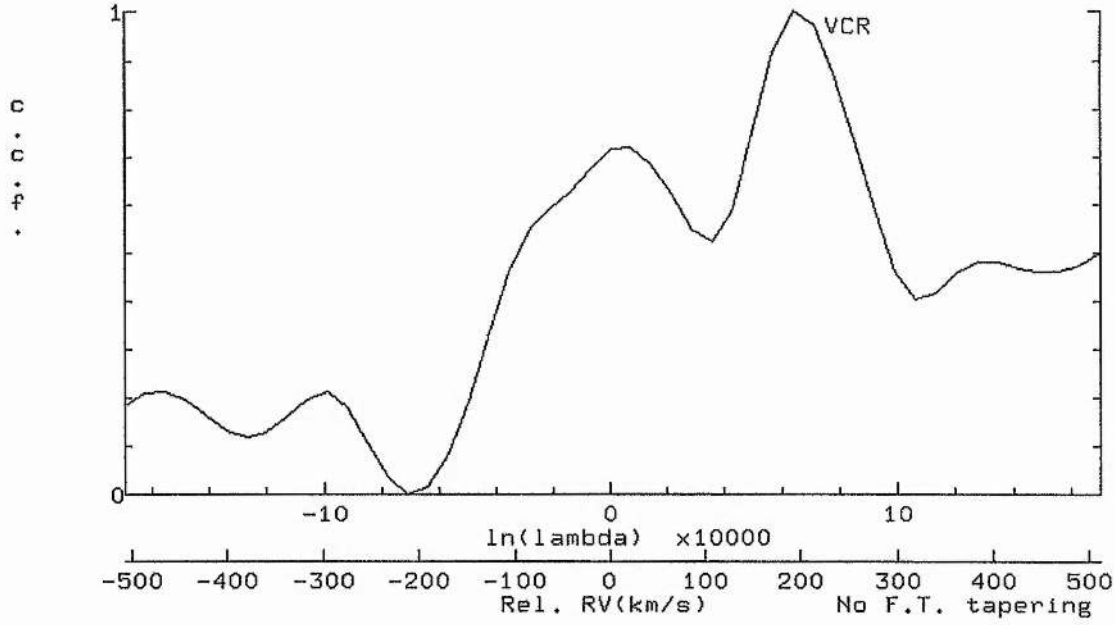

Figure 5.1: CCf of TX UMa v. HD 154417. The highest peak is due to the secondary and the lower peak near the center is due to the primary

Keplerian effects. The radial velocity corrections for the primary are found to be negligible ($\leq 0.02 \mathrm{kms}^{-1}$). Using these data we solved the two orbits separately. Any differences in the systemic velocities derived indicates problems in the measurement of the radial velocities. In this case there is good agreement between the systemic velocities derived as can be seen from the orbits shown in Table 5.2. The orbit given for the secondary is the average of the two orbits calculated, one for each template spectrum. The two orbits agree to within the quoted errors. The corrected data and adopted orbits are shown in Fig. 5.2.

5.3 The light curves and their solution

For this study we used the B and V light curves of Koch. In common with other investigators we found problems in the solution of the light curves. This appears to be due to the large colour changes involved in the deep eclipse of the primary by the much cooler and redder secondary. In particular the U filter is affected by the Balmer decrement in the primary which is not present in the secondary. The U filter is also strongly affected by atmospheric features and so we chose to ignore the U light curve. We found all solutions to the light curves indicate a semi-detached configuration, but they all showed systematic differences between the observations and the model calculations of at least $0\overset{m}{.}04$, particularly around primary eclipse. We therefore elected

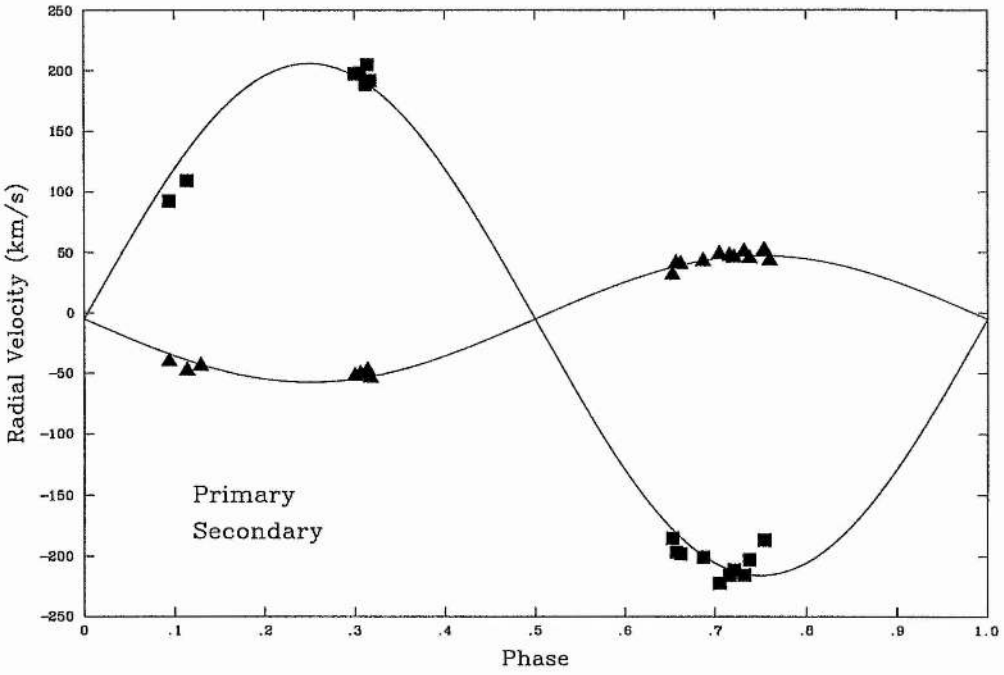

Figure 5.2: Radial velocity measurements for TX UMa and the adopted spectroscopic orbit. The radial velocity measurements have been corrected for non-Keplerian effects

to exclude all data within the phase range 0.98–0.02 from the solution since it is during these phases that the effects of the variations in effective wavelength are greatest. In terms of the depth of primary minimum we exclude one quarter of the eclipse in B and one fifth in V. Using this rather drastic approach we were able to produce model fits to the remaining data that were very good. We also tried solutions to the light curves excluding data in the phase range 0.99–0.01, but these solutions also showed large systematic errors. The solutions to the partial light curves predict depths of eclipse that are too deep by $0\overset{m}{.}3$ in B and $0\overset{m}{.}2$ in V. Errors of this magnitude are of the order of those to be expected given the change in effective wavelength during primary eclipse. However, this situation is clearly far from satisfactory but is unlikely to be improved upon until a light curve in a narrow-band filter system becomes available for TX UMa. We therefore resign ourselves to the use of only those parts of the light curve that seem unaffected by the variations in effective wavelength. It seems reasonable to assume that of all the parameters derived from the solution, the radii will be the least affected by the use of a partial light curve since they are determined primarily by the width of the eclipses. Those parameters which should be treated cautiously are the inclination and secondary temperature since they are determined primarily by the total and relative depths of the eclipses respectively. This is not as great a handicap to the derivation of the absolute parameters of the system as it might seem since the masses of the components are only weakly dependent upon the inclination of the orbital plane for any system with eclipses as deep as those seen in TX UMa i.e. for which

Table 5.2: The spectroscopic orbit of TX UMa. Values in bold type are assumed.

	This Paper		Swensen &	Hric et al. (1990)	
	Uncorrected	Corrected	McNamara(1968)		
Primary					
$\gamma(kms^{-1})$	-5.1 ± 0.9	—	-11.5	-12.9	-8.9
$K_p(kms^{-1})$	52.2 ± 1.0	—	56.1	52.8	54.8
e	**0.000**	**0.000**	0.080	0.0144	0.0134
$\omega(^\circ)$	—	—	326.6	324.2	324.7
Secondary					
$\gamma(kms^{-1})$	-6.6 ± 2.9	5.0 ± 3.4	—	—	—
$K_s(kms^{-1})$	200.0 ± 3.2	211.3 ± 3.6	—	—	—
e	**0.000**	**0.000**	—	—	—

the inclination is $\approx 90^\circ$, and the secondary temperature can be estimated independently of the light curve solution from the spectral type estimate of Plavec & Polidan (1976). They used the strength of Ca II infrared triplet to estimate a spectral type of G0III-IV. This is in fairly good agreement with the temperature derived from *uvbyI* photometry by Olson (1982) of 5500K.

We therefore present the results of the analysis of the partial B and V light curves of Koch using the program LIGHT2 while bearing in mind the discussion above. We used the mean effective temperature determination for the primary component of Cugier (1989) and the albedo and gravity darkening exponents for the primary adopted were 1.0 and 0.25 respectively. For the secondary component we initially adopted the usual atmospheric parameters for a convective atmosphere (albedo=0.5, gravity darkening exponent=0.08) but a much better match to the out-of-eclipse variations was found if the secondary albedo was left as a free parameter. For the rotation rate of the primary we adopt the value quoted by Cugier of 64kms^{-1}; we assumed synchronous rotation for the secondary. Other free parameters in the solution are the effective temperature of the secondary component at its pole, the polar radius of the primary component relative to the semi-major axis of the orbit and the inclination of the orbital plane. No reasonable solutions were found for a detached configuration and so the secondary was constrained to its Roche lobe as defined by the mass ratio. The results are presented in Table 5.3 for both the corrected and uncorrected spectroscopic mass ratios together with the adopted solution. Note that the radii and temperatures quoted are mean values over the surface of the stars. The light curves and adopted solutions are shown in Fig. 5.3.

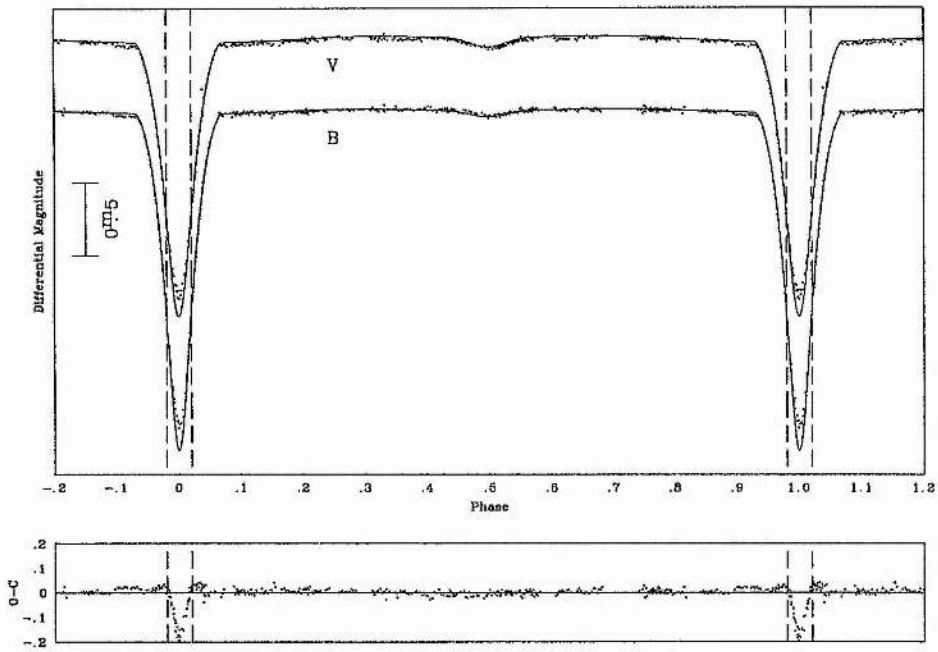

Figure 5.3: The BV light curves for TX UMa and the adopted solutions. Phases between dashed lines were excluded from the solutions and the residuals from the V light curve solution are shown

5.4 The absolute parameters of TX UMa

To derive the absolute parameters of TX UMa we used data from a variety of sources. For the masses we adopt the values derived from the spectroscopic orbit presented here corrected for non-Keplerian effects in combination with the inclination from the adopted light curve solution all with their quoted error. We likewise adopt the radii for the two components from the light curve solution with their quoted error. Since the error in the secondary's radius is derived from the error in the mass ratio it is probably a fair estimate of the true uncertainty. The error in the primary's radius given is assumed to be the formal error from the light curve solution but this may be an underestimate of the true uncertainty since it does not include errors due to uncertainties in the model used to solve the light curve and the effects of circumstellar material. For the effective temperature of the primary and the reddening of the system we adopt the value and error given by Cugier. For the secondary component we adopt the temperature quoted by Olson and adopt an error range sufficient to include the value derived from the light curve solution. This is the least certain of the quoted parameters both in terms of its value and its error and the true uncertainty in this value may be larger than the quoted value by a factor of two or three but in the absence of reliable data to the contrary we adopt the values shown. The bolometric corrections for the two components are generated by LIGHT2 and we assign an arbitrary error of $\pm 0^{m}.01$ to these values. Given that the various parameters used are based on

Table 5.3: Solutions to Koch's BV light curves of TX Uma. Values in bold type are fixed.

Parameter	Uncorrected		Corrected		Adopted
	B	V	B	V	
$< R_p >$	0.1704	0.1721	0.1755	0.1769	0.176
Formal error	0.0011	0.0012	0.0011	0.0012	0.001
$< R_s >$	**0.2684**[a]		**0.2641**[a]		0.2641
Formal error					0.0018[b]
$< T_p >$	**12900**		**12900**		12900
Formal error					300
$< T_s >$	5459	5286	5449	5291	5500
Formal error	64	37	66	38	200
Mass ratio(p/s)	**3.83**		**4.05**		4.05
Formal error					0.10
i (°)	83.21	83.79	83.78	83.28	83.5
Formal error	0.06	0.05	0.07	0.06	0.5
Secondary Albedo	0.75	0.65	0.79	0.69	0.75
Formal error	0.04	0.04	0.04	0.04	0.1

a: Fixed at Roche limit. b: From error in mass ratio

observations taken at a variety of epochs we adopt an error for the period of 0.0001d which reflects the variations in this parameter although this is still small enough to have a negligible effect on the total error in the absolute parameters. The absolute parameters with associated errors derived from these parameters are shown in Table 5.4.

5.5 Conclusion

The use of the cross correlation technique to obtain a spectroscopic mass ratio for the system TX UMa has again highlighted the need to confirm by means of spectroscopic observations

Table 5.4: Absolute parameters of TX UMa

	Primary	Secondary
Mass	$4.76 \pm 0.16\,M_\odot$	$1.18 \pm 0.04\ M_\odot$
Mean Radius	$2.825 \pm 0.04\,R_\odot$	$4.24 \pm 0.07\,R_\odot$
Mean Temperature	12900 ± 300	5500 ± 200
Log ($L/L_\odot$)	2.30 ± 0.04	1.17 ± 0.065
Mean log g	4.21 ± 0.02	3.25 ± 0.02
Absolute bolometric magnitude	-1.05 ± 0.11	1.77 ± 0.16

the mass ratios obtained photometrically for Algol systems. The large discrepancy found in the case of TX UMa is likely to be associated with the ambiguities inherent in the broad-band light curves for TX UMa noted by other workers. Further studies of TX UMa would benefit enormously from a high quality narrow- or intermediate-band light curve. This is primarily since these filter systems are not adversely affected by the large colour changes which occur during primary eclipse. In particular the UPS system (Heintz, 1989) appears to provide excellent results for Algol systems and is also well matched to the response of CCDs.

The results of Allbright and Richards' study of circumstellar matter in TX UMa is certainly valuable in that it should enable future studies to account for the effect of this material on the light curves and spectroscopy of TX UMa. The effect of circumstellar material is the Achilles heel of Algol studies since there is, as yet, no satisfactory method to include these effects, partly because it has not been clear where in these systems the material lies. This information has now become available for TX UMa and other systems. The inclusion of this information into future studies will no doubt not be easy, but will considerably improve our understanding of these systems.

Despite the difficulties associated with the solution of the light curve, data from a variety of sources and over a range of wavelengths have enabled the absolute parameters of the system to be established. A discussion of the evolutionary status of TX UMa can be found in Chapter 9.

Allbright G.E., Richards M.T., 1993. AJ, **414**, 830.

Cugier, H., 1989. A&A, **214**, 168.

Grewing M., Herczeg T., 1966. Zs. f. Ap., **64**, 256.

Heintz J.R.W., Van Gent R.H., 1989. In: Algols, p.257, Batten A.H. (ed.), Kluwer Academic Publishers, Dordrecht.

Hill G., Hutchings J.B., 1973. Ap&SS, **20**, 123.

Hiltner W.A., 1945. ApJ, **101**, 108.

Hric L. Komžík R., Grygar J., 1990. Ap&SS, **169**, 241.

Hric L. Komžík R., 1992. IBVS, **3698**.

Koch R.H., 1961. AJ, **66**, 230.

Kreiner J.M., Tremko J., 1980. Bull. Astron. Inst. Czechosl., **31**, 343.

Olson E.C., 1982. ApJ, **257**, 198.

Papoušek J., Tremko J., Vetešník M., 1985. Facultatis Scientiarum Naturalium Universitatis Purkynianae Brunensis, **15**, 5.

Pearce J.A., 1932. J.R. Astron. Soc. Can., **26**, 382.

Plavec M.J., Polidan R.S., 1976. In: Structure and evolution of close binary stars, p.289, P. Eggleton, S. Mitton, J. Whelan (ed.), Dordrecht,Reidel.

Rugumer H., 1931. Astron. Nachr., **242**, 179.

Schneller H., 1931. Astron. Nachr., **242**, 179.

Swensen P.R., McNamara D.H., 1968. PASP, **80**, 192.

Chapter 6

RU Ursae Minoris

6.1 Introduction

Bell et al. (1993) have obtained a high-precision R-band light curve of RU UMi (V=10.0–10.9, α(2000.0) =13h37m40s, δ = +69°47.7,P=0.5249 days) as part of a programme to study F–K type binary systems approaching contact for the first time . Their analysis of this light curve led them to the conclusion that the system was very close to a semi-detached configuration. However, of the range of solutions presented, including semi-detached configurations, all give good solutions to the light curve. We therefore included RU UMi in our observing programme in order to determine a spectroscopic mass ratio for the system. This has enabled us to draw some more definite conclusion about the configuration of RU UMi and to obtain preliminary absolute parameters for the system.

6.2 Measurement of the radial velocities

We obtained 14 spectra of RU UMi with the Intermediate Dispersion Spectrograph on the 2.5m Isaac Newton Telescope. Details of the observations and reductions can be found in Chapter 2. The phase coverage of the spectra is poor but sufficient to obtain a mass ratio for the system. We also obtained spectra of HR 1380 and HR 1620, both A7V stars, for use in the cross correlation process. From measurements of the cross correlation functions (CCFs) of these spectra with radial velocity standard stars we derive radial velocities for these stars of 32.6 $\mathrm{km\,s^{-1}}$ and 33.8 $\mathrm{km\,s^{-1}}$ respectively. A 40Å window centered on each of the hydrogen lines is excluded from the cross correlation process since their great width broadens the CCF intolerably. To measure the radial velocity of the primary component we used HR 1380 as a

template. All the CCFs showed a large peak corresponding to the primary component with very little noise in the vicinity of this peak. To measure this peak we formed a standard profile from the CCF of HR 1620 with the HR 1380 as a template. This standard profile was then used to measure the radial velocity of the primary by using a least squares fit. The quality of the fit was slightly better than that achieved by using Gaussian profiles. In general the CCF's also showed a very weak peak near the expected position for the secondary. This peak was sufficiently well separated from the primary peak to be measured separately using a single Gaussian profile, the exception being the peaks seen in the CCFs of the two spectra taken a phases ~ 0.15. These CCFs were measured using a simultaneous fit to the primary and secondary peaks using two Gaussian profiles. In order to be sure that the peak measured was due to the secondary component, we formed CCFs using HR 1620 as a template and measured the supposed secondary peak in the same fashion. Only those measurements which agreed to within $2\,\mathrm{km\,s^{-1}}$ were retained in the subsequent analysis. The measured radial velocities are shown in Table 6.1 under the heading "Uncorrected". We also attempted to measure the radial velocity of the secondary using template spectra of later type stars but the increased level of noise in the region of the secondary peak made this impractical.

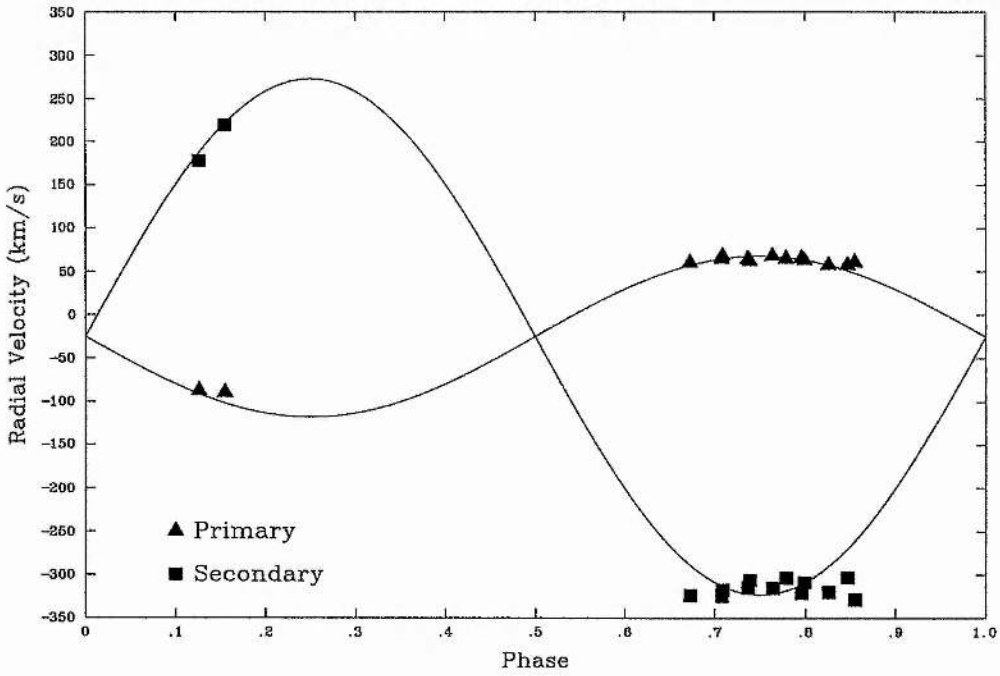

Figure 6.1: Radial velocity measurements for RU UMi and the adopted spectroscopic orbit. The radial velocity measurements have been corrected for non-Keplerian effects assuming the primary component has a convective atmosphere.

Table 6.1: Measured radial velocities for RU UMi in $\mathrm{km\,s^{-1}}$. The phase is calculated from the ephemeris of Bell et al. (HJD min I=2448695.43185 + 0.52492575E)

HJD-2400000	Phase	Uncorrected		Radiative		Convective	
		RV_{pri}	RV_{sec}	RV_{pri}	RV_{sec}	RV_{pri}	RV_{sec}
49027.557	0.709	65.5	—	69.6	—	67.8	—
49027.573	0.739	58.7	-292.5	62.1	-312.5	61.8	-306.3
49027.594	0.779	61.8	-293.7	62.7	-307.3	64.5	-303.6
49027.604	0.799	61.1	-301.4	60.2	-311.5	62.9	-309.1
49027.629	0.847	59.1	-300.1	52.9	-304.1	57.4	-303.4
49027.776	0.126	-92.2	175.5	-83.0	177.9	-87.4	177.6
49027.791	0.155	-91.1	215.9	-85.2	220.0	-89.6	219.4
49029.638	0.673	58.9	—	63.0	—	60.0	—
49029.656	0.708	62.3	-310.2	66.4	-332.5	64.6	-325.1
49029.672	0.737	61.1	-301.3	64.6	-321.4	64.2	-315.2
49029.686	0.764	64.7	-304.0	66.9	-320.2	67.8	-315.5
49029.702	0.796	63.0	-313.1	62.4	-323.8	65.0	-321.1
49029.718	0.826	57.4	-315.4	53.6	-321.5	57.4	-320.3
49029.734	0.855	62.9	—	55.9	—	60.5	—

6.2.1 Spectroscopic orbit

Given the poor phase coverage of the radial velocity data, we decided to solve the primary and secondary orbits simultaneously. We assumed a circular orbit and the free parameters in the least squares solution were the primary and secondary semi-amplitudes and the systemic velocity. All the data were weighted equally. The solution to the orbit is shown in Table 6.2 under the heading "Uncorrected".

Since the configuration of RU UMi is extremely close to contact the ellipticity of the components and their mutual heating (reflection effect) will introduce distortions to the radial velocity data. These non-Keplerian effects can be corrected for using LIGHT2 by calculating the intensity weighted mean of the projected rotational velocity at the required phases using an appropriate light curve solution. Table 6.2 shows two spectroscopic orbit solutions including corrections for non-Keplerian effects derived from the light curve solutions assuming either a radiative or a convective atmosphere for the primary component as described below. Also shown is the orbit of Okazaki et al. (1988) for comparison. The corrected radial velocities are shown in Table 6.1 under the headings "Radiative" and "Convective". The corrected radial velocities and adopted orbit assuming a convective atmosphere for the primary component are shown in Fig. 6.1.

Table 6.2: The spectroscopic orbit of RU UMi

	Uncorrected	Radiative	Convective	Okazaki et al.
$\gamma/\,\mathrm{km\,s^{-1}}$	-25.1 ± 5.3	-25.0 ± 4.6	-25.2 ± 4.8	-12.0 ± 3.1
$K_p/\,\mathrm{km\,s^{-1}}$	91.6 ± 2.9	90.9 ± 2.6	92.8 ± 2.6	91.9 ± 4.2
$K_s/\,\mathrm{km\,s^{-1}}$	290.3 ± 5.8	304.3 ± 5.1	298.4 ± 5.3	—
$m_p \sin^3 i/\,\mathrm{M_\odot}$	2.31 ± 0.09	2.59 ± 0.09	2.49 ± 0.09	—
$m_s \sin^3 i/\,\mathrm{M_\odot}$	0.73 ± 0.03	0.78 ± 0.03	0.78 ± 0.03	—
$(a_p + a_s) \sin i/\,\mathrm{R_\odot}$	3.96 ± 0.07	4.10 ± 0.06	4.06 ± 0.06	—
m_p/m_s	0.315 ± 0.01	0.30 ± 0.01	0.31 ± 0.01	—

6.3 The solution of the light curves

For the solution of the R-band light curve of Bell et al. we adopted the effective temperature for the primary given by Bell et al. (7200±200K). We used the light curve solution of Bell et al. for a primary with a radiative atmosphere and q=0.314 to generate the first approximation to the required radial velocity corrections and re-solved the spectroscopic orbit to obtain a new mass ratio. We are grateful to Steve Bell for providing us with his observations in a convenient format as well as the light curve in the form of 200 normal points. We then attempted two solutions to the light curve using LIGHT2 and the 200 normal points, one with a radiative atmosphere for the primary, and one with a convective atmosphere. Free parameters in the solutions were: the polar radius of both components relative to the semi-major axis of the combined orbit, r_p and r_s; the effective temperature of the cool component at its pole (although the mean temperature is quoted here) and the inclination of the orbital plane, i. These both showed the system to be in a semi-detached configuration and gave slightly different values for the various free parameters. The two solutions therefore imply slightly different radial velocity corrections and thus slightly different mass ratios. The corrected radial velocities and spectroscopic orbit solutions are shown in Tables 6.1 and 6.2 respectively. Since there is little to choose between the quality of the light curve solutions for the two types of primary atmosphere, both are presented here.

Our initial attempts to solve the light curve employed the standard values for the atmospheric parameters of the secondary component i.e. a gravity darkening exponent, $\beta = 0.08$ and an albedo, $\alpha = 0.5$. However the depth of primary eclipse predicted by these solutions were too low by $\sim 0^{\mathrm{m}}.1$ resulting in a (relatively) large value for σ. In order to remove this discrepancy we tried varying the atmospheric parameters of both stars. The most successful approach for both mass ratios was to include the gravity darkening of the secondary component as a free parameter in the light curve solution. The quality of the fit was also slightly improved by also allowing the albedo to vary, but it is the gravity darkening that has the greatest effect on the quality of the light curve solution. These solutions are also shown in Table 6.3. The values for

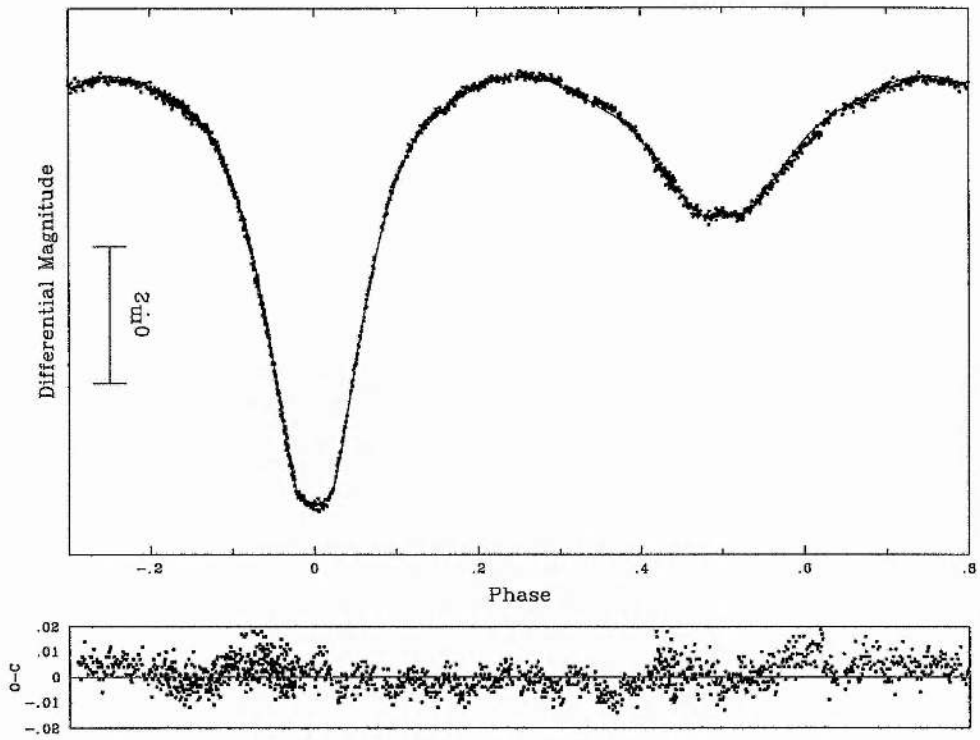

Figure 6.2: The R light curve of RU UMi and the adopted solution. The solution assumes a convective atmosphere for the primary component

the secondary's gravity darkening found to give the best solutions are abnormally high. We believe this is due to the combination of the gravity darkening and reflection effect mimicking the effects of one or several cool spots near the "back end" of the cool component. A comparison of the intensity distribution over the surface of the cool component predicted by the two solutions (normal and abnormal gravity darkening) shows a difference of ~30% in the flux from the back end of the cool component relative to the side of the star. The R-band observations and adopted solution assuming a convective atmosphere for the primary component are shown in Fig 6.2.

The absolute parameters derived from the two light curve solutions and the corresponding spectroscopic orbits are shown in Table 6.4. We have not attempted to estimate the uncertainties in these values since the errors derived from a single light curve solution are likely to be misleading. In any case, until it can be established whether the primary component has a radiative or convective atmosphere, this will continue to be the main source of uncertainty.

Table 6.3: Light curve solutions for RU UMi. Values in bold type are assumed

	Radiative	Convective
r_p	0.4257 ± 0.0004	0.4347 ± 0.0005
r_s	0.2611 ± 0.0014^a	0.2635 ± 0.0014^a
$\langle T_p \rangle$/K	**7200**	**7200**
$\langle T_s \rangle$/K	4781 ± 41	5067 ± 43
m_s/m_p	**0.30**	**0.31**
$i/^\circ$	83.76 ± 0.18	83.14 ± 0.20
α_p	**1.0**	**0.5**
β_p	**0.25**	**0.08**
α_s	0.64 ± 0.03	0.67 ± 0.04
β_s	0.365 ± 0.03	0.34 ± 0.03
σ/mags	0.0038	0.0041

a: Star constrained to Roche lobe, error derived from error in mass ratio

Table 6.4: Absolute parameters of RU Umi

	Radiative		Convective	
	Primary	Secondary	Primary	Secondary
Mass	$2.61\,M_\odot$	$0.78\,M_\odot$	$2.45\,M_\odot$	$0.76\ M_\odot$
Radius	$1.84\,R_\odot$	$1.15\,R_\odot$	$1.86\,R_\odot$	$1.13\ R_\odot$
M_V	2.46	5.66	2.44	5.31

6.4 Conclusion

Given the poor phase coverage of the spectroscopy presented here the absolute parameters derived can only be regarded as preliminary. However it seems safe to conclude that RU UMi is a semi-detached system. It is noticeable that a semi-detached configuration does not give the best fit to the light curve when the parameters used to model the atmospheres of the component stars are set to their standard values. This is an example of the confusion that can arise when the models used to describe eclipsing binary systems are pushed to their limits. This is particularly true in the case of the light curve of Bell et al. for RU UMi where the system is very close to a contact configuration and the light curve is of extremely good quality. Possible sources of problems are: inaccurate modeling of the reflection effect; the presence of star spots and, given that the system is semi-detached, the effects of any mass transfer that may be present.

The positions of both components of RU UMi are shown in the Hertzsprung–Russell diagram (HRD) and mass-radius plane in Fig. 6.3 and Fig. 6.4 respectively. It can be seen that RU UMi conforms to the definition of an Algol system in that it is semi-detached and comprises a main sequence primary and a less massive star that appears to have evolved away from the main sequence. The distinguishing feature of RU UMi is the proximity of the two components. One possible evolutionary scenario for RU UMi is that it is the result of case B evolution in which a magnetic stellar wind has resulting in drastic angular momentum loss (AML). If this were the case then we may expect the AML to continue, in which case a contact configuration would seem inevitable. This will be aided by the evolutionary expansion of the primary but also countered by any mass transfer that may be present. A long term period study may help to find where the balance of these effects lies.

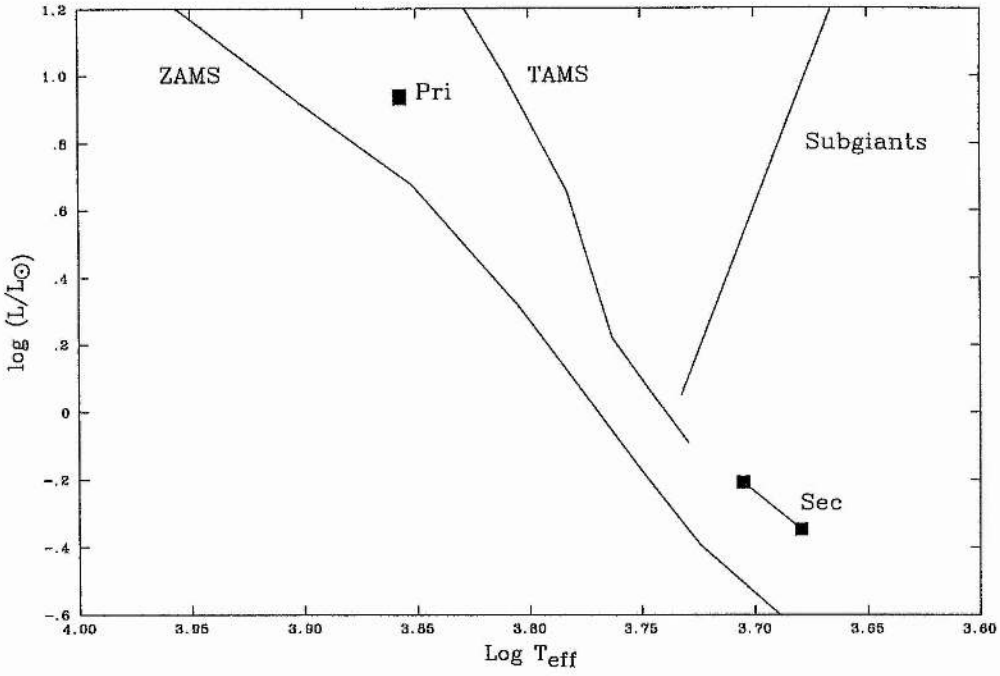

Figure 6.3: RU UMi in the Hertzsprung–Russell diagram. The radiative and convective solutions are both plotted and connected by a line

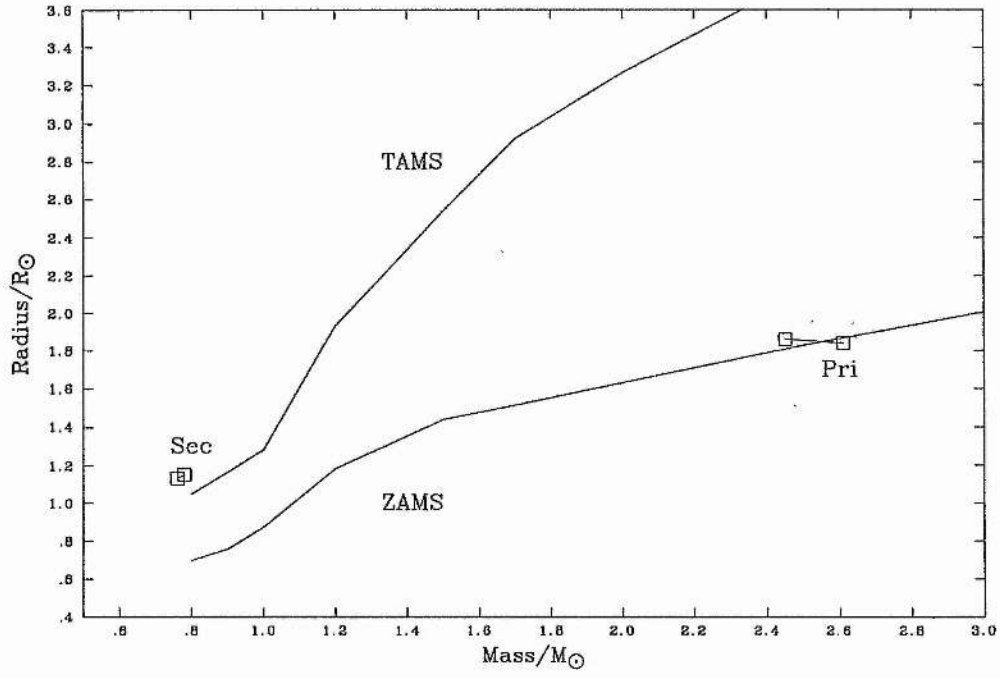

Figure 6.4: RU UMi in the mass–radius plane. The radiative and convective solutions are both plotted and connected by a line

Chambliss C.R., 1982. PASP, **94**, 926.

Hill G., 1982. Publ. Dom. Astrophys. Obs., **16**, 59.

Bell S.A., Hilditch R.W., Edwin R.P., 1993. MN, **260**, 478.

Hill G., Fisher W.A., 1986. Publ. Dom. Astrophys. Obs., **16**, 193.

Popper D.M., 1980. ARA&A, **18**, 115.

Okazaki A., Nakamura Y., Yamasaki A., 1988. PASJ, **40**, 79.

Chapter 7

AF Geminorum

7.1 Introduction

AF Gem (HD 210892, P=1.2435 days, α(2000.0)=6h50m39s, δ = +21°21.9′, B9.5V+G0III-IV, V=10.54–11.83) is a little-studied eclipsing binary star, the main study to date being that of Chambliss (1982). He presents UBV light curves with almost complete phase coverage and reports the discovery of a faint companion star 2" North of AF Gem and approximately four magnitudes fainter. He concludes that AF Gem "appears to be a normal semi-detached system". Spectroscopic observations of AF Gem were obtained with the 2.5m Isaac Newton telescope at the Observatorio del Roque de los Muchachos on the island of La Palma. Details of the observations and reduction procedures can be found in Chapter 2. The spectroscopic orbit derived from 17 spectra is presented here together with new solutions to the light curves of Chambliss. From the light curve solution we obtain corrections for non-Keplerian effects in the spectroscopic orbit and absolute parameters for both components.

7.2 Radial velocity measurements

To measure of the radial velocities of the primary component of AF Gem we formed the CCFs of the spectra using a DAO 1.2m coudé spectrum of Vega (A0Va, -14±1.5, Khallesseh and Hill, 1991) as a template. A 40Å window around the Balmer lines was excluded from all the CCFs since their great width broadens the profiles unacceptably. The CCFs produced showed a clearly defined peak corresponding to the primary component and a weaker peak corresponding to the secondary component. We measured the radial velocity of the primary automatically within VCROSS using a parabola fitted by least squares to the top third of the profile. The resultant

Table 7.1: Measured radial velocities for AF Gem in $\mathrm{km\,s^{-1}}$. The phase is calculated from the ephemeris of Chambliss (HJD min I= $2427162.3095 + 1.24350348E - 1.71 \times 10^{-10}E^2$)

HJD-2400000	Phase	Uncorrected			Corrected	
		RV_{pri}	RV_{sec}		RV_{pri}	RV_{sec}
49026.498	0.775	104.97	-194.36		105.09	-199.79
49026.514	0.787	109.62	-192.20		109.61	-201.01
49026.539	0.808	112.66	-186.04		112.49	-193.81
49027.414	0.511	24.20	—		24.23	—
49028.345	0.260	-56.96	284.87	*	-57.36	298.00
49028.359	0.271	-62.41	275.90	*	-62.85	290.83
49028.375	0.284	-57.74	275.08	*	-58.19	290.94
49028.389	0.295	-51.85	268.57	*	-52.30	285.09
49028.407	0.309	-46.63	262.17		-47.07	279.39
49028.421	0.321	-46.16	249.81		-46.58	267.30
49029.535	0.217	-49.63	253.10		-49.78	261.89
49029.550	0.229	-49.43	231.76		-49.67	240.55
49029.565	0.241	-57.56	243.23		-57.88	253.34
49029.581	0.254	-59.32	242.52		-59.70	254.66
49029.595	0.265	-52.11	241.19		-52.53	255.26
49029.610	0.277	-66.23	242.77		-66.68	258.21
49029.625	0.289	-52.65	257.28		-53.10	273.47

spectroscopic orbit was not appreciably different for any of the combinations of template star, type of profile and manual or automatic fitting with which we experimented but automatic fitting has the advantage of objectivity. The results are shown in Table 7.1 under the heading "Uncorrected".

To measure the radial velocity of the secondary component we used a DAO 1.2m coudé spectrum of HD 211284, a G8IV star for which we adopted a radial velocity of $-104.5\,\mathrm{km\,s^{-1}}$ from measurements of the CCF using DAO spectra of radial velocity standard stars as templates. The CCFs showed peaks corresponding to both the primary and secondary components as well as some spurious features. The peak corresponding to the secondary appeared well separated from the primary peak and any spurious features and so we measured the peak using a single Gaussian profile fitted by least squares to as much of the peak as appeared unaffected by noise. The results are also shown in Table 7.1. It is clear that there is a difference between the measured radial velocities for the secondary component on the dates HJD 2449028 and HJD 2449029 of approximately $30\,\mathrm{km\,s^{-1}}$despite the fact that they cover the same range in orbital phase. No such difference is seen in the primary radial velocities and this difference is seen independently of the template spectrum used to form the CCFs. It should be noted

Table 7.2: The spectroscopic orbit of AF Gem.

	Uncorrected	Corrected
$\gamma(\mathrm{km\,s^{-1}})$	27.2 ± 1.4	27.0 ± 1.4
$K_1(\mathrm{km\,s^{-1}})$	83.2 ± 1.5	83.4 ± 1.45
$K_2(\mathrm{km\,s^{-1}})$	230.7 ± 3.7	243.6 ± 4.3
e	**0.000**	**0.000**
HJD $T_+ - 2449026$	0.487 ± 0.009	0.487 ± 0.009
P/days	**1.24350**	**1.24350**
Mass ratio	2.77 ± 0.07	2.92 ± 0.07

that the spectra marked with an asterisk were taken with a slit width slightly larger than the other spectra (1.11″as opposed to 0.88″). The only other noticeable difference between the two nights was the number of secondary peaks in the CCF's that could be described as "poor" e.g. asymmetric or affected by spurious features, i.e. difficult to measure. There is only one such in the first six spectra and three out of seven for the second night of data. However, the radial velocities measured from these peaks are not noticeably different from those measured from other, better defined peaks. We would expect the effect of using a wider slit to be a widening of the lines in the spectra and thus in the peaks in the CCFs. This effect could introduce blending problems and result in the magnitude of the measured radial velocities being too small, in this case less positive. However the measured radial velocities for spectra taken with a wide slit are *more* positive and so this is certainly not the cause of the problem. It would therefore appear that we have observed real changes in the system that have occurred over the course of one day and have affected the measured radial velocities for the secondary component. Speculation as to what might cause these changes can be found later in this chapter.

Also shown in Table 7.1 are the radial velocities for both components corrected for non-Keplerian effects using corrections derived from the LIGHT2 solutions to the UBV light curves of Chambliss presented below. For the solution of the spectroscopic orbit we assumed a circular orbit and first solved for the the following parameters using the primary radial velocities only: the systemic velocity, γ; the semi-amplitude of the primary orbit, K_1 and the time of maximum positive velocity for the primary, T_+. We then fixed γ and calculated T_+ for the secondary from this solution before solving the secondary radial velocities for K_2 only. The solution for both corrected and uncorrected radial velocities are shown in Table 7.2.

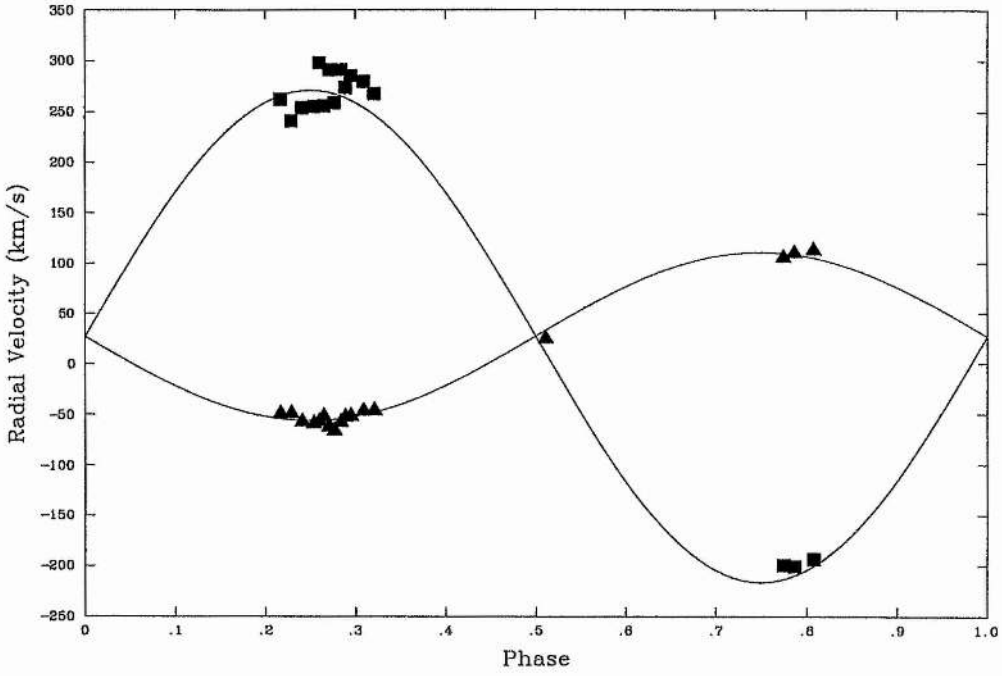

Figure 7.1: Radial velocity measurements of AF Gem and the adopted spectroscopic orbit. The radial velocity measurements have been corrected for non-Keplerian effects

7.3 The light curves and their solution

7.3.1 The effective temperature of the primary component

To establish the effective temperature of the primary component we compared an IDS spectrum of AF Gem obtained near secondary eclipse to IDS spectra of stars of known spectral class. We find that the primary component is a B9.5V star. From Lang's (1980) calibration we derive an effective temperature for the primary component of 10000 ± 500K where the error reflects the standard error for spectral classification of one subtype. IDS spectra taken at other phases give the same result.

7.3.2 Solution of the light curve

To derive absolute parameters we have used the UBV light curves of Chambliss (1976) and the program LIGHT2 (Hill, 1979; Hill and Rucinski, 1993). The light curves are not complete in the phase coverage – the ingress of both eclipses are not covered – and appear to show variations from night-to-night. Chambliss states that although the light curves were obtained with two sets of equipment "it was found that the both sets of observations could be combined without

transformations". It therefore seems likely that, in common with other Algol systems, AF Gem shows intrinsic variability. This is noticeable around the upper section of the egress branch of primary eclipse (phase $\sim$ 0.1), particularly in the V light curve, and so may be a consequence of a variable gas stream due to mass transfer from the secondary component. We attempted to solve light curves assuming a detached configuration but only the V light curve would converge to a reasonable solution. However, the quality of the fit was equally good for a semi-detached configuration so we therefore assumed a semi-detached configuration for subsequent solutions. Free parameters in the solution were then the inclination of the system, the polar radius of the primary relative to the semi-major axis of the orbit and the temperature of the secondary component at its pole. To match the out-of-eclipse variations, we also included the albedo of the secondary component as a free parameter in the solution. The solution of the light curves for the uncorrected and corrected values of the mass ratio are shown in Table 7.3. Since the solution of the light curve is dependent upon the mass ratio, and the corrections to the mass ratio are calculated from the light curve solution, an iterative procedure is used to find a consistent solution for both photometric and spectroscopic data. In this case convergence is achieved in only three iterations. The light curve and solution for the corrected mass ratio are shown in fig. 7.2

7.4 The absolute parameters of AF Gem

To calculate the absolute parameters and their errors for AF Gem we generated a light curve using the mean values for the free parameters shown in Table 7.3. We then used the mean radii, mean effective temperatures and bolometric corrections from this solution with the errors shown in Table 7.3. Other parameters are the reddening and combined V magnitude, for which we use Chambliss' value with an arbitrary 50% error in the reddening, and the orbital parameters from Table 7.2. The results are shown in Table 7.4.

7.5 Conclusion

The variability of the radial velocity measurements for the secondary component presented here appears to be a feature intrinsic to AF Gem but further observations are needed to confirm the reality of this variability. A possible cause for such rapid changes in the appearance of the secondary component may be a combination of two effects seen in other secondaries of Algol systems, chromospheric activity and non-synchronous rotation. The chromospheric activity of Algol secondaries is now well established, characteristic signals having been observed at X-ray, infrared, optical and radio wavelengths (Richards & Albright, 1993). Evidence for non-synchronous rotation has been found by Khallesseh and Hill (1991) in the case of TV Cas. To

Table 7.3: Solutions to Chambliss' UBV light curves of AF Gem. Values in bold type are fixed.

Parameter	Uncorrected			Corrected			Adopted
	U	B	V	U	B	V	
r_p	0.3155	0.3190	0.3237	0.3132	0.3158	0.3245	0.3175
Formal error	0.0011	0.0022	0.0034	0.0007	0.0031	0.0035	0.006
r_s		**0.2747**[a]			**0.2708**[a]		0.2708
							± 0.002[b]
$< T_p >$ /K		**10000**			**10000**		10000
							± 500
$< T_s >$ /K	5990	6000	5850	5910	5800	5770	5830
Formal error	58	90	90	70	100	90	100
Secondary Albedo	0.73	0.58	0.58	0.93	0.83	0.70	0.82
Formal error	0.11	0.13	0.13	0.13	0.13	0.13	0.11
Mass ratio(p/s)		**2.77**			**2.92**		2.92
Formal error							$\pm$ 0.07
Inclination (°)	87.9	87.3	86.2	88.0	87.3	86.8	87.4
Formal error	0.3	0.4	0.5	0.15	0.5	0.5	0.6
σ(mags)	0.0173	0.0205	0.0222	0.0189	0.0208	0.0215	—

a:Fixed at Roche limit. b:From error in mass ratio

Table 7.4: Absolute parameters of AF Gem

	Primary	Secondary
Mass	$3.37 \pm 0.11\,M_\odot$	$1.155 \pm 0.038\,M_\odot$
Mean Radius	$2.61 \pm 0.06\,R_\odot$	$2.324 \pm 0.036\,R_\odot$
Mean Temperature	$10000K \pm 500K$	$5860K \pm 100$
Log ($L/L_\odot$)	1.78 ± 0.75	0.75 ± 0.03
Mean log g	4.13 ± 0.025	3.77 ± 0.02
Absolute bolometric magnitude	0.23 ± 0.22	2.82 ± 0.08

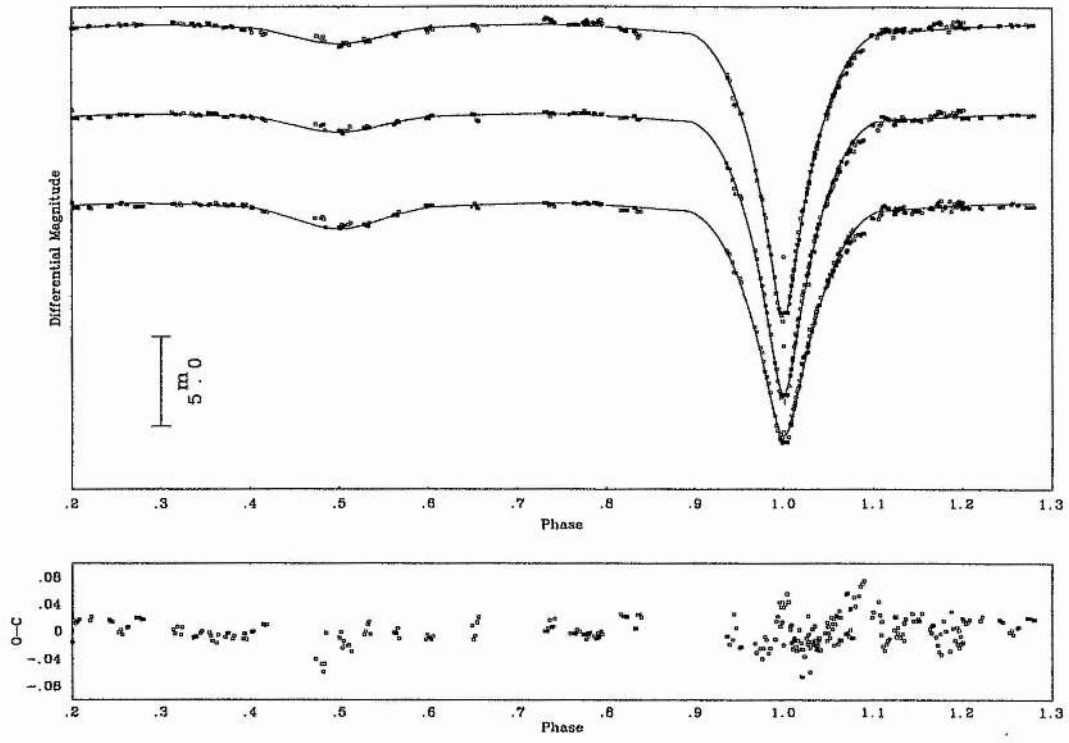

Figure 7.2: The UBV light curves of AF Gem and the adopted solutions. Residuals from the V light curve solution are also shown.

investigate the effects of spot activity on the secondary we generated radial velocity corrections for the secondary component ignoring the reflection effect. This produced an overall drop in effective temperature of between 100 and 200K at quadrature resulting in radial velocity corrections up to $\sim 15\,\mathrm{km\,s^{-1}}$ lower than expected. Therefore if large scale spot activity is present on the secondary of AF Gem it may well produce the required changes in observed radial velocity. However the timescale for the appearance and disappearance of star spots is days as opposed to hours (Maran, 1992; p. 876). We therefore require the secondary to rotate non-synchronously to enable the supposed spot or spots to rotate into or out of view. This scenario is highly speculative and firstly requires confirmation of the radial velocity variability as well as measurement of the secondary star's rotational velocity before serious further consideration.

Comparison of AF Gem with the evolutionary models of De Greve (1993) suggests that AF Gem evolved through case B from a system with an initial mass ratio nearer to 0.6 than 0.9. This is evident both from the position of the mass accreting star on the mass–radius plane (fig. 10 of that paper) and the period of AF Gem compared to the minimum period achieved by the lower mass systems. For example the period of the $4\,M_\odot + 2.4\,M_\odot$ and $4\,M_\odot + 3.6\,M_\odot$ models at minimum luminosity are 1.97d and 4.33d respectively. The period of the $4\,M_\odot + 2.4\,M_\odot$ model is the lowest achieved by any of the models but this still exceeds the period of AF Gem (1.24d) despite the fact that the total mass of the model system during the slow mass transfer phase is

similar to that of AF Gem ($4.7\,M_{\odot}$for the model, 4.53 ± 0.12 for AF Gem). This difference is probably due to the rapid mass transfer phase in AF Gem being different to the one assumed in the model e.g. the value for the angular momentum mass loss adopted for the model may be an underestimate. Further conclusions must await detailed modeling of the evolution of AF Gem which will be possible now that the absolute parameters presented here are available.

Chambliss C.R., 1982. PASP, **94**, 926.

De Greve J.P., 1993. A&AS, **97**, 527.

Hill G., 1979. Publ. Dom. Astrophys. Obs., **15**, 297.

Hill G., Rucinski S.M., 1993. In: Light curve modeling of eclipsing binary stars., p.135, Milone E.F. (ed.), Springer-Verlag,Berlin.

Khalesseh B., Hill G., 1991. A&A, **244**, 75.

Lang K.R., 1980. Astrophysical data: Stars and Planets, Springer–Verlag.Berlin

Maran P. (ed.), 1992. The Astronomy and Astrophysics Encyclopedia, C.U.P..

Richards M.T., Albright G.E., 1993. ApJ Suppl. Ser., **88**, 199.

Chapter 8

HU Tauri

8.1 Introduction

Despite being one of the brighter eclipsing binary systems, HU Tau (HD 29365, P=2.0563 days $\alpha(2000.0)$ =04h38m15.80s, δ =+20°41′05.3″, V=5.87–6.8, B8V+G2) seems not to have aroused much interest in observers compared to fainter systems such as RW Tau and TX UMa. This is principally due to its awkward period. Light curves of the system have been published by Parthasarathy & Sarma (1980) and Melendo (1985) but neither of these is satisfactory in terms of their phase coverage. Giuricin & Mardirossian (1981) from their analysis of the partial B and V light curves of Parthasarathy & Sarma in conjunction with the mass function of Mammano et al. (1967) find that the system is detached but that the secondary is considerably oversized and overluminous for its spectral type – estimated to be early K. Light curves with almost complete phase coverage have been obtained by Tümer & Kurutac (1979) but unfortunately the observations are not available. However, Ito (1988) has obtained complete B and V light curves which he has generously made available to us. A solution to these light curves have since been presented by by Nakamura et. al (1994). They find HU Tau to be a normal semi-detached Algol-type binary star.

The presence of a detached sub-giant in a seemingly normal Algol system is extremely curious. In order to try and confirm the detached nature of HU Tau we obtained over 40 spectra of HU Tau with the Richardson-Brealey Spectrograph (RBS) attached to the 0.5m Leslie Rose Telescope (LRT) at the St Andrews University Observatory during the interval August 1992 to December 1993. These are used in combination with 29 spectra obtained with the 1.2m DAO coudé spectrograph to derive spectroscopic orbits for both components of HU Tau and thus to determine directly and for the first time the mass ratio for the system. The instruments and the data reduction are described in Chapter 2. We also present analysis of the light curves from

Ito using LIGHT2 to derive absolute parameters for the system. We conclude that the system is indeed semi-detached, and have been able to derive much improved absolute parameters for this system.

8.2 The spectroscopic orbit

8.2.1 Radial velocity measurements

To measure the radial velocity of the primary component we formed the CCFs of all the spectra using a DAO coudé spectrum of Vega (A0Va, rv= $-14\pm1.5\,\mathrm{km\,s^{-1}}$, Khalesseh & Hill, 1991) as a template. A 40Å window around the Balmer lines was excluded from all the CCFs since their great width broadens the profiles unacceptably. The cross correlation was performed over the spectral region $\lambda\lambda$ 4000–4509Å. The CCFs produced showed a clearly defined peak corresponding to the primary component and a weaker peak corresponding to the secondary component. The quality of the spectra used shows wide variation. This is reflected in the definition of the peaks in the CCFs due to both the primary and secondary components. We therefore measured the radial velocity of the primary automatically within VCROSS using a parabola fitted by least squares to the top third of the profile. This method has the advantage of being both more objective and less tedious than manual fitting of profiles. It should be noted that the method used to measure the primary peak e.g. type of profile, template star, manual or automatic fitting; has only a small effect on the measured radial velocities.

To measure the radial velocity of the secondary component we formed the CCFs of all the spectra using a DAO coudé spectrum of HD 154417, a radial velocity standard star (G0V, rv= -17.4$\,\mathrm{km\,s^{-1}}$). In general, the CCFs showed a large peak corresponding to the primary component, a weaker peak due to the secondary component and, for the lower quality spectra, a few spurious features. For all spectra which showed a peak due to the secondary sufficiently well separated from the primary peak and any spurious features we measured the radial velocity using a Gaussian profile fitted using a least-squares method to as much of the profile as appeared unaffected by noise. The measured radial velocities for both components are shown in Table 8.1 under the heading "Uncorrected".

8.2.2 The spectroscopic orbit

To find the spectroscopic orbit for HU Tau we solved the data for the primary and secondary components separately. All data were weighted equally except those measurements of a component during eclipse. We used a least squares method to solve each set of data for the systemic

Table 8.1: Measured radial velocities for HU Tau in $km\,s^{-1}$. The phase is calculated from the ephemeris of Ito (HJD min I= 2446485.9967+2.0563056E). Letters in the sixth column signify LRS spectra (L) and DAO spectra (D).

HJD-2400000	Phase	Uncorrected					Corrected	
		RV_{pri}	Wt	RV_{sec}	Wt		RV_{pri}	RV_{sec}
48914.608	0.0556	-20.92	0	—	0	L	-20.91	—
48914.681	0.0911	-35.75	1	—	0	L	-35.73	—
48914.708	0.1043	-35.32	1	—	0	L	-35.29	—
48914.730	0.1150	-46.72	1	118.26	1	L	-46.69	119.56
48914.753	0.1261	-44.43	1	116.05	1	L	-44.40	117.60
48914.776	0.1373	-45.20	1	126.12	1	L	-45.16	128.00
48918.588	0.9911	1.19	0	-25.87	1	L	1.19	-25.97
48919.598	0.4823	-20.61	1	9.08	1	L	-33.04	2.99
48919.632	0.4988	-11.18	1	—	0	L	-3.02	—
48919.661	0.5129	-3.53	1	236.48	0	L	4.63	242.68
48919.684	0.5241	-10.86	1	—	0	L	-2.70	—
48925.522	0.3632	-51.60	1	167.65	1	L	-51.66	180.90
48929.638	0.3649	-45.00	1	—	0	L	-45.06	—
48939.632	0.2250	-69.23	1	203.03	1	L	-69.19	211.68
48940.599	0.6953	44.00	1	-214.82	1	L	44.01	-228.77
48940.648	0.7191	61.84	1	-235.56	1	L	61.82	-248.87
48946.610	0.6185	29.74	1	—	0	L	29.81	—
48955.423	0.9043	24.56	1	-102.74	1	L	24.54	-103.82
48955.464	0.9243	1.15	0	-76.69	1	L	1.13	-77.48
48955.513	0.9481	-4.92	0	-49.99	1	L	-4.93	-50.55
48955.580	0.9807	3.98	0	-24.33	1	L	3.98	-24.55
48968.376	0.2035	-72.16	1	220.19	1	L	-72.11	226.62
48968.453	0.2409	-70.77	1	222.08	1	L	-70.74	232.64
48968.495	0.2614	—	0	199.67	1	L	0.02	212.22
48968.529	0.2779	-69.54	1	—	0	L	-69.54	—
48968.580	0.3027	-75.22	1	205.21	1	L	-75.24	219.15
48975.476	0.6563	45.72	1	-209.05	1	L	45.77	-221.92
48975.514	0.6748	47.65	1	-220.80	1	L	47.68	-234.41
48975.562	0.6981	57.73	1	-203.54	1	L	57.74	-217.45
48976.466	0.1377	-51.42	1	147.78	1	L	-51.38	149.66
48976.517	0.1625	-60.21	1	181.23	1	L	-60.17	184.32
48976.582	0.1941	—	0	179.98	1	L	0.05	185.51
48977.500	0.6406	40.75	1	-216.82	1	L	40.81	-228.67

Table 8.1: Measured radial velocities for HU Tau cont.

HJD-2400000	Phase	Uncorrected					Corrected	
		RV_{pri}	Wt	RV_{sec}	Wt		RV_{pri}	RV_{sec}
48977.589	0.6839	53.04	1	-223.91	1	L	53.06	-237.82
49041.322	0.6778	40.79	1	-207.56	1	L	40.82	-221.27
49329.355	0.7508	52.83	1	-219.32	1	L	52.79	-230.83
49329.397	0.7713	55.15	1	-230.67	1	L	55.11	-239.71
49329.445	0.7946	53.22	1	-212.96	1	L	53.17	-219.58
49329.467	0.8053	59.01	1	-209.44	1	L	58.96	-215.00
49329.493	0.8180	46.61	1	-216.78	1	L	46.56	-221.28
49329.516	0.8291	48.01	1	-199.58	1	L	47.96	-203.23
48213.700	0.1977	-54.63	1	205.27	1	D	-54.58	211.12
48213.730	0.2123	-65.05	1	209.75	1	D	-65.01	217.03
48213.759	0.2264	-67.89	1	211.68	1	D	-67.85	220.44
48213.788	0.2405	-68.73	1	218.08	1	D	-68.70	228.52
48213.818	0.2551	-61.85	1	214.90	1	D	-61.83	226.95
48213.848	0.2697	-59.23	1	214.72	1	D	-59.22	227.63
48213.877	0.2838	-60.62	1	209.86	1	D	-60.62	223.32
48213.931	0.3101	-56.94	1	191.10	1	D	-56.96	205.13
48213.964	0.3261	-55.51	1	184.34	1	D	-55.55	197.96
48214.007	0.3470	-51.97	1	178.34	1	D	-52.02	191.11
48214.036	0.3611	-43.16	1	192.28	1	D	-43.22	204.25
48214.062	0.3738	-44.07	1	167.79	1	D	-44.13	178.73
48214.088	0.3864	-40.61	1	143.28	1	D	-40.68	153.46
48219.019	0.7844	45.79	1	-230.69	1	D	45.74	-238.31
48519.023	0.6791	44.36	1	-217.73	1	D	44.38	-231.48
48609.645	0.7494	48.76	1	-233.28	1	D	48.72	-244.94
48609.673	0.7630	38.18	1	-229.56	1	D	38.14	-239.55
48946.757	0.6900	47.65	1	-235.06	1	D	47.66	-249.04
48946.811	0.7162	49.26	1	-227.11	1	D	49.25	-240.50
48946.822	0.7216	50.33	1	-235.51	1	D	50.31	-248.74
48946.854	0.7371	57.19	1	-225.25	1	D	57.16	-237.83
48946.866	0.7430	56.65	1	-220.25	1	D	56.62	-232.52
48946.898	0.7585	54.76	1	-228.18	1	D	54.72	-238.77
48946.912	0.7654	55.15	1	-216.69	1	D	55.11	-226.44
48946.958	0.7877	54.94	1	-207.92	1	D	54.89	-215.23
48946.969	0.7931	53.83	1	-212.51	1	D	53.78	-219.24
48946.995	0.8057	50.97	1	-226.77	1	D	50.92	-232.31
48947.064	0.8393	45.40	1	-212.67	1	D	45.36	-215.60

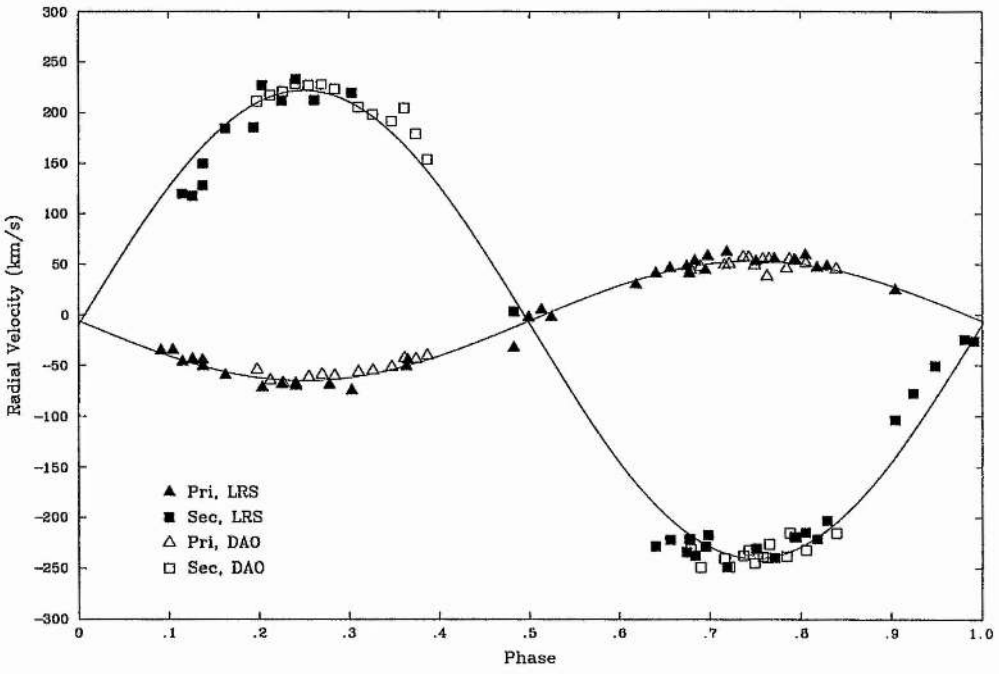

Figure 8.1: Radial velocity measurements of HU Tau and the adopted spectroscopic orbit.

velocity γ and the semiamplitude of the primary or secondary orbit, K_1 and K_2 respectively. The observations were converted to phase units using the ephemeris of Ito. We also attempted solutions including the period and the epoch of maximum positive velocity as free parameters. However, the period derived from the solution of the primary orbit was then unreasonably large and from the secondary orbit, too small. Including the epoch of maximum positive velocity as a free parameter had a negligible effect on the orbit derived. We also attempted a solution for a non-circular orbit but the eccentricity derived was found to be negligible. The solution of the spectroscopic orbit is shown in Table 8.2 under the heading "Uncorrected". The small difference in the value γ between the primary and secondary orbits is within the expected error if we also include the uncertainty in radial velocities of the template stars. Also shown in Table 8.2 under the heading "Corrected" is the spectroscopic orbit derived from the radial velocities corrected for non-Keplerian effects as described below. The radial velocities used are shown in Table 8.1, also under the heading "Corrected".

Given that the spectroscopic orbit is based on radial velocity data from two sources, we were concerned that there may have been a systematic difference between the two data sets. We therefore calculated the mean residual from the adopted orbit for the two data sets. We found the two values to agree to within 1σ for both the primary and secondary orbits. The two data sets are shown in Fig. 8.1 together with the adopted orbit.

Table 8.2: The spectroscopic orbit of HU Tau. T_+ is the epoch of maximum positive velocity.

	Uncorrected	Corrected
Primary:		
$\gamma(\mathrm{km\,s^{-1}})$	-6.1 ± 0.8	-6.0 ± 0.75
$K_1(\mathrm{km\,s^{-1}})$	59.3 ± 1.0	59.3 ± 0.85
$T_+ - 2446400$	**87.5303**	
Secondary:		
$\gamma(\mathrm{km\,s^{-1}})$	-9.9 ± 2.5	-9.4 ± 2.2
$K_2(\mathrm{km\,s^{-1}})$	230.3 ± 2.8	231.2 ± 2.2
$T_+ - 2446400$	**86.5108**	
System:		
e	**0.000**	
P/days	2.0563056	
Mass ratio	3.88 ± 0.08	3.90 ± 0.07

8.3 The light curve solutions

We used the light curves of Ito together with the program LIGHT2 in combination with the spectroscopic orbit above to derive the absolute parameters of HU Tau. The data were made available to us is the form of instrumental B and V magnitudes versus Heliocentric Julian Date. The residuals from the ephemeris of Ito for her own times of primary minimum are relatively large. We therefore derived an ephemeris using two of the times of primary minimum given. The third has a relatively large uncertainty and so we chose to ignore it. The resulting ephemeris used to convert the observations to phase units is:

$$\mathrm{HJD\,min\,I} = 2446485.9948 \pm 0.0003 + 2.0562915 \pm 0.0000023$$

The data were binned into phase intervals 0.0025 phase units wide in the phase interval 0.92–1.08 and 0.025 phase units wide at other phases. We therefore used 96 points in the B and V light curve solutions. No attempt was made to convert the instrumental magnitudes to the standard system.

The spectral type of the primary star is B8V (Cowley et al., 1969). We therefore adopted an effective temperature for the primary of 12000 ± 1000K (Popper, 1980) where the error reflects a typical uncertainty in a spectral classification of one subtype. From the catalogue of Fukuda (1982) we find the rotational velocity of the primary to be $V_{\mathrm{rot}} \sin i = 80\,\mathrm{km\,s^{-1}}$ which is approximately synchronous rotation for the parameters given by Giuricin and Mardirossian and so we assumed this to be the case in our initial solutions of the light curve. For later solutions we set the parameter FSYNH=1.3 where FSYNH=primary rotation rate/synchronous rotation rate. For our adopted solution this provides the correct projected equatorial rotational

velocity.

Parameters appropriate for radiative and convective atmospheres were adopted for the primary and secondary respectively and the mass ratio was fixed at the value derived from the uncorrected spectroscopic orbit above. Free parameters in the solution were initially the primary and secondary polar radii as a fraction of their separation, the effective temperature of the secondary component at its pole and the inclination of the system to the line of sight. For our initial values of these parameters we used the values given by Giuricin & Mardirossian. We found that a solution exists for a detached configuration in which primary eclipse is an annular transit i.e. the inclination $\approx 89°$ and the primary star is larger than the secondary. However we discount this solution for the following reasons.

i As can be seen from Fig 8.2, an annular transit gives a poor fit to the shape of primary eclipse. We attempted to improve the fit to the light curves by including either third light or the limb darkening of the primary component as a free parameter, but neither of these approaches were successful.

ii The light curves of Tümer & Kurutac are of sufficient precision to show a disturbance around phase 0.15 in the form of a dip in the B light curve and a bump on the V light curve, both of size $\approx 0^{m}.02$. The most natural explanation for this disturbance is the projection of a mass transfer stream across the face of the primary star. It is difficult to see how such a stream would be produced in a detached system.

iii A semi-detached configuration is more likely given the subgiant nature of the secondary and the main sequence primary.

iv The luminosity ratio in the B band derived from a solution for a detached configuration is $\approx$ 4magnitudes c.f. 2.5 magnitudes for a semi-detached configuration. It is unlikely that the secondary component would have been detectable in the CCFs if the luminosity ratio had indeed been so large.

We therefore attempted a solution for a semi-detached configuration i.e. the secondary constrained to its Roche Lobe as defined by the mass ratio. The solution derived is shown in Table 8.3. From the mean of the B and V solutions we derived radial velocity corrections for non-Keplerian effects for both components using the intensity weighted mean of the projected rotational velocity and used these corrected radial velocities to derive a new spectroscopic orbit. Since the solution of the light curve is dependent upon the mass ratio and the corrections to the mass ratio are calculated from the light curve solution, an iterative procedure is used to find a consistent solution for both photometric and spectroscopic data. In this case convergence is achieved in only four iterations. We also included the secondary albedo as a free parameter in the latter solutions. The match to the out-of-eclipse variations is then much improved. The

difference in the value of the secondary albedo for the B and V light curve solution may reflect a real dependence of this parameter with wavelength. Since the spectra from which the radial velocities were measured were obtained over a wavelength range similar to that covered by the B filter, we derived a mass ratio including non-Keplerian calculated from the mean light curve solution but using the value for the secondary albedo obtained from the B light curve solution. This new mass ratio differed from the adopted value by less than half the quoted error i.e. the adopted solution is not sensitive to the uncertainty in the secondary albedo.

The solutions to the B and V light curves for the adopted mass ratio and the mean solution are shown in Table 8.3 under the headings "Corrected" and "Adopted" respectively. The B and V light curves and solutions are also shown in Fig. 8.3. The residuals from the V light curve solution are also shown. It is apparent that the fit to primary eclipse is superior for this solution compared to the solution for an annular transit.

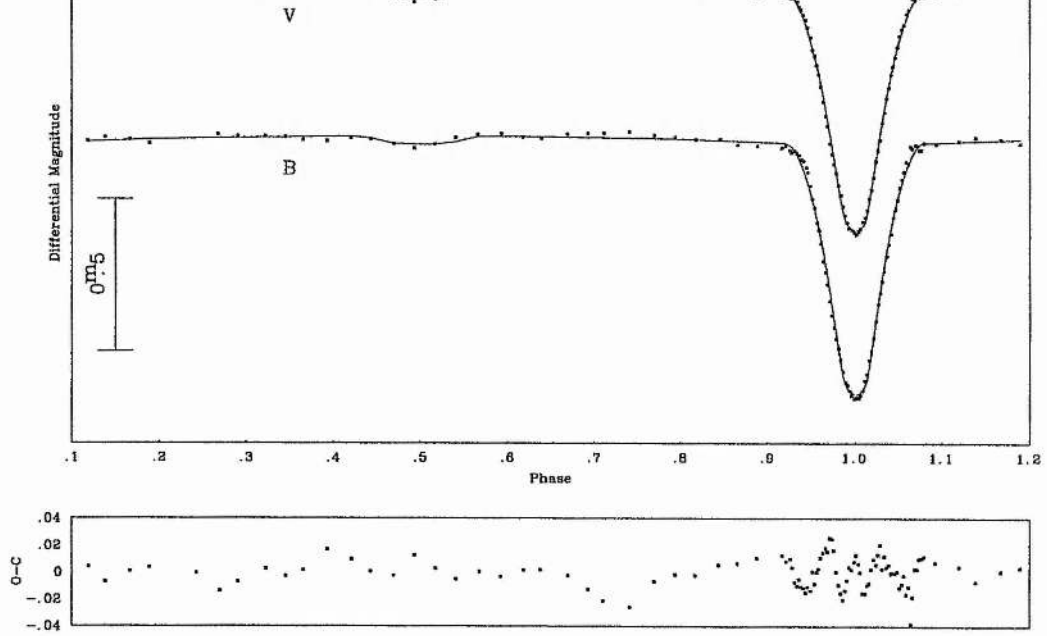

Figure 8.2: The BV light curves of HU Tau and the solution for a detached configuration. The residuals from the V light curve solution are shown.

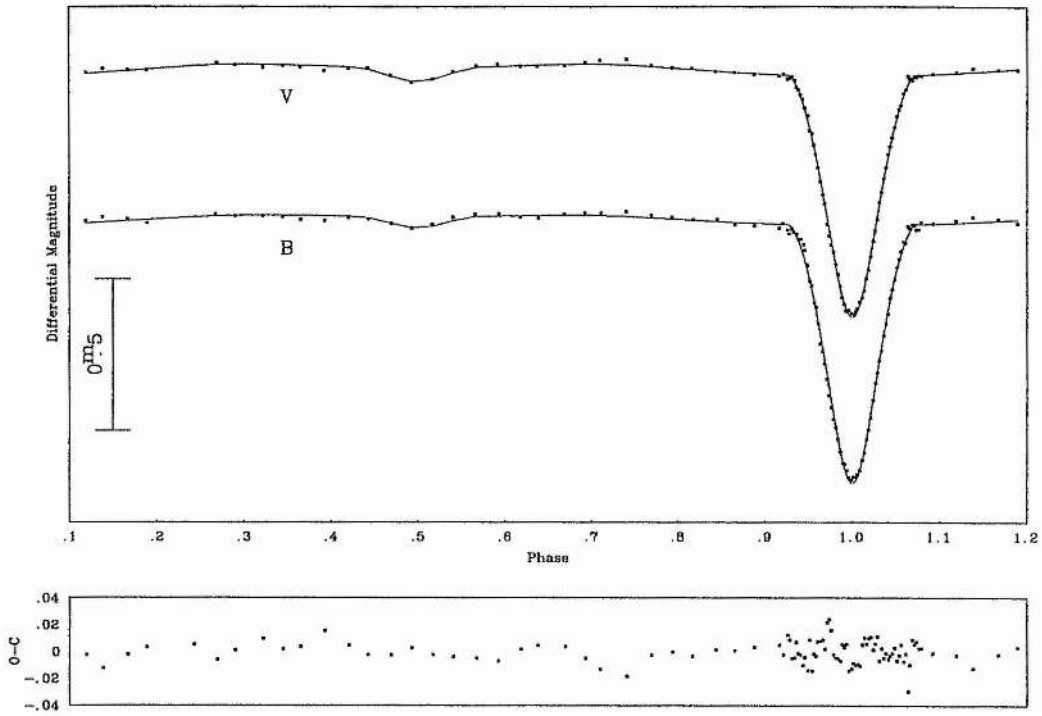

Figure 8.3: The BV light curves of HU Tau and the adopted solutions. The residuals from the V light curve solution are shown.

8.4 The absolute parameters

To derive the absolute parameters we generated a V light curve using the adopted solution shown in Table 8.3 to find the mean radii of both stars as a fraction of their separation and the mean effective temperature of the secondary. The inclination is taken from the mean light curve solution and the bolometric corrections from Lang (1980) are -0.8 ± 0.2 and -0.27 ± 0.07 for the primary and secondary respectively. For the V magnitude we use Oja's value of V=5.90±0.02. Combining Oja's (1983) value of $(B-V)$ for HU Tau, Lang's values of $(B-V)_0$ for B8V and G2III stars and a luminosity ratio of 10 in the V band from the light curve solution, we find $E(B-V) = 0.15 \pm 0.04$, which gives a distance to HU Tau of 115 ± 20pc. The absolute parameters and associated errors are shown in Table 8.4.

8.5 Conclusion

HU Tau serves as an object lesson in treating the conclusions derived from light curve solutions of poor quality with caution. Even for good quality light curves such as those of Ito there may be more than one apparently reasonable solution. However, given the arguments against a detached

Table 8.3: Solutions to Ito's BV light curves of HU Tau. Values in bold type are fixed.

Parameter	Uncorrected		Corrected		
	B	V	B	V	Adopted
r_p	0.2122	0.2090	0.2125	0.2109	0.2117
Formal error	0.0025	0.0015	0.0027	0.0019	0.0017
r_s [a]	0.2530		0.2499		0.2499
Formal error[b]	0.0014		0.0014		0.0014
$< T_p >$ /K	**12000**		**12000**		12000
T_s /K	5665	5240	5600	5300	5450
Formal error	270	110	280	130	150
Secondary Albedo	**0.5**	**0.5**	0.91	0.63	0.77
Formal error	—	—	0.14	0.10	0.09
i/°	78.3	78.1	78.5	78.3	78.4
Formal error	0.1	0.1	0.1	0.1	0.1
σ/mags	0.0130	0.0082	0.0127	0.0084	—

a: Secondary constrained to Roche Lobe b: Derived from error in mass ratio

Table 8.4: Absolute parameters of HU Tau

	Primary	Secondary
Mass	$4.43 \pm 0.09\,M_\odot$	$1.14 \pm 0.03\ M_\odot$
Mean Radius	$2.57 \pm 0.03\,R_\odot$	$3.21 \pm 0.03\ R_\odot$
Mean Temperature	$12000K \pm 1000K$	$5470K \pm 150$
Log (L/Lsolar)	2.09 ± 0.15	0.92 ± 0.05
Mean log g	4.26 ± 0.014	3.48 ± 0.014

configuration given above, it seems safe to conclude that HU Tau is indeed a normal Algol-type binary star. A large number of radial velocity measurements have been obtained for both components. This has been made possible by the cross correlation technique in combination with good access to telescopes of modest aperture equipped with detectors of high efficiency. We have therefore been able to derive masses with a precision of 2–2.5% and radii to a precision $\approx$1%. The accuracy of these parameters is ensured by the consistency of the photometric and spectroscopic solutions. The evolutionary status of HU Tau is discussed in Chapter 9.

Cowley A., Cowley C., Jaschek M., Jaschek C., 1969. AJ, **74**, 375.

Fukuda I., 1982. PASP, **94**, 271.

Giuricin G., Mardirossian, F., 1981. A&A, **97**, 411.

Ito Y., 1988. IBVS, **3212**.

Khalesseh B., Hill G., 1991. A&A, **244**, 75.

Lang K.R., 1980. Astrophysical data: Stars and Planets, Springer–Verlag.Berlin

Mammano A. Mannino, G., Margoni R., 1967. Mem. Soc. Astron. Ital., **38**, 459.

Melendo E.G., 1985. I.A.P.P.P Com., **20**, 1.

Nakamura Y., Yamasaki A., Ito, Y., 1994. PASJ, **46**, 267.

Oja T., 1983. A&ASS, **52**, 131.

Parthasarathy M., Sarma M.B.K., 1980. Ap&SS, **72**, 477.

Popper D.M., 1980. ARA&A, **18**, 115.

Tümer O., Kurutac M., 1979. IBVS, **1547**.

Chapter 9

Comparison of accurate absolute parameters of Algol systems with evolutionary models

9.1 Introduction

The comparison of reliably determined absolute parameters for Algol systems with the latest evolutionary models provides a stringent test of the latest models of stellar structure and evolution. The classic test beds for stellar models are those stars for which the absolute parameters can be determined accurately. The Sun is the best studied star for obvious reasons and is the starting point for any comparison. Otherwise, only eclipsing binaries provide absolute parameters of sufficiently high accuracy (1-2 % ; Andersen, 1991) to provide meaningful tests of models of stellar structure and evolution. For Algol systems where the mass transfer rate does not cause excessive complications, the accuracy of the parameters obtainable now approaches that achieved for detached main sequence stars. This has been made possible by improvements in detector technology and in the methods of analysis such as those used in this thesis. Algols may also offer a unique opportunity to study the chemical structure of a star during a critical phase of its evolution. In this chapter we compile a list of Algol systems from both this thesis and from other published studies for which reliable absolute parameters are available. The properties of these systems will be considered as a group and their evolutionary status will be discussed in the light of recent evolutionary models.

9.2 A compilation of accurate absolute parameters for Algols.

9.2.1 Criteria for selection

We have used two criteria for selection in this compilation, one relating to the type of star included, the other is a measure of the quality of the available absolute parameters.

We must first decide upon a suitable definition of an Algol system. Since we are concerned here with comparison to models designed to explain the evolution of classical Algol systems we use the following definition. For the purposes of this compilation an Algol system is *an eclipsing binary star comprising a main sequence star of spectral type B or A and a less massive subgiant/giant star of spectral type F or later.* Note that we assume nothing concerning the evolutionary path that leads to this combination.

There is inevitably a degree of subjectivity involved in deciding whether the available data for a system are of sufficient quality to warrant the inclusion of that system in a compilation. This degree of subjectivity can be minimised by choosing a measure of quality that is unambiguous and easily testable in an individual case. To minimise the systematic errors present in our compilation we have decided to include only those systems for which *the absolute parameters are based on a self-consistent solution of both the light curve(s) and radial velocity curves for both components including the effects of non-Keplerian distortions.*

9.2.2 The compilation

The nine systems in the compilation are shown in Table 9.1 together with some of their observational characteristics. Some notable exceptions to this compilation are the systems U Cep, U Sge and Algol itself. In the first two cases the disagreement between the mass ratio derived from the light curves and the radial velocity curves has yet to be resolved. Algol, in common with systems such as RY Aqr, R CMa and δ Lib, has published radial velocity data for both components and published light curves. However, there does not appear to be a self-consistent solution for both sets of data available for any of these systems.

The nine systems are discussed individually below and the adopted masses, radii, luminosities and effective temperatures for both components are shown in Table 9.2

RZ Cas The absolute parameters for this system are taken from Maxted et al. (1994a) and are the same as those given in Chapter 3. New BV light curves have been published by Riazi

Table 9.1: Observational data for the nine Algol systems

Name	Coordinates (2000.0)	V mag. Eclipse type	Period (days)	Spectral type
S Cnc	08h43m56.17s	8.45–11.10	9.4845	B9V
HD 74307	+19d02m03.2s	Total		G8–K0 III–IV
RZ Cas	02h48m55.41s	6.38–7.89	1.1953	A3V
HD 17138	+69d38m01.5s	Partial		~K0III-IV
TV Cas	00h19m18.39s	7.30–8.39	1.8126	B9V
HD 1486	+59d08m20.9s	Partial		~G5
U CrB	15h18m11.26s	7.04–8.35	3.4522	B7V
HD 136175	+31d38m50.3s	Partial		G0 III-IV
AF Gem	06h50m39s	10.2–11.3	1.2435	B9.5V
HD 264750	+21d21.9m	Partial		~G0IV
TT Hya	11h13m12.48s	7.5 – 9.5	6.9534	B9.5V
HD 97528	-26d27m54.9s	Total		G9–K1 III-IV
AT Peg	22h13.4m	9.50–10.34	1.1461	A4V
HD 210892	+8d25.5m	Partial		~G8 III-IV
HU Tau	04h38m15.80s	5.9–6.8	2.0563	B8V
HD 29365	+20d41m05.3s	Partial		~ G2 III-IV
TX UMa	10 45 20.45	7.06–8.76	3.0632	B8V
HD 93033	+45 33 58.5	Partial		G0 III-IV

et al. (1994) and UBV light curves by Narusawa et al. (1994). The analysis of these new light curves in conjunction with the radial velocity data of Maxted et al. would provide a better determination of the uncertainty associated with the parameters presented here but are unlikely to alter their values significantly.

S Cnc Van Hamme & Wilson (1993) present a simultaneous solution to the light curves of Crawford & Olson (1980) and the radial velocity data of Popper & Tomkin (1984) from which they derive the absolute parameters used in this study. Since they have not given any estimate of the uncertainty in these values we have adopted the following probable errors. The probable errors in the absolute radii are a combination of the quoted errors for the separation of the stars and the relative radii. From the mass ratio and the separation of the stars we compute the velocity semi-amplitudes for the two stars. To these values we assign errors of $1.05\,\mathrm{km\,s^{-1}}$and $0.94\,\mathrm{km\,s^{-1}}$from the standard deviations of the velocity points given for the primary and secondary respectively. The effective temperatures of the two components are taken from the spectrophotometric study of Etzel & Olson (1985). The effective temperature of the secondary is given as 4500–4750 K. The effective temperature of the primary is 10500K but no error in this value is given. However it appears that a 10000K model does not match the observed flux distribution and so we have an upper limit for the uncertainty of 500K. We therefore adopt a probable error of 250K.

TV Cas The absolute parameters given here are taken from the study by Khallesseh & Hill (1992).

U CrB The masses and radii with the standard errors quoted are taken from Heintze & van Gent (1988a) from their analysis of the UPS light curves of van Gent(1989) and the radial velocity measurements of Batten & Tomkin (1981). The effective temperature of the primary is taken from Cugier (1989). Although this is not the primary temperature used in the analysis of Heintze & van Gent, Heintze (1990) states that the results depend "only a little bit on the adopted T_1". The possibility of third light in the system is also discussed therein but no firm conclusions are drawn. The effective temperature of the secondary is taken from the spectral type estimate of Plavec & Polidan (G0 III–IV; 1976) with the standard uncertainty of one subtype. The luminosities and their uncertainties have been recalculated for these adopted effective temperatures and radii.

AF Gem The absolute parameters presented here are taken from Chapter 6.

TT Hya Van Hamme & Wilson (1993) have used the light curves of Kulkarni & Abhyankar (1978) and the radial velocity observations of Popper (1989) to derive absolute parameters for this system. The effective temperatures are from Etzel (1990). The probable errors quoted here are derived in a similar fashion to those described for S Cnc. The large scatter in the radial velocity data for the primary component is due to the presence of an accretion disk. The probable errors quoted here for the masses and radii are therefore

rather large ($\gtrsim 10\%$). Given that the light curve solution does not account for the effects of the accretion disk (Plavec, 1989) it seems appropriate to adopt these rather pessimistic errors.

AT Peg The absolute parameters for this system are taken from Maxted et al. (1994b) and are the same as those given in Chapter 4.

HU Tau The absolute parameters are taken from Chapter 8.

TX UMa We are in no doubt that much work remains to be done on this system before a coherent picture emerges. A set of light curves in a narrow-band system would be extremely valuable for the future study of this system. Nevertheless, the absolute parameters presented in Chapter 5 satisfy the criteria outlined above and are therefore included here.

9.3 Comparison with evolutionary models

9.3.1 General properties

The positions of the nine systems in the Hertzsprung-Russell diagram (HRD) and mass–radius plane are shown in Fig. 9.1 and Fig. 9.2 respectively. The Zero-age main sequence (ZAMS) and Terminal-age main sequence (TAMS) are shown and are based on the models of Schaller et al. (1992) for standard solar chemical composition.

In the HRD we see that the primaries are indeed all main-sequence stars and that the secondaries lie close to, but not on, the main sequence. The subgiant nature of the secondaries is more apparent in the mass-radius plane. The secondaries of the longer period systems (TT Hya, S Cnc, U CrB) lie well above the main sequence with radii four or five times that of a main sequence star of the same mass, while the shorter period systems tend to lie just above the main sequence with radii 50–100% larger than that of a main sequence star of the same mass. This is simply a reflection of the size of the Roche lobes in these systems. The primary component of RZ Cas appears to lie slightly below the main sequence in the mass-radius plane but not significantly so. Any small difference in the radius of RZ Cas and a model star of the same mass can be explained in terms of a small metallicity difference.

9.3.2 The evolutionary models of Iben & Tutukov, 1984

Iben & Tutukov (1984) have described the evolution of Algol systems including the effects of angular momentum loss (AML) via gravitational radiation and a magnetic stellar wind (MSW).

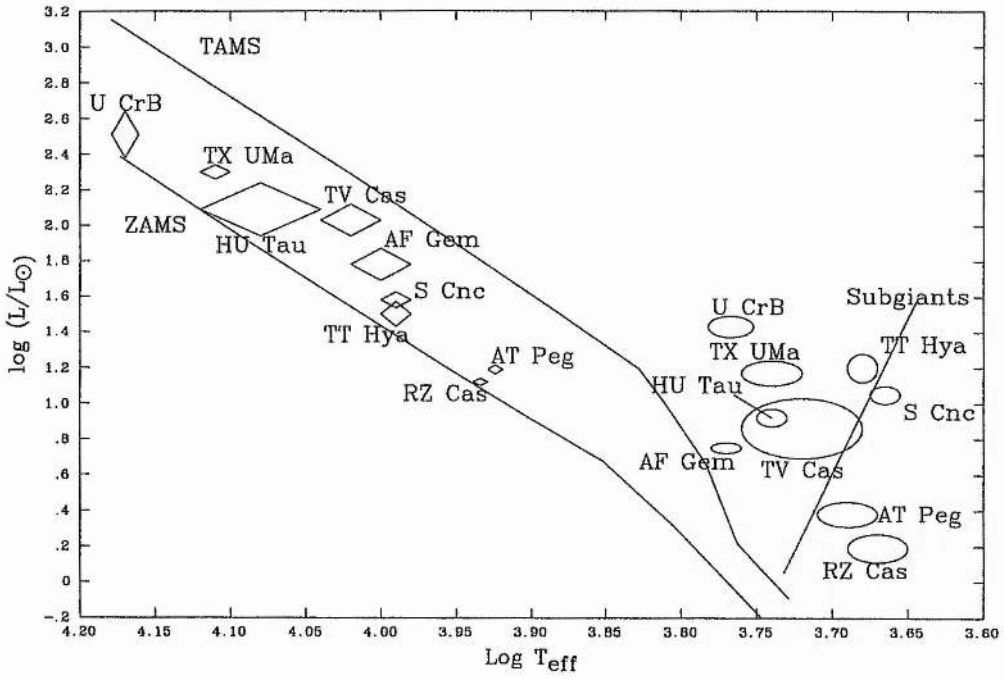

Figure 9.1: The nine systems in the Hertsprung-Russell diagram. Error boxes are in the form of diamonds for the mass gaining stars, and ellipses for the moss losing stars

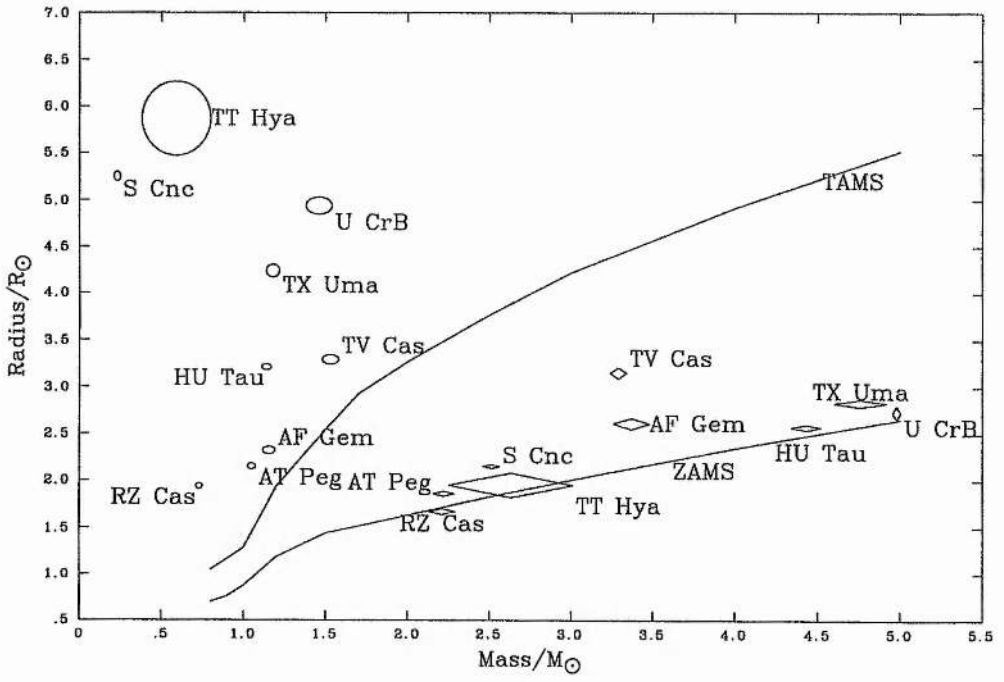

Figure 9.2: The nine systems in the mass-radius plane. Error boxes are in the form of diamonds for the mass gaining stars, and ellipses for the moss losing stars

Table 9.2: Accurate absolute parameters of nine Algol systems

Name	$M/M_\odot$	$R/R_\odot$	Log $(L/L_\odot)$	Log T_{eff}
S Cnc	2.51 ± 0.05	2.15 ± 0.02	1.58 ± 0.045	3.99 ± 0.01
	0.23 ± 0.02	5.25 ± 0.05	1.05 ± 0.05	3.665 ± 0.01
RZ Cas	2.21 ± 0.08	1.67 ± 0.03	1.12 ± 0.02	3.934 ± 0.005
	0.73 ± 0.02	1.94 ± 0.03	0.19 ± 0.08	3.67 ± 0.02
TV Cas	3.29 ± 0.05	3.15 ± 0.06	2.03 ± 0.09	4.02 ± 0.02
	1.53 ± 0.05	3.29 ± 0.05	0.86 ± 0.17	3.72 ± 0.04
U CrB	4.98 ± 0.025	2.73 ± 0.07	2.51 ± 0.13	4.170 ± 0.009
	1.46 ± 0.08	4.94 ± 0.09	1.43 ± 0.06	3.767 ± 0.015
AF Gem	3.37 ± 0.11	2.61 ± 0.06	1.78 ± 0.09	4.00 ± 0.02
	1.155 ± 0.038	2.32 ± 0.04	0.75 ± 0.03	3.77 ± 0.01
TT Hya	2.63 ± 0.38	1.95 ± 0.13	1.50 ± 0.07	3.99 ± 0.01
	0.59 ± 0.21	5.87 ± 0.40	1.20 ± 0.08	3.68 ± 0.01
AT Peg	2.22 ± 0.065	1.86 ± 0.025	1.19 ± 0.025	3.924 ± 0.005
	1.05 ± 0.025	2.15 ± 0.03	0.38 ± 0.07	3.69 ± 0.02
HU Tau	4.43 ± 0.09	2.57 ± 0.03	2.09 ± 0.15	4.08 ± 0.04
	1.14 ± 0.03	3.21 ± 0.03	0.92 ± 0.05	3.74 ± 0.01
TX UMa	4.76 ± 0.16	2.83 ± 0.04	2.30 ± 0.04	4.11 ± 0.01
	1.18 ± 0.04	4.24 ± 0.07	1.17 ± 0.07	3.74 ± 0.02

They describe the evolutionary status of Algols in terms of the parameters M_{a0} and P_0. M_{a0} is an estimate of the initial mass of the mass-gaining star assuming zero mass loss from the system and an initial mass ratio of 1 i.e. M_{a0} is half the total mass of the system. P_0 is an estimate of the initial orbital period of the system if zero AML is also assumed, i.e.:

$$P = 2^6 \frac{M_1^3 M_2^3}{(M_1 + M_2)^6} P$$

The positions of the nine systems from our compilation on the M_{a0}–P_0 plane are shown in Fig 9.3 in the form of error bars. Positions for five of these systems in the M_{a0}–P_0 plane were given by Iben & Tutukov based on the catalogues of Giuricin & Mardirossian (1981) and Giuricin et al. (1983, 1984) and are also shown in Fig 9.3 (small circles). It is interesting to note that, for all of the five systems, the values of M_{a0} and P_0 derived from these catalogues disagree with our own determinations. The differences appear to be random and occasionally very large (e.g. TX UMa).

Below each system is given an estimate of the mass of the He core of the mass losing star. This is based upon a He-core-mass – radius relation via the mass ratio of the system since this determines the size of the Roche lobe and thus the size of the mass losing star. If the time scale for AML is shorter than the nuclear time scale of the mass losing star then the mass of the He core will not change significantly during the semi-detached phase. The two timescales are approximately equal for $P=50h(M_{a0}/M_\odot)^{0.125}$ which is shown in Fig 9.3 by a dotted line. All the systems under consideration lie to the left of the line and so the time scale for AML is indeed shorter than the nuclear time scale of the mass losing star.

Also shown in Fig 9.3 are dashed lines of constant He core mass as marked. By comparing the estimated He core mass for each system with these lines (remembering that M_{a0} is assumed to be constant for any particular system) we can estimate the position on the M_{a0}–P_0 plane of that system prior to the semi-detached phase. All systems lie leftwards of this initial position by varying amounts. The evolution leftwards in the M_{a0}–P_0 plane is due to AML which for Algols is due principally to a MSW. The dashed-dotted line labelled $A_0/R_\odot=6(M_{a0}/M_\odot)^{1/3}$ is a lower limit on the period ($\approx$ 29 hrs) of newly formed binary stars from a separation limit given by Kraicheva et al. (1978) assuming an initial mass ratio of 1. For systems with $M_{a0} < 1.5\,M_\odot$, AML prior to RLOF may bring them below this limit since at least one of the stars will have a convective atmosphere and therefore a MSW. This would appear to be the case for RZ Cas, which presumably started as a binary with $A_0/R_\odot \geq 6(M_a0/M_\odot)^{1/3}$. It then suffered AML which reduced the separation of the components sufficiently that, combined with the evolutionary expansion of the donor, it overflowed its Roche Lobe. Iben & Tutukov find that for all the systems with $M_{a0} > 1.5\,M_\odot$, the present He core mass indicates that the period prior to RLOF was greater than this limit. Of the nine systems presented here, seven have $M_{a0} > 1.5\,M_\odot$ and of these seven, five satisfy the condition $A_0/R_\odot > 6(M_{a0}/M_\odot)^{1/3}$. However, both AF Gem and AT Peg exceed this limit by about 10hrs.

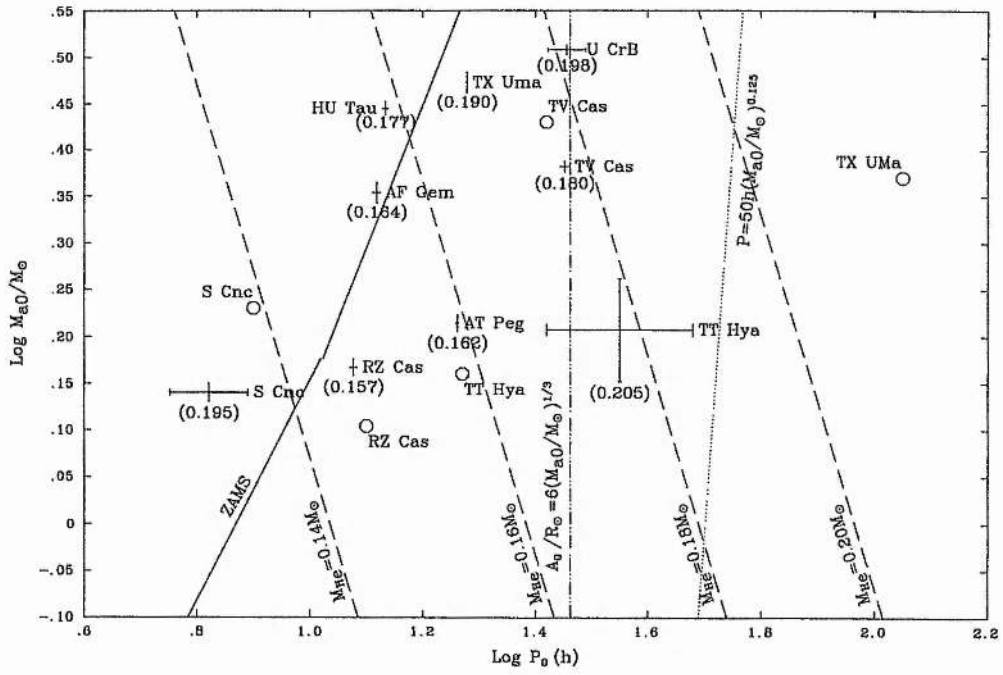

Figure 9.3: The nine systems in the M_{a0}–P_0 plane. See text for explanation

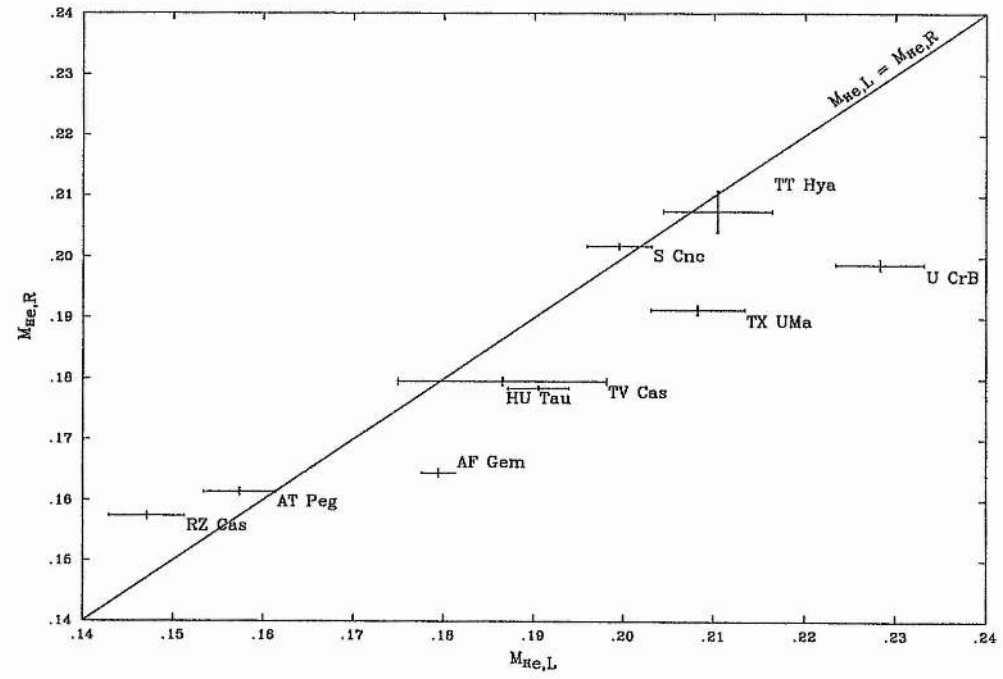

Figure 9.4: A comparison of the mass of the He core of the nine systems estimated from the radii and from the luminosities.

Given that the total mass of AT Peg is $3.27 \pm 0.07\,M_{\odot}$, the initial mass ratio need only have been 0.88 or less for the less massive star to have a MSW which would provide the required AML. A similar argument for AF Gem provides an upper limit for the initial mass ratio of 0.5. There is however a flaw in this argument. It has been assumed that the He-core-mass – radius relation for single subgiants is valid, despite the fact that the secondaries in Algols are constrained by their Roche lobes.

The radius and luminosity of a single star with a degenerate helium core depends only on the He core mass. Therefore, if the He-core-mass – radius relation is valid for Algol secondaries then He core mass given by this relation would agree with He core mass given by the He-core-mass – luminosity relation. To see if this is the case for the nine systems studied here we have used the He-core-mass – radius and He-core-mass – luminosity relations of Kraicheva et al. (1986). The He core masses derived from the radius and luminosity are shown in Fig 9.4. We see that for AF Gem the He core mass derived from its radius ($M_{He,R}$) is too small compared to that derived from its luminosity ($M_{He,L}$). If the value of $M_{He,L}$ is to be believed then the initial mass ratio of AF Gem need not be as extreme as that derived above.

AF Gem is not the only Algol in which the secondary does not obey the He-core-mass – radius relation for single subgiants. For those systems which lie to the right of the line $M_{He,L}$=$M_{He,R}$ in Fig 9.4 (AF Gem, TX Uma, U CrB and HU Tau) this is easily explained as the effect of the Roche lobe. For the longer period systems (S Cnc and TT Hya) the He-core-mass – radius relation appears to be valid. For RZ Cas (and possibly AT Peg) the He-core-mass – radius relation appears to *over-estimate* the He core mass.

9.3.3 The evolutionary models of De Greve, 1993

De Greve (1993) has presented a grid of models for non-conservative evolution of Algol systems. The grid covers the mass range 3 to 8 $M_{\odot}$ for the mass of the primary and for the initial mass ratios 0.9 and 0.6 evolving through case B as well one model for case AB and one late case B (both $6\,M_{\odot}$ primaries). These sophisticated models include the effects of both mass and angular momentum loss from the system. They are based on modern stellar structure models including the effects of convective core overshooting and stellar wind mass loss. It is assumed that 50% of the mass lost from the donor star is captured by the other component ($\beta = 50\%$), while the rest of the material is lost from the system.

Given that the minimum total mass in any of the models is 3.52 $M_{\odot}$, we shall not consider further in this section systems with total masses less than this value (S Cnc, RZ Cas, TT Hya, AT Peg). To determine which of the models is likely to best represent the five remaining systems (TV Cas, U CrB, AF Gem, HU Tau and TX UMa) we refer to Fig 9.5, in which

the mass gaining stars are shown in the mass–radius plane. Also shown are the results of the evolutionary models at the beginning and end of the slow mass transfer phase (SMT) for the initial mass ratios 0.9 and 0.6. There is a well defined trend for mass gaining stars of systems with more extreme initial mass ratios to lie closer to the ZAMS. This is a consequence of the rejuvenation of their hydrogen core i.e. hydrogen rich material from the donor star is mixed into the core of the gainer. This effect is more pronounced for smaller mass ratios since there is more hydrogen rich material donated. From Fig. 9.5, and remembering that all the systems are in the slow mass transfer phase, we can estimate the following initial mass ratios: TV Cas, $q_i \approx 0.8$; AF Gem, $q_i \approx 0.7$, TX Uma, $q_i \approx 0.6$; U CrB, $q_i \lesssim 0.5$; HU Tau, $q_i \lesssim 0.5$. These estimates must be regarded as extremely tentative since the actual value of β is likely to differ from 50% and this will in turn affect the amount of rejuvenation e.g. U CrB may be a system for which $q_i \approx 0.6$ and $\beta > 50\%$, resulting in more efficient rejuvenation.

The donor stars of the four systems are shown in the mass–luminosity plane in Fig. 9.6. This clearly shows the main point of disagreement between the models and the observations. Assuming for the moment that all five systems are at the start of the SMT phase, we see that the donor stars are 10 to 20 times fainter than the model predictions for stars of the same mass. The disagreement is slightly worse if the systems are in reality more further into the SMT phase. At this point we should consider the assumption that the systems are in the SMT phase. The definition of the start of the SMT phase used by De Greve is the point at which the mass transfer rate drops below the average mass transfer rate for the entire mass transfer phase. The typical value of this average mass transfer rate is between 10^{-6} and $10^{-7}\,M_\odot/yr$ for the lower mass systems. Mass transfer rates are difficult to determine observationally. The most common method is probably the modelling of the period. This is not a straightforward task since the period variations are influenced not only by the mass transfer rate, but also by the rotation of the primary component (Biermann & Hall, 1973) and by the the magnetic cycle of the secondary. The mass transfer rates derived are therefore only rough estimates. For example, for TX UMa Allbright & Richards (1993) quote a value $\sim 10^{-9}\,M_\odot/yr$ but also give an upper limit of $10^{-6}\,M_\odot/yr$. For TT Hya the properties of the accretion disk have enabled Plavec (1989) to determine a mass transfer rate $\approx 10^{-6}\,M_\odot/yr$. A precise estimate of the mass transfer rate has been made for U CrB by Olson & Bell (1989). They used a non-LTE analysis of the light losses due to the projection of the accretion stream on the face of the primary component in the *uvby* and I bands. They find a mass transfer rate of $4 \times 10^{-8}\,M_\odot/yr$. Given that the disturbances to the spectroscopic orbit due to mass transfer seen in TT Hya are not seen in the other systems studied here, the mass transfer rate observed for U CrB may be regarded as typical for these other systems. All the systems, with the possible exception of TT Hya, are therefore well into the SMT phase.

A similar problem can be seen in Fig. 9.7 in which we see the five systems in the mass-ratio–period plane. The two evolutionary models shown ($5{+}3\,M_\odot$ and $4{+}2.4\,M_\odot$) achieve the

lowest period of any of the models in the appropriate mass range. It can be seen that the predicted periods are between 0.45 and 3.0 days too long.

The most likely culprit for these differences is the way in which the mass and angular momentum loss is treated. For example, it may be the case that the value of β is appreciably different from 50%. Alternatively, it has been shown on the M_{a0}–P_0 plane that AML via a MSW is an important factor in the evolution during the SMT phase for most Algols. It may be that the efficiency of this mechanism is underestimated by the model. In any case it seems that definitive conclusions must await further evolutionary model calculations tailored to individual systems.

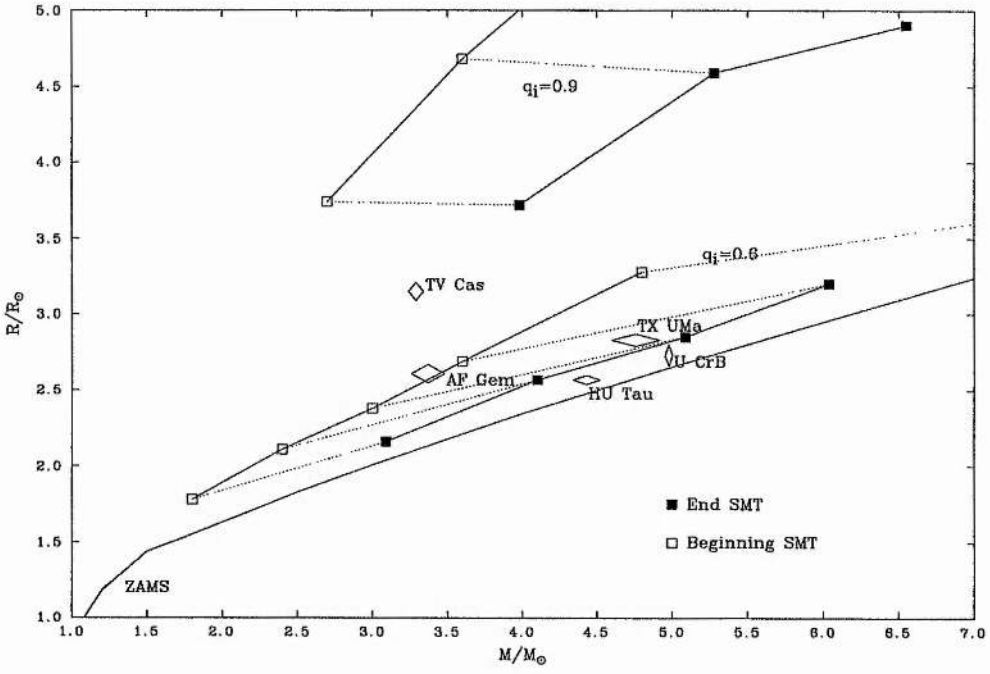

Figure 9.5: The mass gaining stars in the mass–radius plane and the evolutionary models of De Greve for mass gaining stars during SMT. The evolution of the models in this plane is indicated by a dotted line

9.4 Conclusion and future directions

Our conclusions are limited simply because of the lack of suitable models for the evolution of low mass Algol systems. For the very low mass systems such as RZ Cas and S Cnc no detailed non-conservative models appear to exist at all. For the higher mass systems the models of De Greve appear to be the best available. However, there is limited agreement between these models and the available observational data. Whether this is due to the models not covering

the required parameter space or a more fundamental problem remains to be seen. However, from the general model of Iben & Tutukov we have been able to show that AML due to a MSW is an important factor in the evolution of most Algols during the SMT phase.

Individual evolutionary scenarios exist for a few systems (β Per; Sarna, 1993; TV Cas De Greve et al., 1985; U Sge; Sarna & De Greve, 1994). However, the quality of the absolute parameters for these systems is not as high as that for the systems collected here. The individual modelling of several systems with high quality absolute parameters will doubtless shed more light on the processes at work in the evolution of Algol systems. Whether this will challenge our beliefs concerning Algols or reinforce them remains to be seen.

We may expect high quality absolute parameters to become available for several systems over the next few years as the new data analysis techniques used in this thesis are applied to the existing data for systems such RY Aqr, R CMa, δ Lib and β Per. An interesting problem will be the modelling of the Na D λ5890 line radial velocity measurements for these systems since this line is sensitive to both temperature and gravity. Since both these quantities are variable across the surface of the secondary component, this is not a straightforward problem and would involve the combination of a sophisticated light curve modelling program and model atmosphere calculations.

The use of tomography and related techniques for separating binary star spectra will certainly be of great importance if it proves to be reliable for extracting the spectra of the cool components. In this case it will be possible to establish the surface composition of the cool component. This will be an enormously valuable datum which will offer a unique insight into the chemical profile of stars in a crucial stage of their evolution.

The number of Algols for which high quality data will become available in the future will doubtless increase but at what rate remains to be seen. Certainly the new generation of high aspect ratio CCDs can provide excellent spectroscopic data in combination with telescopes of modest aperture. In terms of photometry, it is to be hoped that the increased used of robotic telescopes will benefit the study of Algol systems. This is likely to be particularly useful for longer period systems since robotic observatories are well suited to long term programmes. For both short and long period systems the use of narrow band filter systems circumvents many problems associated with the solution of broad band filter light curves, particularly for Algols (Heintze & van Gent, 1988b) and their use should certainly be encouraged.

Another promising development which will certainly help to increase the quality and number of absolute parameters for Algol systems is the mapping of the circumstellar material in Algols. There is much interest in the accretion processes at work in Algol systems (several articles can be found in Batten, 1988). These processes are interesting in their own right and their study may well lead to higher quality absolute parameters for a whole range of Algols for

which mass transfer currently masks the underlying properties of the stars.

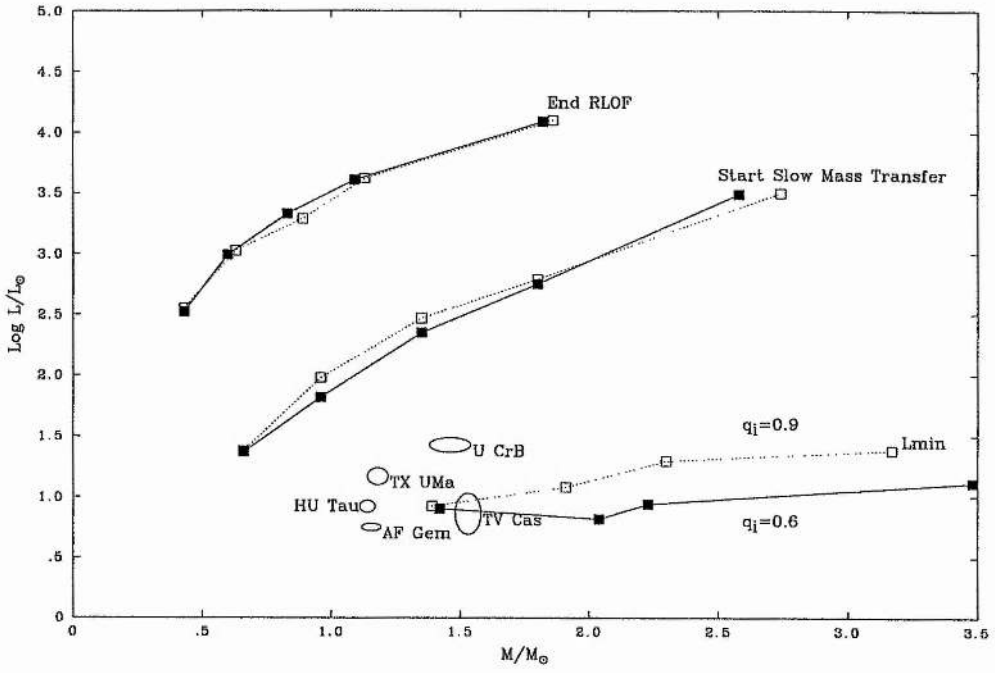

Figure 9.6: The mass donors in the mass–radius plane and the evolutionary models of De Greve for two mass ratios at three significant phases of their evolution

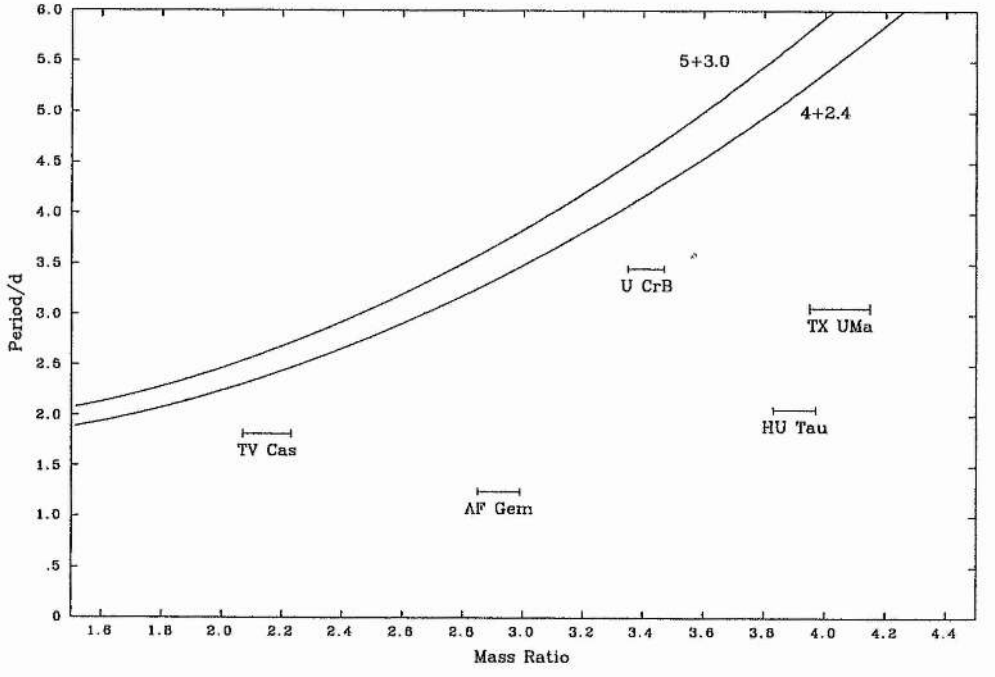

Figure 9.7: The mass ratio–period plane. The evolution of the orbital period for two of De Greve's models are shown as well as the observed periods for the five more massive systems

Andersen J., 1991. A&A Rev., **3**, 91.

Allbright G.E., Richards M.T., 1993. AJ, **414**, 830.

Batten A.H. (ed.), 1988. Algols, Kluwer Academic Publishers, Dordrecht.

Batten A.H., Tomkin J., 1981. Publ. Dom. Astrophys. Obs., **15**, 419.

Biermann P., Hall D.S., 1973. A&A, **27**, 249.

Crawford R.C., Olson E.C., 1980. PASP, **92**, 833.

Cugier, 1989. A&A, **214**, 168.

De Greve J.P., 1993. A&AS, **97**, 527.

De Greve J.P., de Landstheer, A.C., Packet, W., 1985. A&A, **142**, 367.

Etzel P.B., 1990. In: Active Close Binaries, p.189, İbanoğlu (ed.), Kluwer Academic Publishers, Dordrecht.

Etzel P.B., Olson E.C., 1985. AJ, **90**, 504.

Giuricin G., Mardirossian F., 1981. ApJS, **46**, 1.

Giuricin G., Mardirossian F., Mezzetti M., 1983. ApJS, **52**, 35.

Giuricin G., Mardirossian F., Mezzetti M., 1984. ApJS, **54**, 421.

Heintze J.R.W., 1990. In: Active Close Binaries, p.121, İbanoğlu (ed.), Kluwer Academic Publishers, Dordrecht.

Heintze J.R.W., van Gent R.H., 1988a. In: Algols, p.264, Batten A.H. (ed.), Kluwer Academic Publishers, Dordrecht.

Heintze J.R.W., van Gent R.H., 1988b. In: Algols, p.257, Batten A.H. (ed.), Kluwer Academic Publishers, Dordrecht.

Iben I., Tutukov A.V., 1984. ApJ, **284**, 719.

Khallesseh B., Hill G., 1992. A&A, **257**, 199.

Kraicheva Z.T., Popova E.I., Tutukov A.V., Yungelson L.R., 1978. Astron. Zh., **55**, 1176.

Kraicheva Z.T., Tutukov A.V., Yungelson L.R., 1986. Astrofizika, **24**, 287.

Kulkarni A.G., Abhyankar K.D., 1978. Contrib. Nizamiah Japal-Rangapur Obs.. 9

Maxted P.F.L., Hill G., Hilditch R.W., 1994a. A&A, **282**, 821.

Maxted P.F.L., Hill G., Hilditch R.W., 1994b. A&A, **285**, 535.

Narusawa S.-Y., Nakamura Y., Yamasaki A., 1994. AJ, **107**, 1141.

Olson E.C., Bell D.J., 1989. PASP, **101**, 907.

Plavec M., 1989. AJ, **96**, 755.

Plavec M., Polidan R.S., 1976. In: Structure and evolution of close binary systems, p.289, Eggleton P. et. al (ed.), Reidel, Dordrecht.

Popper D.M., 1989. ApJS, **71**, 595.

Popper D.M., Tomkin J., 1984. ApJ, **285**, 208.

Sarna M.J., 1993. MN, **262**, 534.

Sarna M.J., De Greve J.P., 1994. A&A, **281**, 433.

Riazi N., Bagheri M.R., Faghini F., 1994. A&SS, **211**, 293.

Schaller G., Schaerer G., Meynet G., Maeder A., 1992. A&AS, **96**, 269.

van Gent R.H., 1989. A&AS, **77**, 471.

Van Hamme W., Wilson R.E., 1993. MN, **262**, 220.

Appendix A

Automatic Rectification of spectra

A.1 Introduction

PRESS is an automatic rectification program for use with linearised DAO FITS spectra specifically designed to produce spectra for use with VCROSS but of more general use. This appendix describes how the use of PRESS as well as the associated programs XPRESS, which is a version of PRESS that is quicker to use, and DPRESS, which handles spectra stored in ASCII format. The algorithm used to rectify the spectra is also described.

A.2 The aim of rectification

A spectrum can be described in terms of two components, a continuum that varies slowly with wavelength and, generally, a large number of absorption or emission lines. The lines are also described in terms of two components, a sharp line core and the broader line wings. We therefore have three scales at which the spectrum varies, that of the continuum (broadest) the line wings and the line cores (narrowest).

In its purest sense, rectification entails dividing the entire spectrum by the continuum leaving only the lines as variations about an arbitrary intensity level (usually set to I=1). In spectra where regions of the continuum are clearly defined, rectification is generally straightforward. Rectification becomes more problematic as the density of lines in the spectrum increases because the overlapping line wings depress the level of the continuum and make it less clearly

defined. The density of lines at which the continuum becomes invisible depends upon the quality of the observed spectrum both in terms of its resolution and signal-to-noise ratio, and the intrinsic strength and width of the lines. In spectra where fitting the continuum is problematical, alternative approaches usually involve fitting some smooth function to the data or small sections of the data and using this "pseudo-continuum" to rectify the data.

The degree of care required in defining the continuum is dependent upon the use to which the spectra will be put. For example, if the spectra are to be used for equivalent width measurements and line profile studies, great care must be taken not to fit a continuum that "divides-out' the broad line wings. For spectral classification studies, rectification involves little more than dividing the spectra by a function to simply flatten them out. For radial velocity work based on cross-correlation, we are only interested in the sharp line cores and so a pseudo-continuum is used that removes the larger scale features that add noise to the CCF.

A.3 The rectification algorithm

The rectification algorithm used in PRESS is described in terms of a flow chart in Fig A.1. The idea is to form a pseudo-continuum by taking a smoothed version of the spectrum and using this to form an approximately rectified spectrum. The presence of absorption lines has the effect of lowering the value of this smooth function below the value of the actual continuum. PRESS therefore calculates the flux above the continuum as a function of wavelength – the "residual flux". The residual flux is then a measure of the amount by which the lines reduce the level of the continuum so we can use a smoothed version of this function to apply a correction to the initial version of the pseudo-continuum. This process is then iterated until the mean value of the residual flux is acceptably small or for a fixed number of iterations.

The two most important parameters in the process are the smoothing interval **wsmooth** and the limiting value of the mean residual flux **climit** (or alternatively the maximum number of iterations **nmax**. The choice of these parameters strongly affects the appearance of the rectified spectrum and need to be chosen with care. For example, if a value of **wsmooth** is used that is less than the typical width of a line wing then measurement of equivalent widths will be systematically too low. However, this type of spectrum would be ideal for forming CCFs provided that **wsmooth** is not so low that the adopted pseudo-continuum is affected by the line cores since this disrupts the shape of the line cores. The value of **climit** should be matched to the signal-to-noise ratio of the spectra since the noise is randomly distributed about the continuum and so we would expect a certain amount of residual flux.

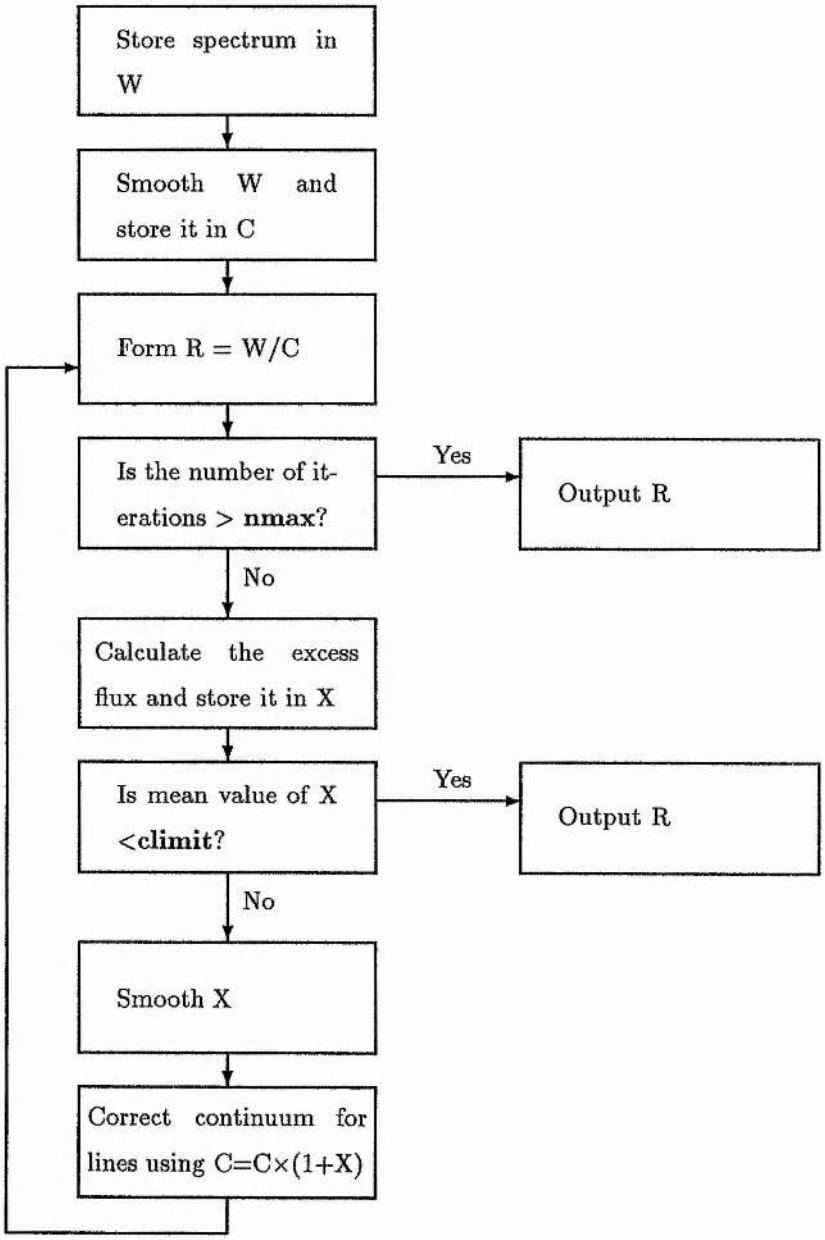

Figure A.1: The rectification algorithm

A.4 Using PRESS

Once press is installed, typing PRESS produces a title sequence and the first prompt:

```
Are you using a master list ? [Y] >
```

The filenames of the spectra can either be entered one-by-one from the terminal or can be read from a file – a master list. If a master list is to be used a response of <CR> or Y will result in a prompt asking for the name of the master list. Any other response results in PRESS prompting for file names individually.

Most spectra contain features that are much stronger and broader than the average e.g. the Balmer lines in early type stars. To cope with these features PRESS enables the user to specify regions that are to be ignored in the formation of the continuum and it will then simply use a linear interpolation in these regions. The next prompt enables a file containing these regions to be entered:

```
Are you using selected wavelength regions ? [N] >
```

Pressing <CR> or entering N will result in the entire spectrum being rectified. Otherwise the name of the file containing the required regions is prompted for. The file should contain pairs of wavelengths in free format, one pair per line. For example the following file would be used to make PRESS interpolate 100Å across Hγ and Hδ:

```
4050.0  4150.0
4290.0  4390.0
```

The next three prompts enable the user to enter the required values of **wsmooth** in units of pixels, **climit** and **nmax** or to adopt the default values by pressing <CR>. A typical use of PRESS might be as follows:

```
   PPPPP    RRRR   EEEEEE   SSSS     SSSS
   P    P   R   R  E       S        S
   P    P   R   R  E       S        S
   PPPPP    RRRR   EEE      SSS      SSS
   P        RR     E           S        S
   P        R R    E           S        S
   P        R  R   EEEEEE  SSSS     SSSS

                                    P. Maxted

                               Manual available in
                               pressdir:manual.tex

================================================

Are you using a master list ? [Y] > N
 Reading single file

Are you using selected wavelength regions  ? [N] > Y
 Using selected spectral range

Enter name of spectral region file > HLINES.DAT
Spectral region file is HLINES.DAT



Enter smoothing interval [20] > 30

Smoothing interval set at  30


Enter maximum number of iterations [20] >

Maximum number of iterations is  20


Enter convergence limit [0.001] >
```

```
convergence limit is .0010000
Enter name of spectrum to be rectified, E to end > W0135
Current file is W0135

 Iteration   Delta
     2       .00885
     3       .00555
     4       .00393
     5       .00295
     6       .00234
     7       .00191
     8       .00159
     9       .00137
    10       .00118
    11       .00104
    12       .00093
Convergence limit reached
Enter name of spectrum to be rectified, E to end > W0138
Current file is W0138

 Iteration   Delta
     2       .00648
     3       .00432
     4       .00322
     5       .00254
     6       .00208
     7       .00174
     8       .00148
     9       .00129
    10       .00113
    11       .00101
    12       .00090
Convergence limit reached
Enter name of spectrum to be rectified, E to end > E
```

The output spectra from PRESS are than stored in files with the same name as the input files with the exception of the initial symbol which is changed to the letter 'V'. In the example above the rectified spectra would be stored in the files `V0135.FTS` and `V0138.FTS`. Note that if the file extension is not specified `.FTS` is automatically assumed.

Some experimentation is required to find the values of **wsmooth**, **climit** and **nmax** suited to any particular task. For example, to flatten out spectra for convenience sake, a large value of **wsmooth**, say equivalent to 10Å, should be used with a file of wavelength regions to avoid disrupting large features such as the Balmer lines. In these cases we are generally not concerned with having the continuum level exactly set I=1 and so a relatively large value of **climit** can be used e.g. **climit**=0.01, or alternatively a **nmax** can be set to a low value such as 3 or 4.

For spectra which are to be used with VCROSS more care is required. In particular it is found that if **wsmooth** is set too low, large spurious features appear symmetrically either side of the central peak. The value of **climit** should be chosen such that the residual flux is matched to the signal-to-noise ratio. For spectra with a signal-to-noise ratio of 50–200 a value of 0.0001 gives good results.

A note of caution is appropriate concerning the spectra of early-type stars. It was found that if the hydrogen lines were included in the rectification procedure and the cross correlation process, the resultant CCF's were extremely good and very easy to measure but that the values for the radial velocities measured were systematically incorrect. The hydrogen lines should not therefore be included in the cross-correlation process.

A.5 XPRESS and DPRESS

For a large set of homogeneous spectra the user may specify a file of default parameters to be used by XPRESS. This version of PRESS saves time by using these default values without prompting the user and also does not print the details of the rectification procedure. The default parameters are stored in the file `pressdir::xpress_default.dat`. The first twelve columns contain the parameter name followed by the value of the parameter in the next twelve columns. For example:

```
nmax        10
wsmooth     20
climit      0.001
```

DPRESS works in the same fashion as PRESS but the files are stores in ASCII format as a simple list of wavelengths versus intensities. The default file extension in then `.dat`

Appendix B

Tomography

B.1 Introduction

Tomography is a technique borrowed from medical physics for recovering an N dimensional object from a set of compressed N-1 dimensional images of the object viewed from different angles. In the case of a binary star the images are the combined spectra of a binary star where the Doppler shift plays the rôle of the viewing angle and the object is taken to be the intrinsic spectra of the individual stars placed one behind the other (c.f. Bagnuolo & Gies, 1991). This is illustrated in Fig. B.1. This technique has been used to recover the individual spectra of the component stars in a binary system from the observed composite spectra, for example, by Bagnuolo & Gies for AO Cas and by Hill et al. (1994) for CC Cas. These systems are both OB type binaries.

Using a code developed by Graham Hill including the modifications described below we have investigated the reliability of tomography when it is used to recover the spectra of the components of Algol type binary stars. Using a set of synthetic combined spectra we have investigated the effect of the signal-to-noise ratio and radial velocity errors (random and systematic) on the recovered secondary spectrum. We find that the secondary spectrum can be recovered reliably but only under certain conditions.

B.2 The synthetic spectra

To create a set of synthetic Algol spectra we used two high signal-to-noise spectra obtained with the Richardson-Brealey spectrograph (RBS) and Reticon detector attached to the Leslie Rose

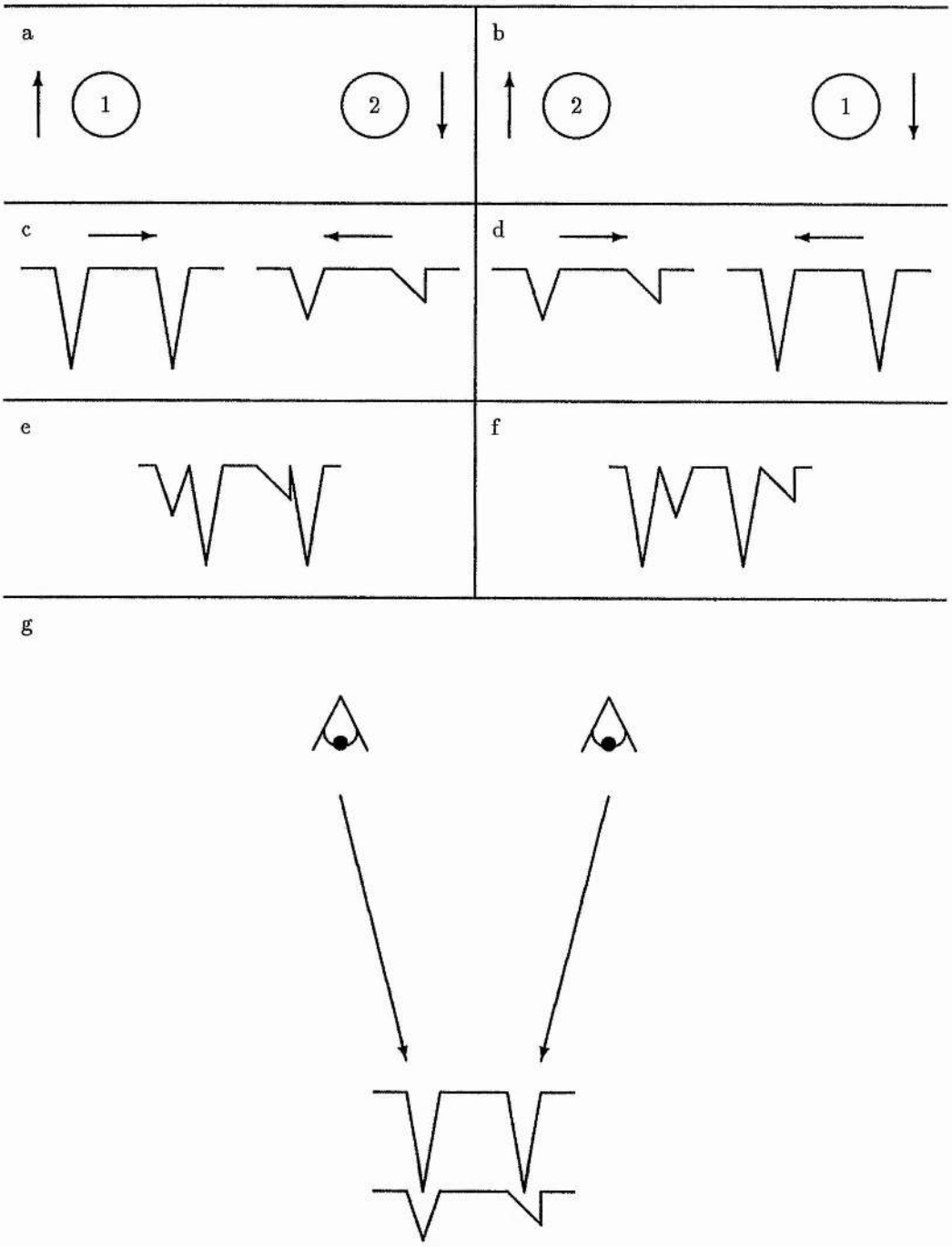

Figure B.1: The principle of Tomography as applied to binary star spectra. a),b) The orbital motion of the stars at two phases. c),d) The individual spectra of the stars and the Doppler shifts at the corresponding phases. e),f) The combined spectra. g) The object and viewing angles that mimic the effect of the Doppler shifts.

Telescope at the St Andrews University Observatory. The spectra are approximately 600Å long and centered at 4250Å and the resolution is slightly better than 1Å. For the primary we used a spectrum of Vega (α Lyr, A0Va) and for the secondary we used a spectrum of Hamal (α Ari, K2IIIab).

For stars of similar spectral type the luminosity ratio in the continuum is not wavelength dependent for the range of wavelengths found in a typical spectrum. This is not the case in Algols where the large difference in spectral type between the two stars implies a change in luminosity ratio of as much as 25% over the wavelength region covered by our spectra. To mimic this effect using our rectified spectra we multiplied the secondary spectrum by a linear function such I(4000Å)/I(4500Å)=0.75.

To the mimic the radial velocity variations due to orbital motion we adopted a mass ratio of 2.5 and a primary radial velocity semi-amplitude of $80\,\mathrm{km\,s^{-1}}$. Since radial velocity measurements are usually made only near quadrature we used primary radial velocities of magnitude $\sim 70\,\mathrm{km\,s^{-1}}$ equally distributed in sign. The corresponding secondary radial velocity is then simply $-2.5\times$(primary radial velocity). The effects of the Doppler shifts on the spectra were then applied. The effects of gravity darkening and mutual heating in Algols produce variations in the luminosity ratio with phase and so the spectra were added using random luminosity ratios in the range 18–22. The spectra were then re-normalised. In fact the variations in luminosity ratio reflect a non-uniform effective temperature distribution on the surface of both stars but particularly the secondary component. This in turn suggests that the spectrum of the secondary star varies with phase. However for the range of luminosity ratios considered here (which is typical for short period Algols) the corresponding change in spectral type for the secondary is only one subclass. The RBS spectra are shown in Fig. B.2

B.3 Summary of the method

Tomography is an iterative technique whereby approximations to the individual spectra are refined by applying a correction based on the difference between the observed and calculated combined spectra. For the case where the luminosity ratio is constant Bagnuolo & Gies give the following equations for the calculation of the correction:

$$\Delta f_{p,i} = \delta \times \frac{\sum_{k=1}^{m} p_{k,i} - (f_{p,i} + f_{s,i+s_k})}{m}$$

$$\Delta f_{s,i} = r\delta \times \frac{\sum_{k=1}^{m} p_{k,i-s_k} - (f_{p,i-s_k} + f_{s,i})}{m}$$

where:

$\Delta f_{p,i}, \Delta f_{s,i}$ are the corrections to the ith pixel of the primary and secondary spectra

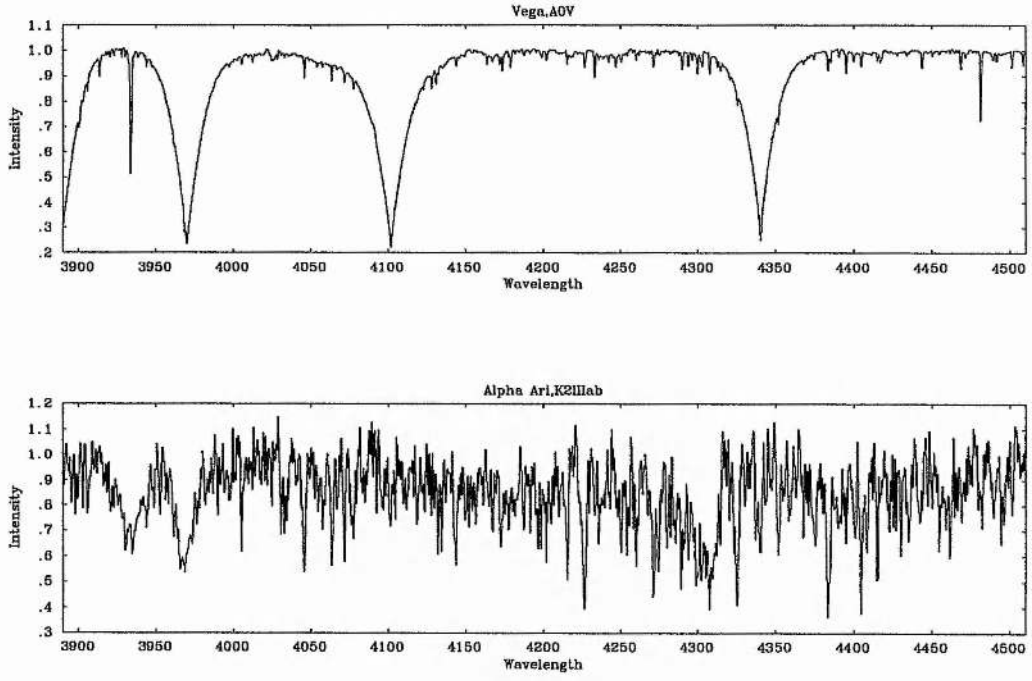

Figure B.2: The RBS spectra of Vega and Hamal

	respectively;
m	is the number of combined spectra;
$p_{k,i}$	is the ith pixel of the kth combined spectrum in the rest frame of the primary component;
$f_{p,i}, f_{s,i}$	are ith pixels of the approximations to the primary and secondary spectra respectively;
r	is the luminosity ratio
s_k	is the radial velocity shift of the secondary spectrum relative to the primary for the kth spectrum and
δ	is a number ~ 0.3 which aids convergence (Goitein, 1972).

In the case where the luminosity ratio is phase and/or wavelength dependent we introduce the variable $L_{k,i}$ which is the luminosity ratio of the two stars (primary / secondary) for the ith pixel of the kth spectrum. The corrections for the primary and secondary spectra can then be generalised as follows:

$$\Delta f_{p,i} = \delta \times \overline{L_{p,k,i}} \times \frac{\sum_{k=1}^{m} p_{k,i} - (L_{p,k,i} \times f_{p,i} + L_{s,k,i} \times f_{s,i+s_k})}{m}$$

$$\Delta f_{s,i} = \delta \times \overline{L_{s,k,i}} \times \frac{\sum_{k=1}^{m} p_{k,i-s_k} - (L_{p,k,i} \times f_{p,i-s_k} + L_{s,k,i} \times f_{s,i})}{m}$$

where:

$$L_{p,k,i} = \frac{1}{1 + L_{k,i}}$$

and

$$L_{s,k,i} = \frac{1}{1 + 1/L_{k,i}}$$

are the fractional luminosities of the primary and secondary stars respectively.

The tomography code of GH was modified to enable these generalised corrections to be used. For each combined spectrum the appropriate values of $L_{k,i}$ are interpolated from a table of user-supplied values at a range of wavelengths. In the case of the synthetic spectra where the wavelength dependence is linear, only two values are required for each combined spectrum. In reality these values would be generated from a light curve solution using LIGHT2.

B.4 Results

Using the modified version of the tomography code we attempted to reconstruct the primary and secondary spectra using the correct values of the radial velocities and the luminosity ratios. The results are shown in Fig. B.3 for the entire spectral region used. It should be noted that 200 iterations were required to achieve convergence and that after the first few iterations convergence was very slow. Recovery of the primary spectrum appears to be successful at this scale but the secondary spectrum is clearly affected by large features in the primary spectrum. This is particularly noticeable around the Balmer lines, but also near other strong metallic lines. This disruption is caused by the large and rapid change in the luminosity ratio near these features. Implicit to the method used to derive the corrections given above is the assumption that the luminosity ratio does not vary significantly near spectral lines. For stars of similar spectral type this is indeed the case since the luminosity ratio is less extreme in the continuum and this ratio does not change significantly near weak spectral lines. This is not the case for Algol systems, particularly near the strong spectral lines of the primary. Away from these features, recovery of the secondary spectrum is remarkably good. In Fig. B.4 we compare the actual primary and secondary spectra to the recovered spectra over the spectral region $\lambda\lambda$4150–4300Å. We first note that the recovery of the primary spectrum is indeed very accurate. A comparison of the original and recovered spectra shows them to be the same to within 1% for most of the spectral region used with systematic errors of $\sim$5% around the Balmer lines.

For the secondary spectrum we see that most spectral lines are recovered at the correct positions, and at the correct relative strengths, although there appears to be a slight scaling problem. Comparison of this spectrum with other K star spectra shows that spectral classification with this spectrum leads to the correct spectral type to within a subclass if several criteria are used e.g. the ratio of the Fe to Cr lines.

The main advantage of tomography as far as the recovery of the primary spectrum is concerned is the increase in the signal-to-noise ratio. This is demonstrated in Fig. B.5 where we

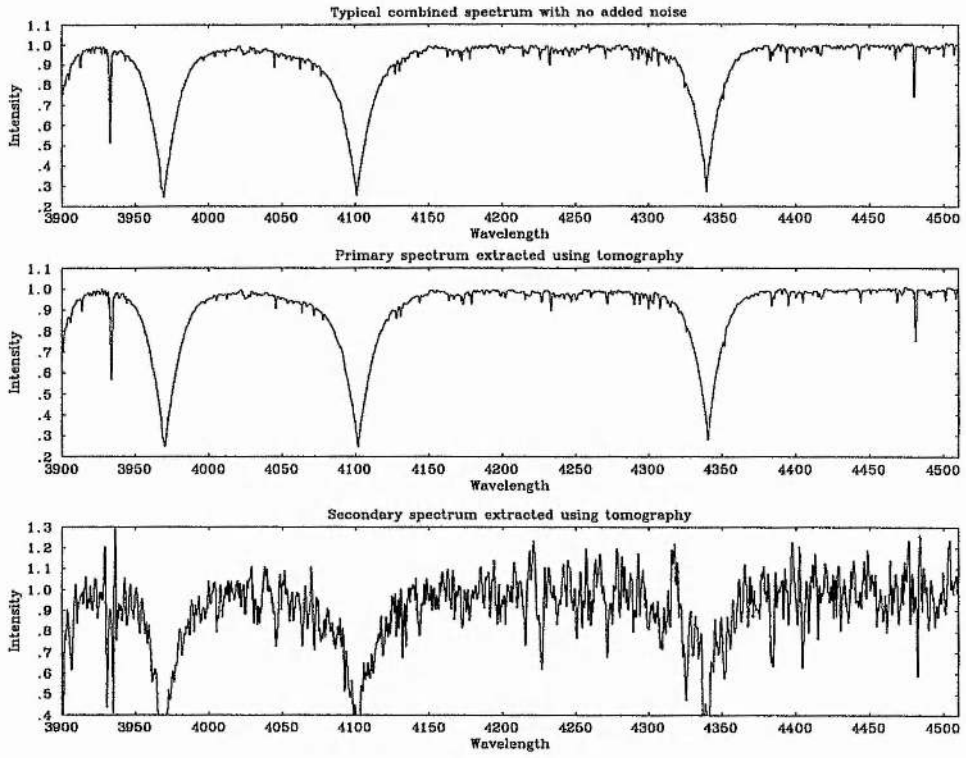

Figure B.3: A typical combined spectrum and the spectra recovered using tomography

compare the original primary spectrum to a primary spectrum with pure Gaussian noise added such that the signal-to-noise is 50. The increase in signal-to-noise provided by tomographic separation of 20 such spectra is evident. Tomography has the advantage over simple shift-and-add techniques of being less prone to systematic errors due to the presence of the fainter component. Recovery of the secondary component in these situations is still surprisingly good although the error in the spectral classification may be as much as three or four subtypes at this level.

We also investigated the effect of errors in the adopted radial velocities on the recovered spectra. For random errors typical of those found in Algol spectra e.g. $\sigma_{\rm pri} = 3\,{\rm km\,s^{-1}}$, $\sigma_{\rm sec} = 15\,{\rm km\,s^{-1}}$, we found very little effect on the primary spectra, but the spectral features in the secondary spectra tended to be broader, as might be expected given that the radial velocity errors translate into errors in the positions of these features. We also looked at the effect of systematic errors in the radial velocities and found that errors of up to $10\,{\rm km\,s^{-1}}$ in the primary semi-amplitude and $30\,{\rm km\,s^{-1}}$ in the secondary semi-amplitude were required before errors in the shapes of the spectral features in the recovered spectra became noticeable.

For all of the cases discussed above we started the iterative process using completely featureless spectra because we found that using "initial guesses" resulted in misleading results for the secondary component. In particular, we note that, for the secondary, convergence is

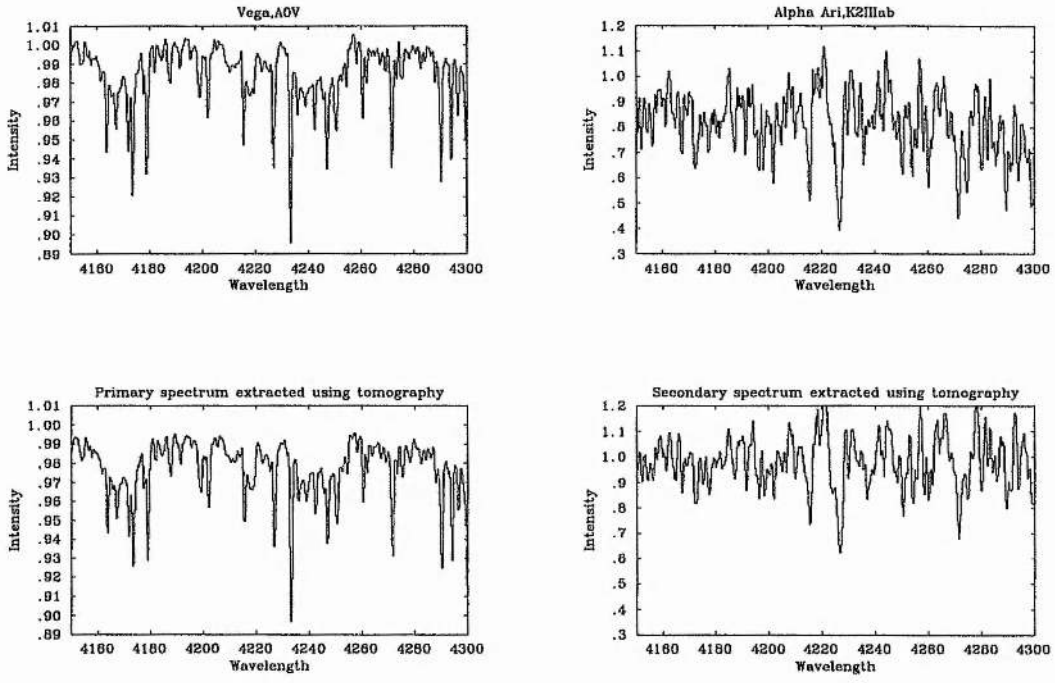

Figure B.4: Detail of spectra recovered using tomography and the original spectra for comparison.

equally slow for both featureless initial spectra and "initial guesses". However the slow rate of convergence could lead the unwary to believe that the spectrum produced after 50 iterations was a fair reflection of the underlying secondary spectrum, whereas in reality this spectrum would be determined principally by the "initial guess". Since there is nothing to be gained from using an "initial guess" it would seem prudent to avoid its use.

B.5 Conclusion

We can summarise the results above as follows: recovery of the individual spectra from combined Algol spectra is feasible except near strong spectral features in the primary spectrum where the secondary spectrum will be unreliable; the method is robust in terms of its ability to cope with noise and radial velocity errors; convergence is slow and is not helped by the use of "initial guesses".

The disruption of the secondary spectrum by strong primary spectral features is clearly the biggest restriction to the use of the method. Given that recovery of the primary spectrum appears to be very reliable it may be possible to modify the algorithm further to take account of variations in the luminosity ratio produced by these features. However for these difficult

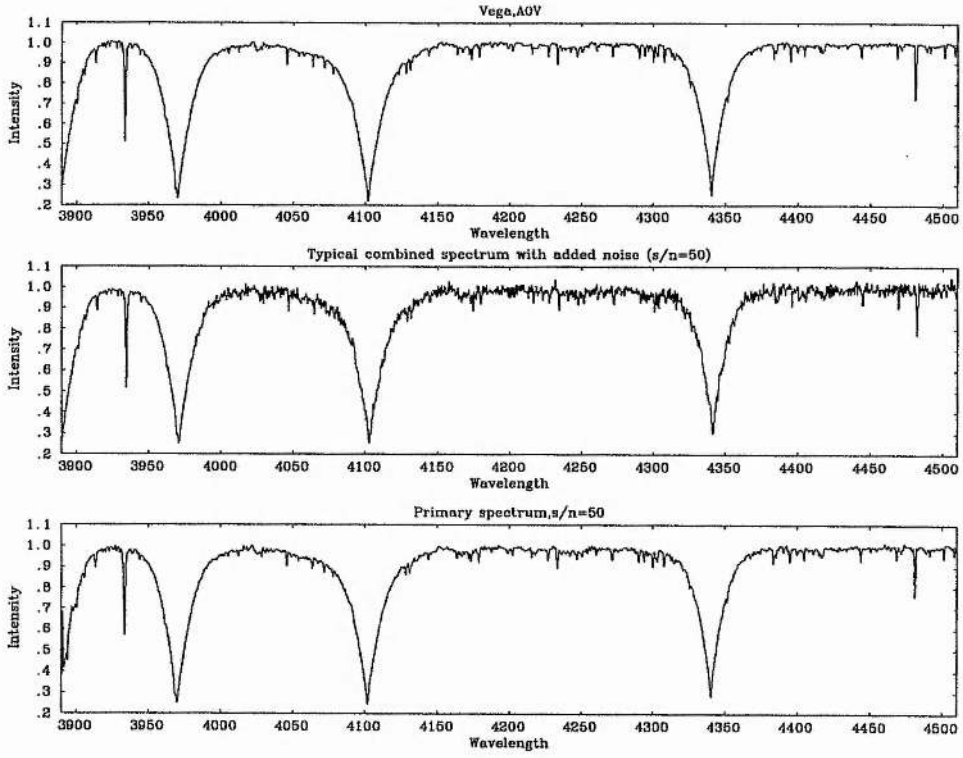

Figure B.5: The improvement in signal-to-noise for the primary

cases alternative approaches such as the disentangling method of Simon & Sturm (1992) should (and are) being investigated. The results presented here would suggest that such studies would provide useful improvements.

Bagnuolo, W.G., Gies D.R., 1991. ApJ, **376**, 266.

Goitein M., 1972. Nucl. Instr. Meth., **101**, 509.

Hill G., Hilditch R.W., Aikman G.C.L., Khallesseh B., 1994. A&A, **282**, 455.

Simon K.P., Sturm E., 1994. A&A, **282**, 92.